

THESIS APPROVAL

The abstract and thesis of Carol Stack for the Master of Science in Geology presented October 26, 1998, and accepted by the thesis committee and the department.

COMMITTEE APPROVALS:

Kenneth M. Cruikshank, Chair

Ansel G. Johnson

Richard H. Thoms

Leland A. W. Buddress
Representative of the Office of Graduate Studies

DEPARTMENT APPROVAL:

Ansel G. Johnson, Chair
Department of Geology

Abstract

An abstract of the thesis of Carol Stack for the Master of Science in Geology presented October 26, 1998.

Title: An examination of folded Eocene turbidites, Douglas County, southwestern Oregon.

Located in a fold and thrust belt in southwestern Oregon, the folded early Eocene Umpqua Group turbidites of this study have a N-S exposure approximately 360 m long and 20 m high. Nearly a down plunge view, the exposure of short wave trains, 1 to 1½ wavelengths of 10 to 28 m, is dominated by asymmetric chevron-like folds, but includes a symmetric concentric-like fold and kink-like folds.

A folding mechanism consistent with the fold and fault patterns of the outcrop is layer-parallel shortening. The form of theoretical multilayers produced in layer-parallel shortening is related to the conditions of folding: contact strength of the layers, relative strength of the layers, and layer thickness. The folding units within the outcrop exhibit contrast in layer strength. The concentric-like fold is bounded above by a unit of thicker beds having relatively less shale, acting as a stiff medium in a confined multilayer since the unit thickness is greater than the wavelengths of the folds. The package of chevron-like folds does not appear to have a comparable theoretical multilayer in form. Within the kink-like fold, nonlinear slip at layer

contacts, necessary in forming ideal monoclinial kink folds, may be evident in localized tan siltstone and associated calcareous nodules.

Asymmetry in the outcrop, short limbs of chevron-like folds facing south and kink-like fold facing north, is consistent with the regional setting in a NNW verging thrust sheet and top-to-the-south layer-parallel shear. Top-to-the-south bedding thrusts on the long, north-dipping limbs of the chevron-like folds, and duplex-like structures in some sandstone beds are evidence of the sense of shear.

Minimum shortening in the outcrop is 35 to 40 percent attributable to folding, but not including bed thickening in layer-parallel shortening and shortening in bed repetition by faulting.

The fold package appears to be in a relatively thin unit near the base of a thrust fault within a larger NNW verging thrust sheet. As a relatively thin unit bounded by muddier units above and below, there is sufficient contrast in strength over the thickness, enabling shorter wavelength folds to develop.

AN EXAMINATION OF FOLDED EOCENE TURBIDITES,

DOUGLAS COUNTY, SOUTHWESTERN OREGON

By

CAROL STACK

A thesis submitted in partial fulfillment of the
requirements for the degree of

MASTER OF SCIENCE

in

GEOLOGY

Portland State University

1998

Dedication

This thesis is dedicated to the curious who ask questions, in memory of my late brother, Leo, a model of never-ending curiosity and invention. Leo and I had many conversations regarding the folds. To all the Garden Valley residents passing by the outcrop who stopped to ask questions, keep asking.

Acknowledgments

My husband Michael provided ladder detail and company on numerous trips to the site; his constant support and encouragement is much appreciated. My advisor, Ken Cruikshank, provided timely insight and perspective to the study. I appreciate his patience in allowing the project to unfold at a nonlinear pace. Thanks to committee members, Ansel Johnson, Dick Thoms, and Lee Buddress, for their constructive review and comments.

Thank you to Lou Clark for the trip south during a not so typical Oregon rain (can't believe we did that). Special thanks to the couple concerned for my welfare during the period of slides and rockfall in December of 1997, and for the hospitality of Dale and Betty Woodruff, Garden Valley neighbors to the south.

Stereonets used in the analysis were drawn with GEORient 5.1© for Windows95, a product of Rod Holcombe, Department of Earth Sciences, University of Queensland, Australia, (<http://www.earthsciences.uq.edu.au/~rodh/software/>).

Table of Contents

Abstract	1
Dedication	i
Acknowledgments	ii
Table of Contents	iii
List of Tables	v
List of Figures	vi
Introduction	1
Regional Geologic Setting	3
Geographic Location	3
Regional Physiography and Geology	3
Stratigraphy	5
Siletz River Volcanics	5
Umpqua Group	7
Tye Formation	12
Structure	13
Folds	13
Faults	15
Tectonic History	17
Geologic Setting of the Study Area	21
Methods	25
Outcrop Observations	28
Bedding	28
Fractures	33
Fold Form	34
Section I	35
Bed Form	35
Fold Form	38
Fractures	39
Section II	43
Section III	45
Sections IV and V	49
Section VI	52
Discussion	58
Outcrop Fold Package	58
Folding Mechanism	59
Fold Form	59
Asymmetry	66
Unit Thickness	69
Outcrop Setting	75
Conclusion	78

Bibliography82
Appendix A.....86
Appendix B87
Appendix C.....102

List of Tables

<i>Number</i>	<i>Page</i>
Table 1. A summary by section of bed thickness and sandstone to shale ratios.....	30
Table 2. Summary of fold form by section (Figure 8).....	35
Table 3. A summary of bed thickness and sandstone to shale ratios by folding unit. .	61
Table 4. Results of applying the model relating multilayer thickness, number of structural units, and viscosity contrast in a multilayer with free slip.....	74

List of Figures

<i>Number</i>	<i>Page</i>
Figure 1. Location of study area.	2
Figure 2. Location of study area in Sutherlin subbasin..	4
Figure 3. Stratigraphic nomenclature for the region containing the study area.....	6
Figure 4. Schematic fence diagram of wells and measured sections surrounding the study area (after Ryu and others, 1992).	
Figure 5. Paleogeographic reconstruction of the Pacific Northwest at 55±5 Ma (after Heller and others, 1987, Fig. 5).	18
Figure 6. Cross-section of Sutherlin subbasin through study area.....	22
Figure 7. Estimated thickness of Umpqua Group units in the study area.....	24
Figure 8. N-S cross-section of folds with axial survey points, and map view of axial survey points.	26
Figure 9. Schematic showing thickness of measured fold limbs from north to south.	29
Figure 10. Bed deformed into low-amplitude sine wave with wavelength of about two meters.....	31
Figure 11. Duplex-like feature.....	32
Figure 12. Asymmetry of folds defined.....	34
Figure 13. Section I folds.....	36
Figure 14. Folds 3 and 4 of Section I.....	37
Figure 15. Envelopes of a bed traced through the folds of Section I.....	39
Figure 16. Bedding thrusts and sub-horizontal faults in the concentric-like fold of Section I.	40
Figure 17. Section I folds and faults not at low angle to bedding.	42
Figure 18. Section II and Section III folds.....	44

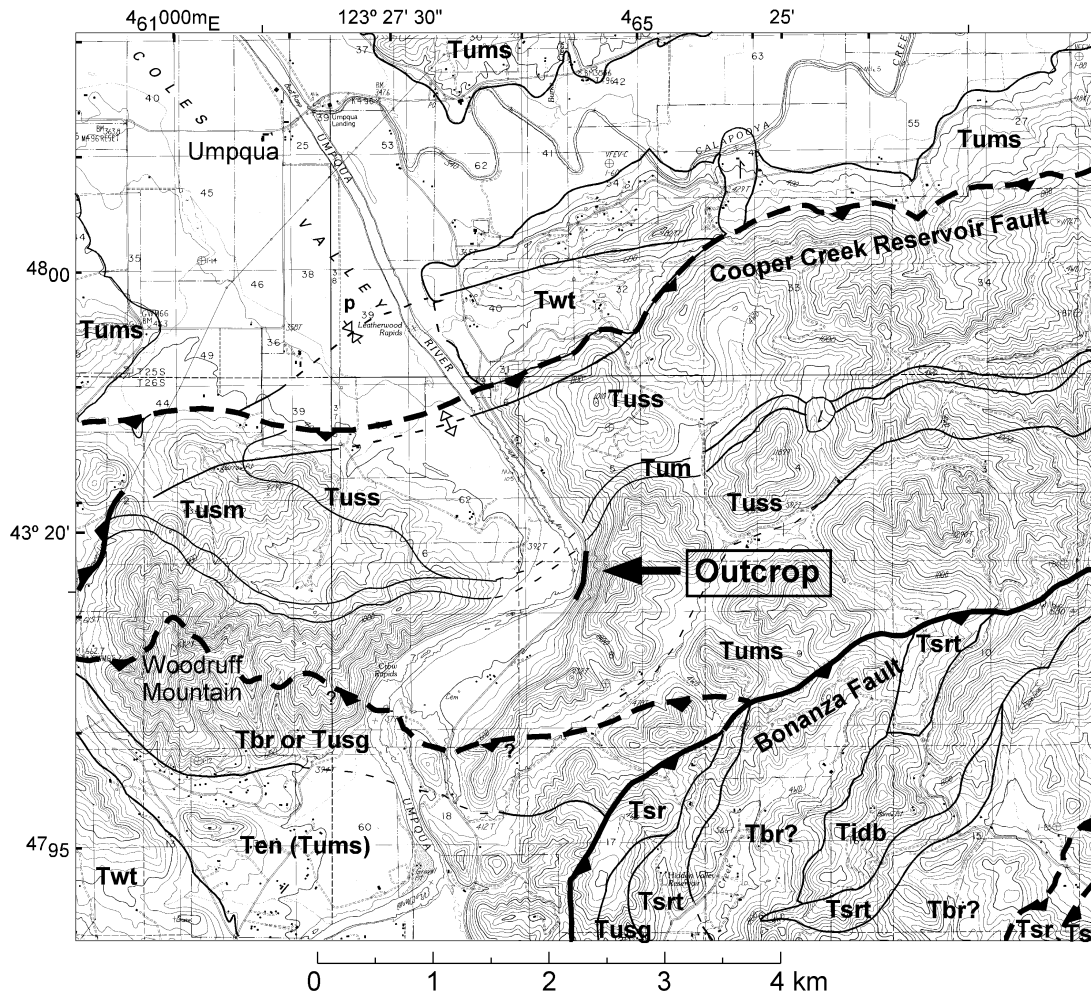
Figure 19. Idealized kink form imposed on schematic drawing of kink-like fold.....	46
Figure 20. Fractures and contacts in kink-like fold.	47
Figure 21. Tan siltstone and associated calcareous nodule at base of kink-like fold of Section III.....	48
Figure 22. Thrust fault zone immediately north of (stratigraphically below) the kink-like fold.	49
Figure 23. Section IV and Section V folds.	50
Figure 24. Jointed hinge of fold 14 in Section IV.....	51
Figure 25. Section VI asymmetric chevron-like folds.	53
Figure 26. Schematic folding of conjugate fault zones in layers of Section VI.	54
Figure 27. Anticlinal fold 21 in Section VI.	55
Figure 28. Duplication of layers in south anticline of Section VI.	56
Figure 29. Boudin layer in curve of drag fold in fold 21, Section VI.....	57
Figure 30. Model of folding units in the study outcrop.	60
Figure 31. Theoretical multilayer folds.	62
Figure 32. Fold form of Section I.	64
Figure 33. Parameters for multilayer folding models.	65
Figure 34. Opposite sense of asymmetry of monoclinial kink and drag folds.....	67
Figure 35. Sense of fold asymmetry for the outcrop setting in a thrust sheet.....	69
Figure 36. Chart of layer to average media viscosity.	71
Figure 37. Chart of initial thickness as a function of layer to average media viscosity contrast.....	72
Figure 38. Relation of the wavelength to thickness ratio in rigid and soft media, for various ratios of media to normal viscosity of the multilayer.	73
Figure 39. Order of deformation.....	79

Introduction

This study describes folds exposed in an outcrop of the late Paleocene to early Eocene Umpqua Group in the Umpqua River valley, northwest of Roseburg, southwestern Oregon (Figure 1). Within a sequence of continental slope, shelf, and deltaic deposits, the folds are part of a larger fold and thrust belt on the Klamath Mountain borderland stretching from the Oregon Cascade Range to the Pacific Ocean.

Approximately 360 meters long and normal to the strike of the folds, the outcrop consists of rhythmically bedded sandstone and shale layers up to 70 cm thick. Wavelengths are 9 to 28 m and amplitudes, 3 to 7 m. Plunge of the folds ranges from 2° to 34°, W and E, giving much of the outcrop close to a down plunge view, a relatively undistorted view of the folds. The folds are predominantly asymmetric chevron-like folds with a concentric-like fold and kink-like folds (Johnson and Pfaff, 1989). The many faults and joints are evidence of a complex interplay of folding and fracturing, creating ramps, wedges, and shear zones within the sequence of fold forms.

The objective of this study is to examine and describe the exposed folds, mapping the fold forms and faults in general and detail of the best exposures. Multilayer fold theory (Johnson and Fletcher, 1994) is used to address two questions: a) why did folds form in these layers, and b) what conditions in the multilayer contributed to the present fold form. Any constraint on the conditions of folding will enhance the understanding of the formation of the outcrop and provide a glimpse into the Paleogene setting of the region.



Umpqua Group undifferentiated

- Tuss: sandstone dominated turbidites, thick to massive
- Tum: mudstone
- Tusm: sandstone dominated turbidites, thin to medium bedded
- Tums: mudstone dominated thin turbidites
- Tusg: pebbly, gritty sandstone, Bushnell Rock lithology

Umpqua Group differentiated

- Twt: White Tail Ridge Formation
- Ten: Tenmile Formation
- Tbr: Bushnell Rock Formation

Tsr: Siletz River Volcanics

- Tsrt: tuff
- Tidb: intrusive diabase

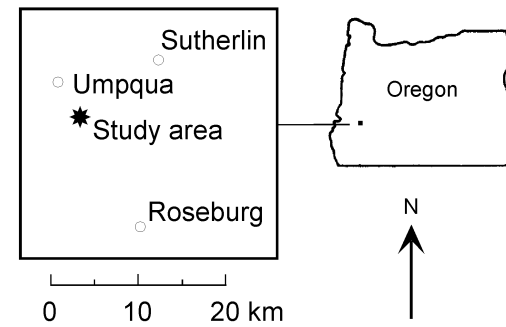


Figure 1. Location of study area. The outcrop is along Garden Valley Road, 4.2 km SSE of Umpqua. Base map is from USGS Garden Valley 7.5' Quadrangle. The geology is from Wells (1998).

Regional Geologic Setting

Geographic Location

The folds of the study area are exposed in a roadcut between milepost 11 and 12 on Garden Valley Road northwest of Roseburg, Douglas County, southwestern Oregon. They are 4.3 km south of Umpqua (Figure 1). The regional topography is one of domed hills and resistant ridges, up to 700 m in elevation with relief of 600 m, clustered between river and creek valleys. Density of vegetation on hills is thick to sparse depending on the substratum, with mostly madrone, oak, and fir trees. At an elevation of 120 m, the outcrop overlooks a bend in the Umpqua River as it flows from the High Cascades to the Pacific Ocean at Reedsport.

Regional Physiography and Geology

Near the convergence of the Oregon Coast Range, Western Cascades, and Klamath Mountains, the study area is in the Sutherlin subbasin at the southern end of the Oregon Coast Range (Figure 2). The subbasin contains Umpqua Group sedimentary rocks overlying Siletz River Volcanics (Baldwin and Perttu, 1980; Molenaar, 1985), the basement rock of the Oregon Coast Range (Duncan, 1982). To the west, Siletz River Volcanics and Umpqua Group strata are buried in the Tyee basin, then resurface in the Myrtle Point subbasin (Baldwin, 1974; Molenaar, 1985). Tyee sandstone forms higher ridges west and north of exposed Umpqua Group strata (Molenaar, 1985; Perttu and Benson, 1980). At the eastern edge of the basin is the

boundary of the Oregon Coast Range with the late Eocene-early Miocene Western Cascades (Baldwin, 1974).

South of the Sutherlin subbasin, the Oregon Coast Range converges with the Mesozoic Klamath Mountains. An effect of this convergence is seen in the parallel NE-SW structural alignment of the Umpqua arch, Sutherlin subbasin, Bonanza fault zone, and the faulted boundary of the Klamath Mountain province (Molenaar, 1985; Perttu and Benson, 1980; Ryberg, 1984) (Figure 2). The Klamath Mountains were the major source of sediment for Umpqua Group rock (Molenaar, 1985; Ryberg, 1984).

Stratigraphy

The stratigraphy of the Umpqua region consists of Paleocene age Siletz River Volcanics, regarded as basement rock, underlying up to 3700 m of Eocene turbidite sediments and deltaic deposits (Baldwin and Perttu, 1980; Molenaar, 1985) (Figure 3). The lower to early middle Eocene units, which include the units of the study area, comprise the Umpqua Group (Molenaar, 1985; Ryu and others, 1992). The younger units above the Umpqua Group belong to the Tyee Formation. Following is an overview of these units from oldest to youngest.

Siletz River Volcanics

Underlying the Umpqua Group, the Paleocene to early Eocene Siletz River Volcanics have K/Ar and Ar/Ar dates of 50.7 ± 3.1 to 62.1 ± 1.0 Ma with ages typically decreasing from south to north (Duncan, 1982). A date of 62.1 Ma was recorded for

Series	Foram Stage	Sequence	Ryu and others (1992)		Molenaar (1985)	Baldwin (1974) Baldwin and Perttu (1989)					
			N	S							
Eocene	Middle	Narzian	Spencer Fm. and Bateman Fm.		Elkton Fm.	Bateman Fm.					
			Lorane Fm. and Elkton Fm.			Elkton Fm.					
		Ulatisian	III	Tyee Fm.	Baughman Mbr.	Tyee Fm.	Deltaic facies ?	Tyee Fm.	Baughman Mbr. ?		
					Hubbard Creek Mbr.		Upper slope-outer shelf ?		Hubbard Creek Mbr. ?		
			Tyee Mountain Mbr.			Deep-water fan facies ?		Tyee Mountain Mbr. ?			
	Lower	Penutian	Umpqua Group	Umpqua Group undifferentiated	Camas Valley Fm.	Umpqua Formation	Umpqua Formation	Camas Valley Mbr.	Camas Valley Mbr.	Umpqua Group	
					Rasler Ck tongue			White Tail Ridge Fm.	White Tail Ridge Mbr.		White Tail Ridge Mbr.
					Coquille River Mbr.			Remote Mbr.	Ollala Creek Mbr.		Ollala Creek Mbr.
		Berry Creek Mbr.			Tenmile Fm.			Tenmile Mbr.	Tenmile Mbr.		
		Slater Creek ss. Mbr.			Bushnell Rock Fm.			Bushnell Rock Mbr.	Bushnell Rock Mbr.		
		pre-Tertiary			Siletz River Volcanics (basement)			Roseburg Formation (basaltic)			
Bullitian	I										
Paleocene											

Figure 3. Stratigraphic nomenclature for the region containing the study area. This study uses the nomenclature of Ryu and others (1992).

volcanics in the Drain anticline in the heart of the Umpqua arch northeast of the study area (Figure 2). Extending from the foothills of the Oregon Cascades east of the study area to the west and northwest, the volcanics form the basement of the Oregon Coast Range. Estimated to be up to 25 km thick in the central Oregon Coast Range, the base of the volcanics has not been observed. The Siletz River Volcanics consist of pillow basalt, tuff-breccia, massive lava flows, and sills with some aerial deposits in its southern extent (Baldwin, 1974; Duncan, 1982; Snavely and others, 1968).

Exposure of the Siletz River Volcanics is widespread in the Roseburg area north to the Bonanza fault zone (Figure 1) and in the cores of anticlines east and west of the Tyee basin (Figure 2). Umpqua Group strata lap onto and thin across the Umpqua arch, a volcanic high north of the study area (Molenaar, 1985). Northeast of Sutherlin, Mobil Oil Corporation drilled into 3 km of Siletz River basalt without reaching its base (Ryu and others, 1992).

Umpqua Group

Unconformably overlying the Siletz River Volcanics, the Umpqua Group continental margin deposits are Paleocene to early Eocene. Foraminifera of the Umpqua Group are referable to the Lower Penutian-Upper Ulatisian Stages (Thoms, 1975). Paleoecology indicator fossils show deposition of the units took place in warm shallow waters of sublittoral to neritic depths with occasional connections to the open ocean (Thoms, 1975). The oldest microfauna in the group, in sedimentary beds within volcanics east of Myrtle Point, are of the Paleocene (Thoms, 1975). Planktonic foraminifera of the Tenmile Formation are indistinguishable from those of the lower undifferentiated Umpqua Group (Ryberg, 1984). In the uppermost Camas Valley Formation, foraminifera are characteristic of the early Ulatisian Stage of earliest middle Eocene age (Ryberg, 1984). Just as fossils do not easily distinguish the formations of the Umpqua Group, neither do contacts within the group. Formation and member contacts are generally conformable with interfingering facies and local unconformities (Ryu and others, 1992).

Stratigraphic Nomenclature

The interfingering of deposits and complexity of the setting has prompted revision of the stratigraphic nomenclature of the Umpqua Group several times as additional mapping and correlation of the units has been completed (Figure 3).

Umpqua Group strata were first described by Diller (1898) as the Umpqua Formation.

Baldwin (1974) upgraded the formation to the group status composed of three formations, the Roseburg, Lookingglass, and Flourney, with the study area in the Roseburg Formation. The sedimentary part of Baldwin's Roseburg Formation is based on an exposure of turbidite beds on the south side of the Dickinson Mountain anticline, north of Sutherlin (Figure 2). Baldwin (1974) estimated the interbedded sandstone and shale is 2400 m thick.

The basement Siletz River Volcanics were included with the sedimentary strata of the Umpqua or Roseburg Formation by Baldwin and Diller (1974; 1898). Molenaar (1985) used Umpqua as a formation name with four members but separated the volcanics which were now shown to be equivalent to the type Siletz River Volcanics to the north (Snively and others, 1968; Thoms, 1975).

More recently, work of Ryu and others (1992) maintains the Umpqua Group status but builds on prior work for redefining the subdivisions of the group. This recent nomenclature divides the differentiated Umpqua Group into the Bushnell Rock, Tenmile, White Tail Ridge, and Camas Valley formations, and units not assigned to formations are referred to as the undifferentiated Umpqua Group.

Differentiated Umpqua Group

In the lower Umpqua Group, the Bushnell Rock Formation unconformably overlies Siletz River Volcanics and in areas, Mesozoic rock of the Klamath Mountains. The formation consists of thick massive units of pebble-cobble conglomerate with minor interbeds of sandstone. Clasts are derived from the Klamath Mountains to the south (Molenaar, 1985). Near Woodruff Mountain (Figure 1), an isolated well-bedded sandstone and conglomerate unit about six hundred meters thick, was interpreted by Molenaar (1985) as a local deep water channel facies of the Bushnell Rock Formation.

Thickness of the Bushnell Rock Formation varies to 1200 m (Molenaar, 1985; Ryberg, 1984; Ryu and others, 1992). Thickest in the south and southeast regions of the Tyee basin, the unit rapidly thins to the north within 8 to 16 km, grading into the undifferentiated Umpqua Group strata (Ryu and others, 1992). South of the study area, the Bushnell Rock formation is in possible fault contact with undifferentiated Umpqua Group units (Figure 1). A fence diagram of the Umpqua area shows the formation in all columns south of Umpqua to a vertical thickness of 600 m (Figure 4).

Conformably overlying the Bushnell Rock Formation, the Tenmile Formation is mainly composed of thin-bedded turbidites alternating with deep marine mudstone, (Baldwin, 1974; Molenaar, 1985). In its southern extent, three isolated tongues of pebbly sandstone with mudstone rip-ups and pebble to boulder conglomerate are associated with the turbidites, one of which, the Rasler Creek tongue, has rounded,

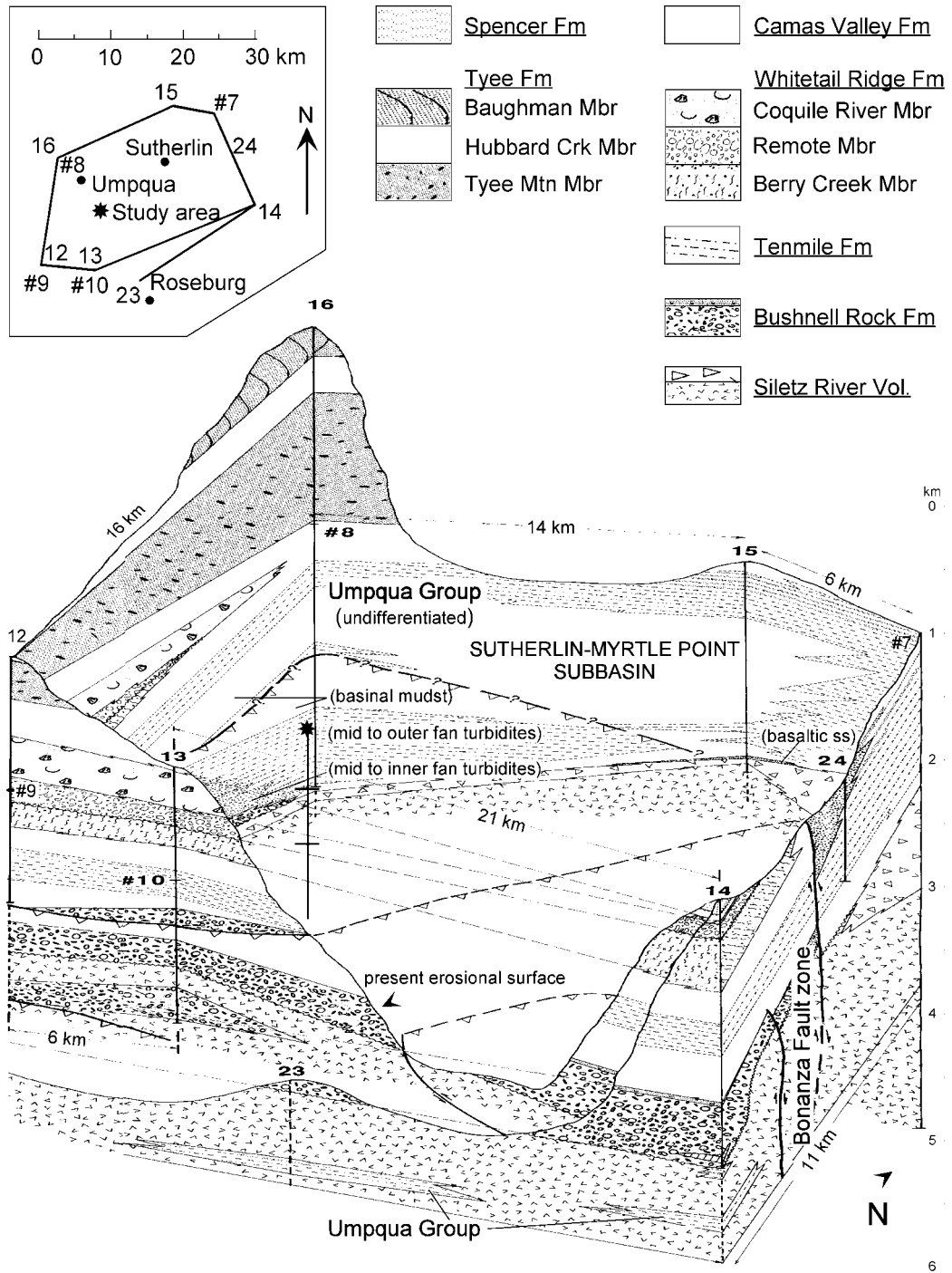


Figure 4. Schematic fence diagram of wells and measured sections surrounding the study area (after Ryu and others, 1992). The location of the study area is indicated by the symbol and post in the interior. Lines from well #9 to well #7 connecting the upper and lower boundaries of the Tenmile Formation turbidites cross this interior post at the horizontal line segments on the post.

white calcareous concretions (Ryu and others, 1992). The turbidite beds consist of poorly sorted, medium to coarse grained, lithic sandstones alternating with dark gray mudstone. Sandstone to mudstone ratios are 1:1 to 2:1 (Ryu and others, 1992). Up to 450 m thick, the turbidite beds commonly overlie slope mudstone and grade out toward the north and northwest. Locally overlying the turbidite sequence is an upper slope/shelf mudstone. Up to 900 m thick, the deep marine mudstone unit is widespread in the south, southeast, and eastern Tye basin (Baldwin and Perttu, 1980; Molenaar, 1985; Ryu and others, 1992). In the Umpqua area, the Tenmile Formation occurs as a mudstone, turbidite, mudstone sequence up to a vertical thickness of 850 m (Figure 4) (Ryu and others, 1992).

Conformably above the Tenmile Formation is a deltaic sequence, the White Tail Ridge Formation. Up to 1000 m thick, the formation thins to the north into deep marine mudstone of the undifferentiated Umpqua Group (Ryu and others, 1992). The fence diagram of Figure 4 has White Tail Ridge Formation in columns south of the study area with vertical thickness up to 750 m (Ryu and others, 1992).

Consistently above the White Tail Ridge Formation, the widespread Camas Valley Formation, uppermost Umpqua Group unit, consists of massive, shelf to slope mudstone up to 550 m thick (Baldwin, 1974; Molenaar, 1985; Ryu and others, 1992). In the Umpqua area, the Camas Valley Formation is about two hundred fifty meters thick (Figure 4) (Ryu and others, 1992).

Undifferentiated Umpqua Group

The formations of the Umpqua Group are not recognized basin-wide because of poor exposures, lateral facies changes, and complex structure. The category of undifferentiated Umpqua Group accommodates these problematic areas typically in the northern, distal sections of the basin where Bushnell Rock conglomerate and White Tail Ridge deltaic deposits are absent (Figure 4). A sedimentary sequence of turbidites and mudstone, the distal deposits are laterally equivalent facies of formally recognized Umpqua Group formations, though the lower undifferentiated strata in the Sutherlin area might be older than the Bushnell Rock Formation (Molenaar, 1985). The undifferentiated name is also applied to sedimentary rocks interfingering with Siletz River Volcanics (Ryu and others, 1992).

Tyee Formation

Stratigraphically above the Umpqua Group, the widespread middle Eocene Tyee Formation crops out over an area 80 km wide and 280 km long, from a latitude of 42°41' N to 45°11' N (Molenaar, 1985). The thick bedded micaceous arkosic sandstone and minor mudstone sequence ranges from 2000 to 3000 m thick (Molenaar, 1985; Ryu and others, 1992). Provenance of the sandstone is mixed, though Rb/Sr ratios of coarse muscovite flakes indicate the Idaho batholith is the main source of sediments (Heller and others, 1985). Column 16 of the fence diagram in Figure 4 shows the Tyee Formation is about one kilometer thick northwest of Umpqua (Ryu and others, 1992).

Structure

The structure of the Sutherlin subbasin is dominated by a NE-SW trend parallel to the accretionary contact between the Mesozoic Klamath Mountain terrane and Cenozoic Siletz River Volcanics (Ryberg, 1984). To the west, structural trends in the Tyee Formation are N-S within an E-W extension regime (Perttu and Benson, 1980) overprinted by a series of NW-SE anticlinal plays (Ryu and others, 1996). The larger scale anticlines and synclines in the subbasin accommodate the volcanic highs in the north (Figure 2). Major faults in the south expose Siletz River Volcanics and Umpqua Group strata adjacent to the Klamath terrane.

Folds

Folding is at several scales in the region. First-order folds have wavelengths of 10 km and amplitudes of 1 km (Perttu and Benson, 1980). Fold axes parallel the accretionary lineament (Figure 2) south of Roseburg. Perttu and Benson (1980) report anticlines are tighter in the hinge than the broader synclines, and north limbs are steeper. Ryu and others (1996) describe the folds as broad, and the Oakland anticline in particular, as a symmetrical broad fold with dips of 10° to 30° on its limbs, except near faults. The Oakland anticline and Dickinson Mountain anticline to the north appear to form the skeleton of the Sutherlin subbasin structure (Figure 2). The beds of the study area are on the southeast limb of the first-order Oakland anticline.

Second-order folds occur as syncline-anticline pairs on the limbs of first-order folds. The fold pairs have axes that extend 1 to 5 km and half-wavelengths of 0.4 to

1.1 km. The second-order folds are locally developed; three of the anticlines and synclines are mapped in the Umpqua to Sutherlin area (Ryberg, 1984, Wells, 1998). One pair crosses the Umpqua River south of Umpqua (Figure 1) bordering the Cooper Creek Reservoir fault. The area of the syncline north of the fault is an exposure of the White Tail Ridge Formation.

Third-order folds are highly localized, occurring as sequences of tight chevron-like folds. The folds of the study are third-order, with wavelengths of 10 to 30 m and 3 to 7 m amplitudes. Other third-order folds in the Sutherlin subbasin were reported by Wells and Waters (1934) and by Perttu and Benson (1980). These folds are in the Bonanza area east of Sutherlin, and at two sites along the Umpqua River, south of the Cooper Creek Reservoir fault, and south of Woodruff Mountain. The folds south of Woodruff Mountain described by Perttu and Benson (1980) have fold axes of more variable azimuth and plunge than the folds in the study outcrop. Perttu (Geology of the Stephens and Calapooya proposed nuclear sites, Douglas County, Oregon: Portland State University, c. 1972-76) reported tight chevron folds in calcareous concretionary siltstone at a fault contact near the currently mapped Cooper Creek Reservoir fault.

The third-order folds of the Umpqua basin are in turbidite beds of the lower Umpqua Group, the Tenmile Formation and its lateral equivalent in the undifferentiated Umpqua Group. These highly localized folds are not generally found in the upper Umpqua Group, the White Tail Ridge sandstone and Camas Valley

mudstone (Ryberg, 1984). However, a distal facies of the White Tail Ridge Formation, the Coquile River member, is locally infolded with Tenmile Formation turbidites (Ryu and others, 1996). Away from faults, upper Umpqua units typically have dips of less than 30° (Ryu and others, 1992). In the study area, the turbidite unit containing the folds overlies a less competent mudstone unit (Figure 1).

Faults

In the eastern Umpqua basin, major faults are south of the Sutherlin subbasin. The Bonanza fault on the southern boundary of the subbasin and the Wildlife Safari fault to the south have a NE-SW strike which is similar to the trend of the regional folds (Figure 2). Farther south, the Canyonville fault has a more E-W strike. Dominant motion on the faults varies from reverse, with hanging wall displaced northwest, in the NE-SW Bonanza fault zone, to E-W right-lateral strike slip on the Canyonville fault (Ryberg, 1984). The Wildlife Safari fault has elements of both with oblique right-lateral reverse displacement.

In the Bonanza fault zone south of the study area, basement Siletz River Volcanics and Bushnell Rock conglomerate are thrust top-to-the-northwest, adjacent to sedimentary beds of the undifferentiated Umpqua Group (Figure 1). The fault was still active after deposition of the White Tail Ridge Formation. Ryu and others (1996) report that reactivation of the Bonanza fault deformed sandstones of the White Tail Ridge Formation and upper Eocene-Oligocene Colestin/Fisher Formation in the foothills of the Western Cascades east of Sutherlin. At the Bonanza mine east of

Sutherlin, the fault dips about 45° SE, parallel to bedding. Dip separation is estimated at 1.5 km maximum (Perttu and Benson, 1980).

The Wildlife Safari fault brings Mesozoic Klamath Mountain rock adjacent to Umpqua Group units, offsetting the Tenmile Formation but not the White Tail Ridge Formation (Ryberg, 1984). The fault dips 70° SE to vertical and has a minimum 5 km right-lateral offset, based on offset of a late Mesozoic thrust fault and associated syncline, and variable reverse offset (Ryberg, 1984). The Wildlife Safari and Bonanza faults generally do not displace beds of the Camas Valley and Tyee formations, restricting their age to about 52 Ma (Ryu and others, 1996).

The near vertical Canyonville fault offsets rocks of the Klamath Mountains at least 30 km in a right-lateral sense. This estimate is based on offset of the intersection of the contact between Riddle and Day Creek Formations with a syncline affecting both units (Ryberg, 1984). Gentle folds in the White Tail Ridge Formation are also offset but to a lesser degree suggesting multiple episodes of movement on the fault (Ryberg, 1984). The Tyee Formation overlaps the fault in the central Coast Range (Baldwin, 1974).

Other faults in the subbasin vary in trend. The Cooper Creek Reservoir fault south of Umpqua has trend and motion similar to the Bonanza fault (Figure 1) (Ryu and others, 1996). It appears to offset the White Tail Ridge Formation, bringing turbidites of the undifferentiated Umpqua Group adjacent to and higher than the formation (Figure 1). West of the study area, faults border Woodruff Mountain. On

the northwest side of the mountain is a N-S trending normal fault, west-side down similar to the Tyee structural alignment (Figure 1). Southwest and southeast of the mountain, faults described by Perttu (1968) offset Bushnell Rock conglomerate, the southeast fault having motion similar to the Bonanza fault (Figure 1). Perttu (1968) also describes a possible fault in the core of the Oakland anticline north of Umpqua, where beds are slightly overturned.

Tectonic History

The rhythmically bedded sandstone and siltstone of the undifferentiated Umpqua Group consists of sequences of inner, middle, and outer submarine fan deposits, and basinal mudstone. Paleogeographic reconstruction of the Northwest done by Heller and others (Heller and others, 1987) has the Umpqua Group sediments being deposited during a phase of basin development between colliding oceanic islands along a continental margin. Coincident with basin development is uplift of the Klamath Mountains, major sediment source to the basins.

The oceanic islands, source of the Siletz River Volcanics, possibly formed over a hot spot or spreading ridge, or along a rifted continental margin. Geochemical analysis by Pyle (1988) indicating an oceanic volcanic setting favors a spreading ridge or hot spot interpretation. Palinspastic reconstruction by Heller and others (1987) to 55 Ma places the islands and basins offshore of a continental margin near the present Oregon-Idaho border (Figure 5).

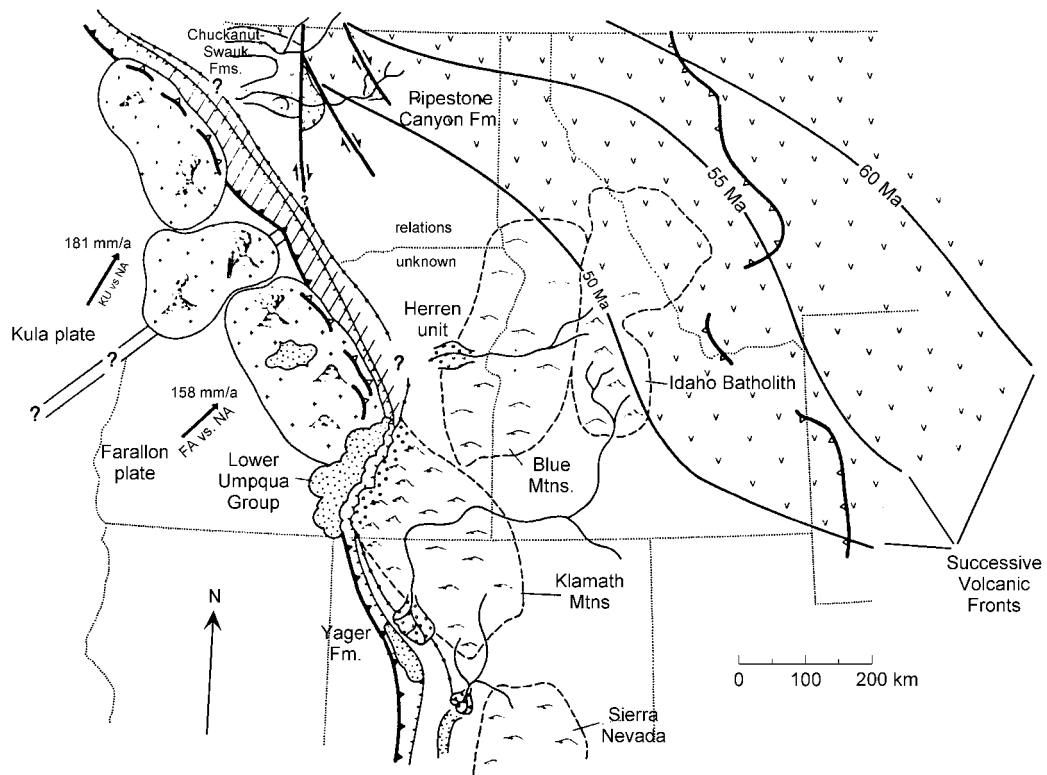


Figure 5. Paleogeographic reconstruction of the Pacific Northwest at 55 ± 5 Ma (after Heller and others, 1987, Fig. 5).

The islands and intervening Umpqua basin were accreted and possibly partially subducted as the oceanic plate collided with the North American plate at the margin of the Klamath Mountain terrane. Continuing uplift and erosion of the Klamaths provided sediment to the basins surrounding the volcanic highs. The exact nature of the suture zone between the Umpqua Group and Klamath Mountains is still being investigated to determine if significant thrusting accompanied accretion or there is a more abrupt juxtaposition along the Wildlife Safari fault (Ryu and others, 1996).

Based on tight folding of the Umpqua Group being confined below the White Tail Ridge Formation, and the Tyee Formation having a N-S structural lineament, Ryberg (1984) constrained major faulting and folding of the Umpqua Group to the early Eocene. The change in deformation style within the Umpqua Group is thought to signal a jump in the subduction zone to its current location west of the Coast Range in late early Eocene and a change to N-S structural alignment in the forearc basin. Subsequent subsidence of the forearc basin allows for the great areal extent and thickness of the Tyee Formation with major provenance in the Idaho batholith (Heller and Ryberg, 1983).

By 40 Ma pre-Basin and Range extension had begun in Idaho, Washington, western Montana, and Oregon causing westward displacement of the Klamaths, accreted islands, and basins. Possibly coupled with extension is some clockwise rotation of these units with additional rotation attributed to dextral shear between the continental and oceanic plates (Wells and Heller, 1988). Paleomagnetism studies indicate the lower Umpqua Group rotated clockwise about 70° (Magill and Cox, 1980). Rotation of the Klamath Mountain terranes is 110° to 40° in older to younger terranes, respectively, extending from the Paleozoic Devonian to the Cenozoic (Irwin and Mankinen, 1998).

Superimposed on the NE-SW structural trends paralleling the Klamath-Umpqua suture zone are N-S and NW-SE trends (Ryu and others, 1996). Major manifestations of the N-S trend are the Oregon Coast Range and the Tyee forearc

basin. Some reactivation of the older NE trending faults is possible during this E-W extension (Ryu and others, 1996). The NW-SE structure is displayed in normal faults and structural culminations of the NE trending anticlines recently described by Ryu and others (1996).

Geologic Setting of the Study Area

The folds of the study area are in sandstone dominated turbidites (Tuss), above a thin mudstone unit (Tum) of the undifferentiated Umpqua Group (Figure 1). The mudstone overlies another sandstone dominated turbidite unit (Tuss) immediately to the north. In the riverbed 120 m to the north, stratigraphically below the mudstone unit, plane parallel sandstone beds up to 1 m thick (Tuss), dip about 30° S (Figure 1). Along the road above, sandstone beds are oriented 110°/05° S, then abruptly change orientation to 050°/42° SE at the contact with the mudstone unit to the south.

Stratigraphically above the study area unit are mudstone dominated turbidites (Tums) (Figure 1). The undifferentiated units crop out between the Bonanza fault zone and the Cooper Creek fault, a distance of 3 to 4 km. The White Tail Ridge Formation, exposed north of the Cooper Creek fault and south of Woodruff Mountain; and the Bushnell Rock Formation, exposed in the Bonanza fault zone, are both near their northward terminus for this longitude (Molenaar, 1985).

A NW-SE cross-section through the study area connecting well #8 and section 23 of the fence diagram (Figure 4), shows the relative position of the study area strata on the south-dipping limb of the Oakland anticline (Figure 6). The cross-section extends from the Camas Valley Formation (uppermost unit of the Umpqua Group) exposed north of Umpqua to Siletz River Volcanics exposed near Roseburg. In constructing the cross-section, two essential elements were addressed, the regional dip of the Oakland anticline and the throw on the Cooper Creek Reservoir fault.

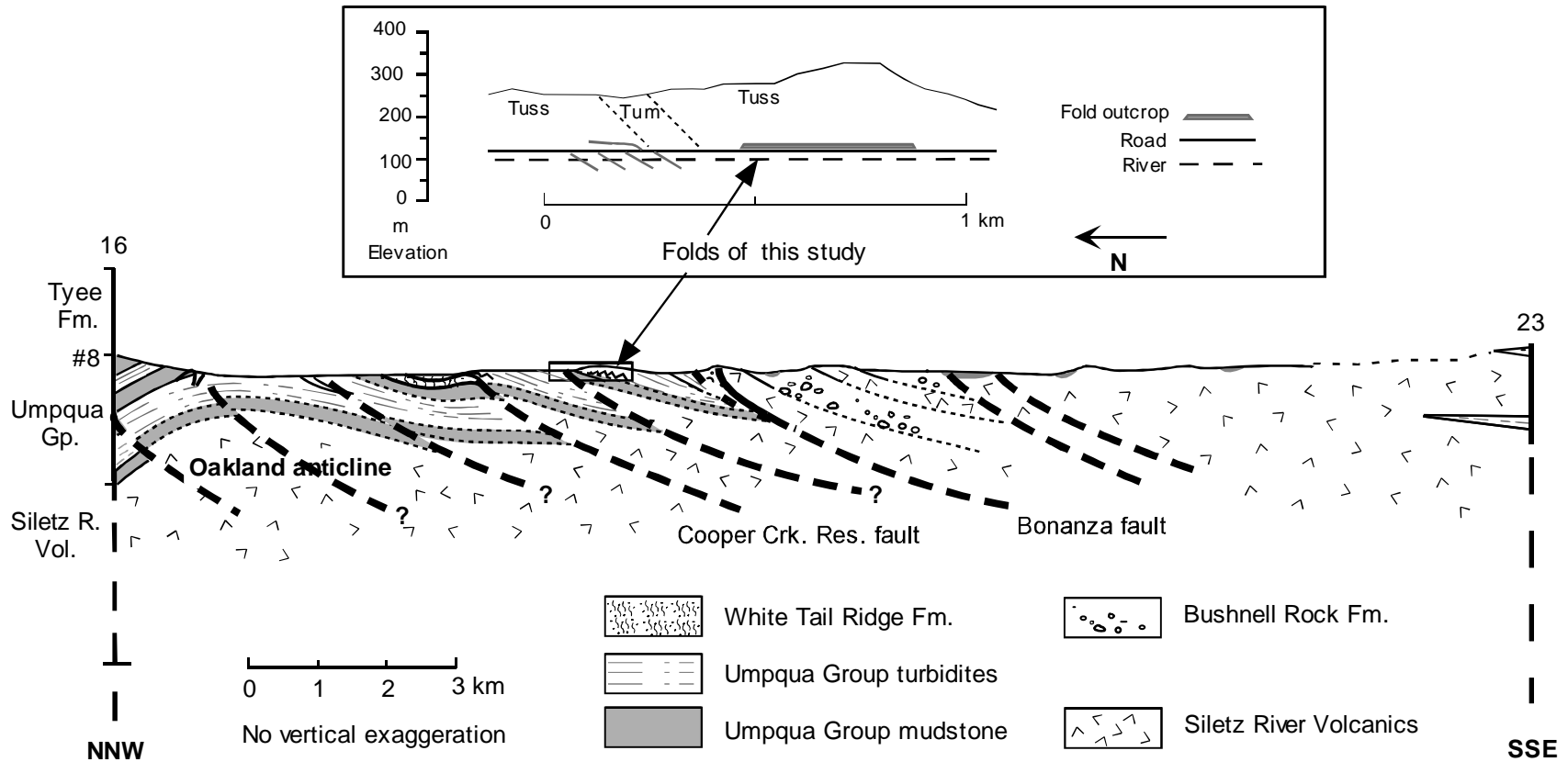


Figure 6. Cross-section of Sutherlin subbasin through study area. Cross-section is from fence diagram section 16 northwest of Umpqua to section 23 near Roseburg (Figure 4), normal to the regional trend of the Oakland anticline. Bedding dip is the general trend of the beds on the Oakland anticline. Local variations, mainly at mudstone contacts, are shown as an overlay to the regional trend. Displacement on the Cooper Creek Reservoir fault has the lower, thick turbidite section brought to the surface to meet unit thickness requirement. The unit containing the outcrop may be a repeat of the lower turbidite unit, also mapped as Tuss (Figure 1). (Perttu, 1968; Ryberg, 1984; Ryu and others, 1992; Ryu and others, 1996, Wells, 1998). The upper cross-section shows the spatial relationship of the outcrop and units to the south, and the exposure in the River. The topographic profile shows the local maximum elevation of outcrop unit, Tuss, 240 m to the east.

The regional dip is assumed to be 15° to 30° , based on data beyond areas of local deformation. The areas of local deformation ignored for the base drawing are the vertical beds immediately north of the anticline, a zone of more steeply dipping beds south of the Oakland anticline, vertical beds and small folds near the Cooper Creek Reservoir fault. The regional trend extends east of Sutherlin where Wells (1934) describes Umpqua Group strata as dipping 20° to 65° SE with an average of 30° , except for small areas of complex structure. Throw on the Cooper Creek Reservoir fault is taken to meet the need of the map distance of the turbidite unit south of the Cooper Creek Reservoir fault. The required thickness matches well with the lower turbidite unit at well #8. Offset on faults nearer the core of the Oakland anticline is relatively small to match the possible offset seen in the well.

An upper limit estimate of the thickness of the undifferentiated units exposed between the Bonanza fault and Cooper Creek fault (Figure 1) is 1600 m (Figure 7) using the geologic units of Figure 1 and average bedding dip. Including the White Tail Ridge Formation above the undifferentiated units totals 2000 m. Maximum thickness of the Umpqua Group sediments in the Sutherlin area was estimated by Ryberg (1984) at 2700 m and Baldwin (1980) at 2400 m. In the Umpqua area, Perttu and Benson (1980) estimated 1460 m, with a muddier section along Calapooya Creek of 760 m and a sandy unit forming the hills to the south of 700 m. Using two turbidite units as in well #8 of the fence diagram, the thickness estimate of the Umpqua Group in the Umpqua area is about 1600 m (Figure 7).

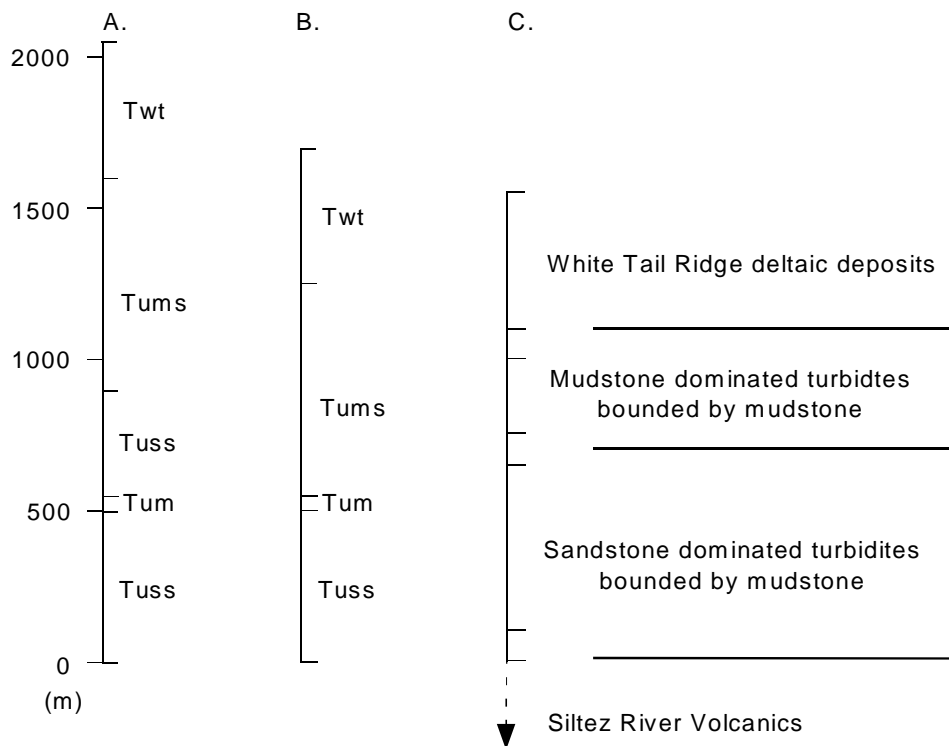


Figure 7. Estimated thickness of Umpqua Group units in the study area. A. Thickness of units is based on average dip and map distance the unit is exposed without consideration of folding. See Appendix A for detail. B. For comparison, column B is the same as column A but with duplication of unit Tuss removed. C. Thickness of units is based on using two turbidite units as in well #8 of the fence diagram (Figure 4).

Methods

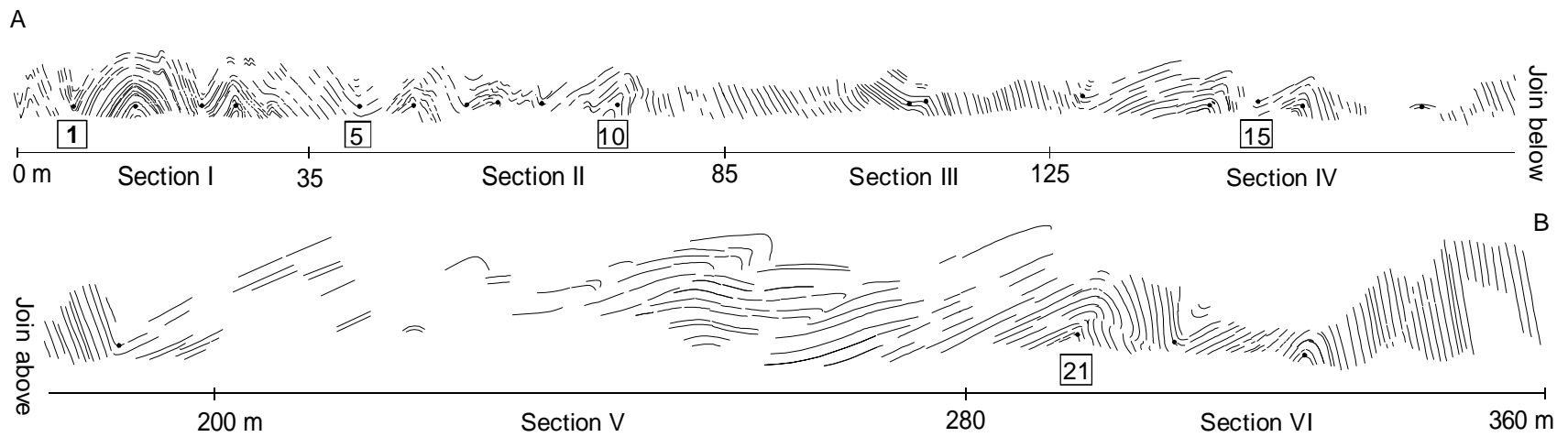
A measured section of the beds comprising the folds of the study area, a survey of control points, and three areas of detailed mapping form the basis for the description and analysis in this study. For ease of reference, the beds are divided into six sections, north to south (younging direction), according to fold form and exposure (Figure 8).

The thickness of beds exposed in the study area was measured or estimated as appropriate for the various levels of exposure:

- a) Sandstone and shale layers of accessible beds greater than 10 cm thickness were measured individually.
- b) Intervals of thinner intervening beds were measured as a whole, denoting the number of beds, and estimating the sandstone to shale ratio.
- c) Thickness of inaccessible and variably covered sections was estimated using road distance and general strike and dip of adjacent beds.

Beds were traced through folded sections if feasible. Where beds disappeared beyond visible access, they were traced one limb to another by reference to distinctive packages of beds. Distinction was based on a combination of factors including patterns of bed thickness, layering or separation tendencies in some beds, calcareous layers and boudins, and relative resistance of beds.

N-S cross-section of folds, no vertical exaggeration



Map view of hinge survey points

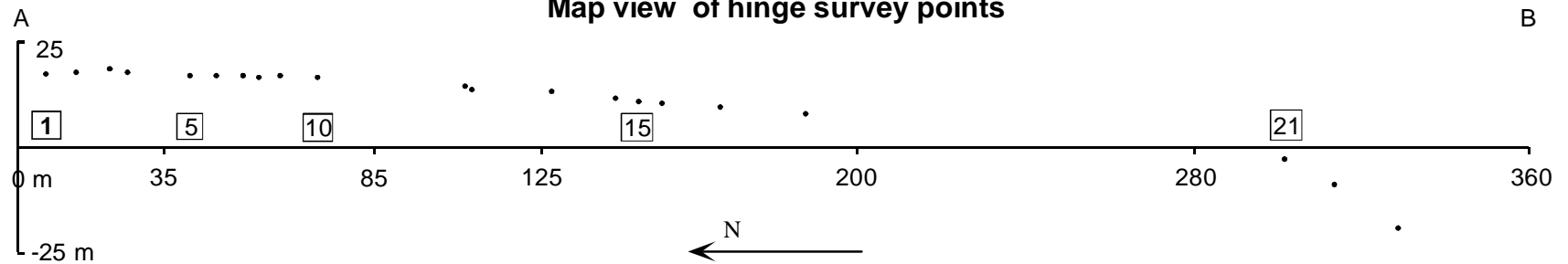


Figure 8. N-S cross-section of folds with axial survey points, and map view of axial survey points. Hinges number 1 to 18 in Sections I to IV and 21 to 23 in Section VI. Appendix C has a set of photographs of the outcrop.

Beds, joints, and faults in the folds of Sections I, III, and VI (Figure 8) were mapped in more detail in the field, at a scale of approximately 1:25 onto 11"x18" photographs. Photography was done with a 50 mm lens mounted on a 35 mm SLR camera. Prior to photography, three nonlinear control points per photo area were flagged on the outcrop along with hinges of folds and camera locations. The flagged points, hinges, and camera locations were then surveyed with a total station. Coordinates of surveyed points were used to determine distances between points and as a basis for removing photographic distortion.

Outcrop Observations

The interbedded sandstone and shale layers of the study area folded into predominantly asymmetric chevron-like folds, accompanied by a symmetric concentric-like fold, and kink-like folds (Figure 8). Folded turbidite beds are also exposed in the bed of the Umpqua River 20 m below the outcrop and downstream to the southeast. In the riverbed 120 m north, stratigraphically below the mudstone unit, Tum, (Figure 1), plane-parallel sandstone beds (Tuss) up to 1 m thick, dip 30° S. Above along the road, sandstone beds exposed for 90 m abruptly change orientation from $110^{\circ}/05^{\circ}$ S to $050^{\circ}/42^{\circ}$ SE at the mudstone contact (Figure 6). Areas to the east are covered.

The exposure of folds is approximately 360 meters long and normal to the fold axes. With plunge of the folds ranging from 2° to 34° west and east, much of the outcrop is close to a down plunge view giving an undistorted view of the folds. Total measured thickness of layers in the outcrop is about 110 m assuming little duplication in covered areas (Figure 9).

Bedding

Bedding relationships (thickness and contrasts in material properties) are extremely important factors in folding. Plane parallel and laterally continuous beds dominate the exposure. The occasional lenticular bed and pinchout in Section I of the outcrop are exceptions. Where bed thickness does vary, the bed is frequently adjacent to a calcareous layer.

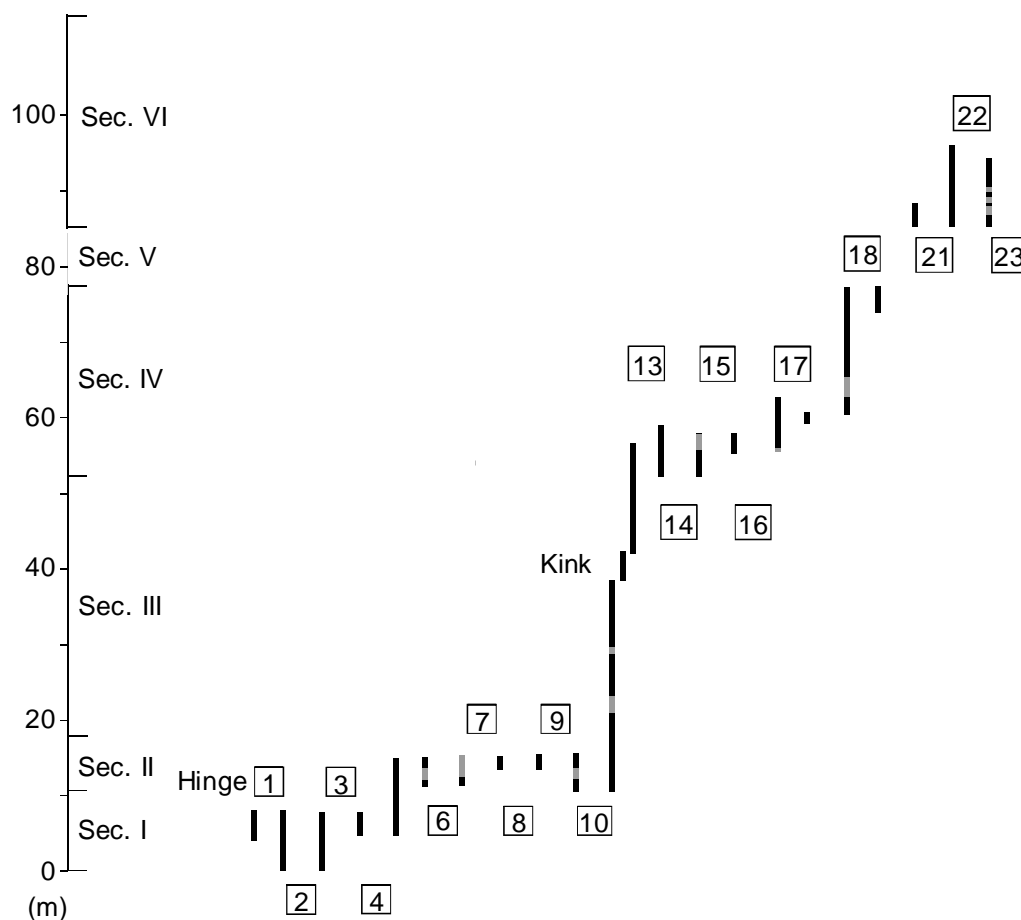


Figure 9. Schematic showing thickness of measured fold limbs from north to south. Gray intervals on columns are covered. The scale at left is not meant to portray a continuous vertical section because of covered areas or unrecognized repetition. See Appendix B for detailed stratigraphic sections.

Arenaceous layers in the outcrop are massive to graded with medium to fine grained lithic sandstone. In the classification scheme of Mutti and Ricci Lucchi (1972) the beds can be classified as turbidites, fitting somewhere between type *C*, an arenaceous-pelitic facies, and type *D*, a pelitic-arenaceous facies (Mutti and Ricci Lucchi, 1972). Bed thickness is less than the range 50 to 159 cm for facies *C* classification but the sandstone/shale ratio is greater than the facies *D* norm of 1:2 to

1:9 (Table 1). These facies imply deposition beyond the distributary system in an outer fan to basin plane setting.

The turbidite beds are up to 70 cm thick with an average of 11 cm. Average thickness increases up section, decreases slightly, then increases again (Table 1).

Within this framework, bed thickness is mostly random with minor fining or thickening up sequences of 3 to 5 beds. Average sandstone to shale ratios in the sections varies from 3.9 to 3, but not directly with average thickness.

Table 1. A summary by section of bed thickness and sandstone to shale ratios. Data used are from representative sequences of beds making up the folds in a section.

Section	Applicable section thickness (m)	Turbidite average thickness (cm)	Sandstone thickness maximum (cm)	Sandstone average thickness (cm)	SS : Shale average of ratios
VI	20	11.7	49	8.1	3.5
IV	28	10.6	32	7.9	3.7
III	36	14.1	60	10.5	3.9
II	8	10.5	58	9.8	3.0
I	10	6.7	31	4.5	3.9

Current structures vary from north to southeast, though Perttu and Benson (1980) determined the dominant paleoflow direction is from the east in the lower Umpqua Group and from the south in the middle and upper Umpqua. Paleoflow in Umpqua Group sections measured by Ryberg (1984) in the Sutherlin area is 150° to

210°. In the classification scheme of Bouma (1962), most beds are an *ae* layer sequence with *b*, *c*, and *d* absent. (The five divisions of the Bouma sequence are from the bottom, *a*: massive to graded sandstone, *b*: sandy parallel laminations, *c*: rippled or convoluted bed, *d*: laminations of silt and mud, *e*: mudstone.) Other beds are *abae*, *ce*, and *ace* layer sequences.

Sharp basal and upper contacts characterize most of the beds in the outcrop. Deformation of the planar bed form occurs adjacent to several deeply weathered brecciated shale zones in Sections II, IV, and VI, where beds have a convoluted, wavy appearance (Figure 10). Some beds are also deformed into duplex-like structures (Figure 11), similar in form though not in shear sense, to the flexural slip duplexes described by Tanner (1992).

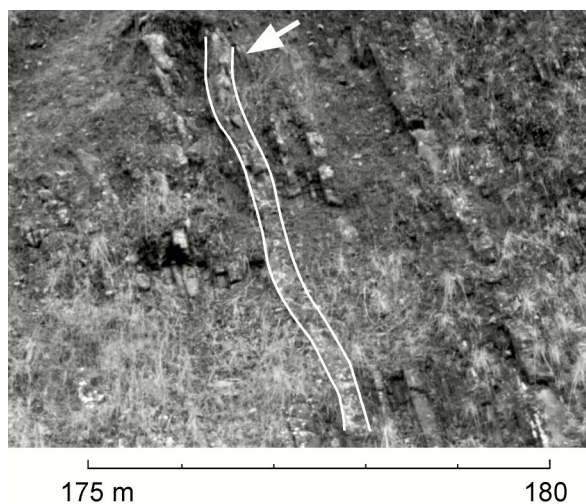


Figure 10. Bed deformed into low-amplitude sine wave with wavelength of about two meters. Immediately below and 1 m above the deformed bed are weathered shale layers. The bed is on the steep limb of fold 18, the south syncline of Section IV. Scale indicates position in outcrop.

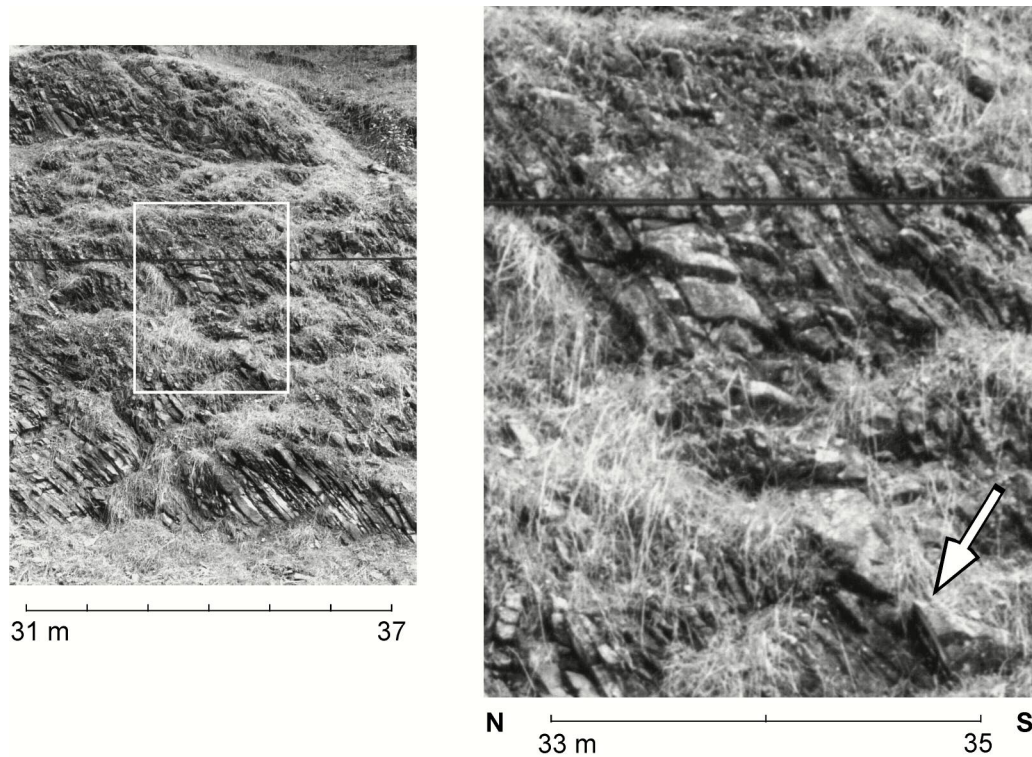


Figure 11. Duplex-like feature. The beds at boundary of Sections I and II (Figure 13) have top-to-the-south sense of layer-parallel shear. The feature appears highly localized, diminishing upward in the exposure and absent at the base of the outcrop. Below the exposed duplex-type feature, the thicker bed is offset in a top-to-the-north sense (arrow).

Deformation of bed form by boudinage is localized in most but not all calcareous layers in the outcrop. Boudins occur on long and short limbs and in at least one hinge. Spacing of the calcareous layers varies from 0.5 to 2 m in Section I, and 1.5 to 3 m in Section VI, a ratio similar to the 0.6 ratio of average bed thickness for the sections (Table 1). The aspect ratio of measured boudins varies from 0.2 to 0.7 with an average of 0.3. Imbrication of boudins occurs at two locations, at another location, boudins are caught up in the hinge of a fold. The sandstone bed closest to the

calcareous boudins and layers is frequently conspicuously jointed or thickened, with thickening up to 100 percent over a distance of 3 to 4 meters.

Fractures

Jointing in sandstone layers is typically 1 to 2 times layer thickness but varies considerably, with closer jointing in zones associated with nearby faults or bed movement. Veins or secondary mineralization are rare. A thin layer of calcite partially covers a small fracture in Section I and several hairline veins were found in Section VI. Calcite or quartz slickenfibers in flexural slip movement horizons (Tanner, 1989) are also not evident. Shale layers are highly jointed with spacing generally less than layer thickness.

Faulting in the outcrop is common with thrusts across single beds, multiple beds, and limbs. Much of the faulting is at low angle to bedding and consistent with layer-parallel shortening, though occasional higher angle faults cut through hinges or across a fold limb. Ramp faults duplicate beds, producing about five meter displacements in several folds, without preference for north or south-dipping limbs. Where thicker sandstone beds yield in the hinges, thinner beds below commonly repeat by thrusting in the hinge in a top-to-the-south sense.

In the asymmetric chevron-like folds of the outcrop, beds on long limbs are repeatedly thrust in a top-to-the-south sense. Faulting in the kink-like fold is consistent with layer-parallel shortening and flexural slip. Steeply dipping beds bordering the kink-like fold have faults consistent with layer-parallel shortening and

with post folding sub-horizontal compression. Faults that are high angle to bedding are mainly confined to Section I, extending across a limb of each fold.

Fold Form

Fold forms vary north to south, from a symmetric concentric-like fold in Section I, asymmetric chevron-like folds in Section II, a kink-like fold in Section III, to asymmetric chevron-like folds in Sections IV and VI (Figure 8). Asymmetry of the folds, defined by $(\lambda_L - \lambda_R) / (\lambda_L + \lambda_R)$ (Figure 12), varies from -0.4 in Section I to near one in Section IV (Table 2).

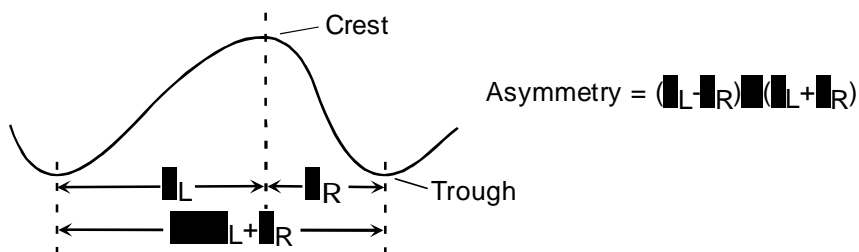


Figure 12. Asymmetry of folds defined.

The concentric-like fold has a broad anticline bordered by narrow synclines. Chevron-like folds have straight limbs and interlimb angles of 45° to 90° . Wavelengths are 9 to 28 m, amplitudes 3 to 7 m, both greatest in Section VI (Table 2). The kink and asymmetric chevron-like folds have top-to-the-south sense of layer-parallel shear. Plunge of the folds is mainly less than 20° with an average of 13° , and the outcrop face has a slope of 75° to 80° . So much of the outcrop is close to a down plunge view providing a relatively undistorted view of the folds.

Table 2. Summary of fold form by section (Figure 8). Because of cover, values for Sections II and IV are based only on axis position and gross fold form without tracing bedding from one axis to another. The average plunge for Section II is calculated separately for east and west plunging folds.

Sec.	Wavelength (m)	Amplitude (m)	Asymmetry $(\lambda_L - \lambda_R) / (\lambda_L + \lambda_R)$	Average plunge	Wavelength: amplitude ratio
VI	28	7	0.5	20° E	4
IV	11 to 20	3 to 7	0.5 to 1	3° W	3.2
III	(Kink)	N/A	N/A	3° W	N/A
II	9 to 14	3 to 4	-0.1 to 0.7	27° E 20° W	3 to 3.5
I	12 to 16	3 to 5	-0.4 to 0.1	17° E	3.1 to 4

Section I

Bed Form

Thickness of beds varies considerably in zones of Section I. Beds pinch out from the top and bottom on the far north and south of fold 2 (folds are numbered just above the horizontal scale), roughly symmetric to the fold axis, at the 7 to 8 m and 21 to 22 m marks on baseline (Figure 13). On the south limb of fold 2, a bed coming down from the kink-like fold at 17 m thickens then thins again at the base of the exposure. Beds on the north-dipping limb of fold 3 are thicker than those of the adjacent south-dipping limbs (Figure 14). Thicker beds extending into the core of fold 4 become lenticular or deformed with variable thickness (Figure 14).

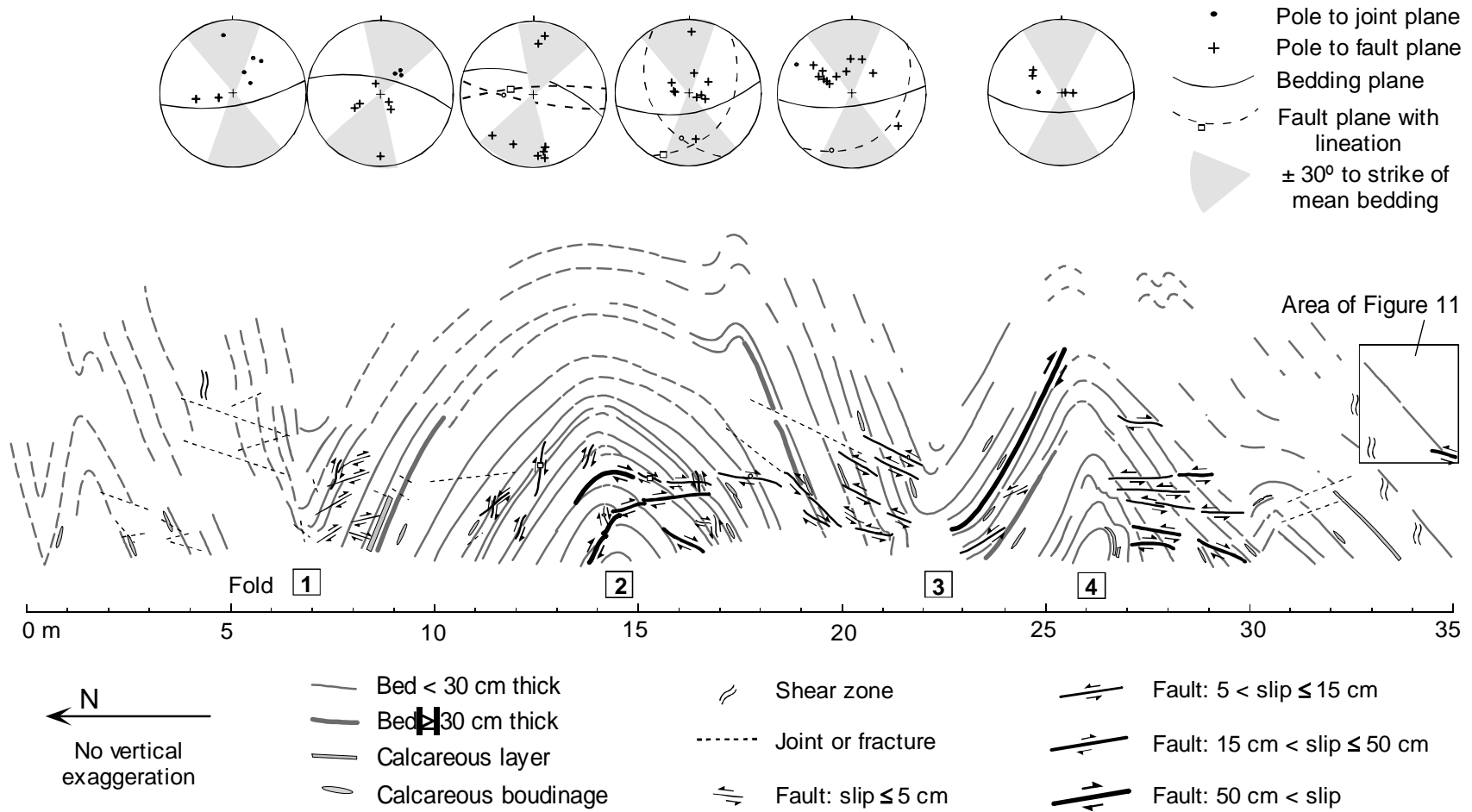


Figure 13. Section I folds. Symmetric concentric-like fold bordered by chevron-like folds. Thrust faults are scattered throughout the section, but dominate the north limb of fold 2. Sub-horizontal faults cross a limb of each fold. Stereonets above the cross-section show orientations of beds, measured faults and joints, and lineations on faults. Lineation symbols are also on the fault path in the cross-section.

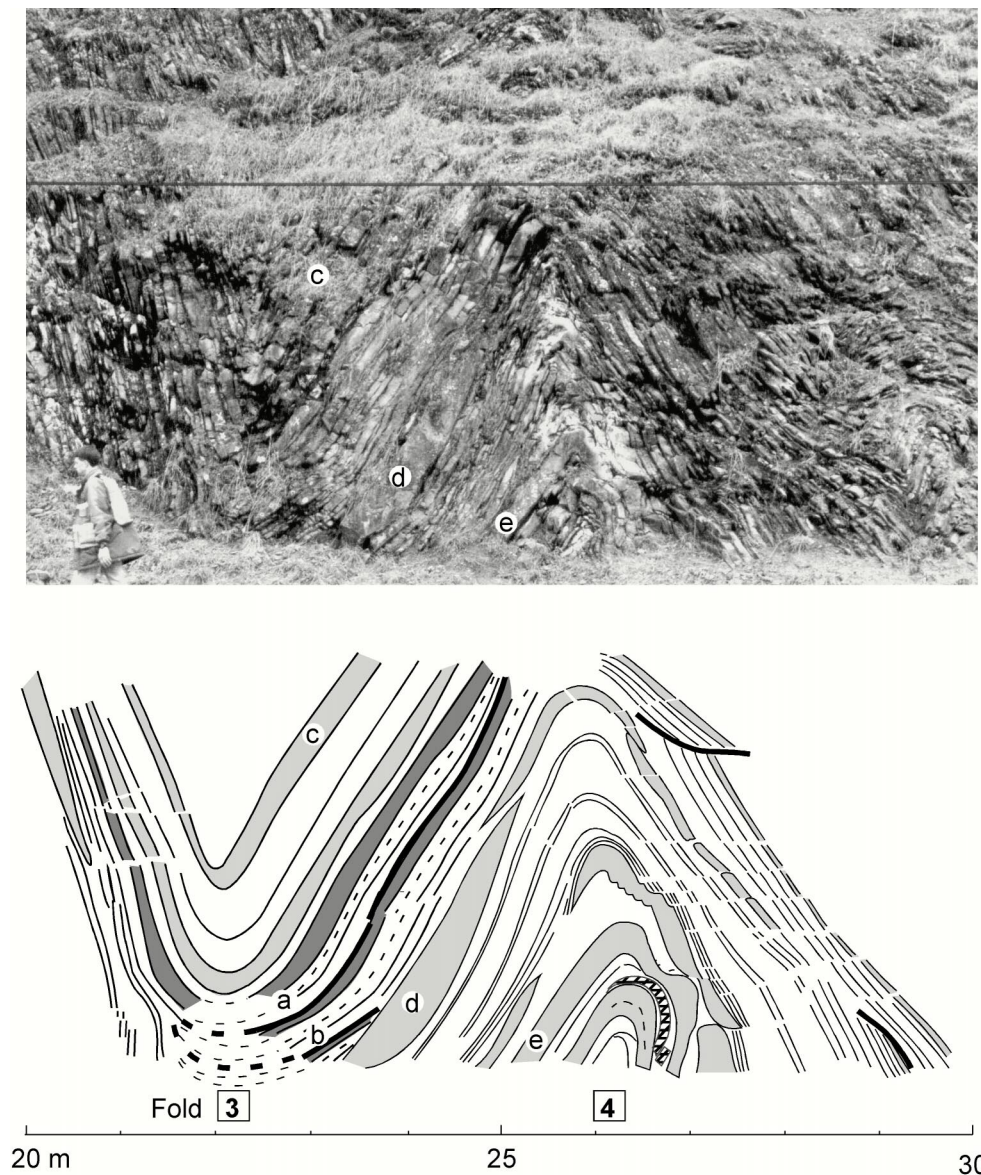


Figure 14. Folds 3 and 4 of Section I. Beds thicken on the north-dipping limb and in the core of fold 4. A set of beds is repeated the length of the north-dipping limb at the contact below *a* and again at *b*. On the south limb of fold 3 these beds are again faulted in a top-to-the-south sense at the top and base of exposure. Stepping offsets in south-dipping, thin beds of fold 4, show the effect of top-to-the-north faults that cut thin beds but indent a larger bed toward the fold interior. Top-to-the-north offset is also seen on the south-dipping limb of fold 3 at lower left and at mid-level. The hatched bed in the core of fold 4, a calcareous layer, appears to influence lateral motion of beds immediately to the south. *c*, *d*, and *e* are points of reference between the photograph and drawing. The black horizontal line crossing the photograph is an overhead wire.

At the south boundary of Section I, a thicker than average bed exhibits layer-parallel shortening with a top-to-the-south sense of shear in the form of duplex-like structures (Figure 11). The feature appears localized above an area of sheared beds to the south and above the kink-like fold south of hinge 4. At base of the outcrop, the duplex-like structures are not present.

Calcareous boudin layers spaced 0.5 to 2 m apart in the section, are more numerous in the limbs of fold 3 than fold 2 (Figure 13). On the south-dipping limb of fold 2 at 17 m, several boudins are thrust one onto another.

Fold Form

The folds of Section I are dominated by a longer wavelength concentric-like fold bordered by shorter wavelength chevron-like folds on each side (Figure 13). North of fold 1 at 0 to 5 m, the exposed chevron-like folds have shorter wavelength and lower amplitude. At the south end of the section, thinner beds are folded into a kink-like feature. A small asymmetric fold with the short limb facing north initiates on the south limb of the concentric-like fold and continues vertically into the upper layers.

Axial planes of the folds in Section I tilt up to 10° N (Figure 15). A bed followed through the section is constrained in an envelope narrowing to the south, with a medial axis dipping 12° S. A distinctive calcareous layer below the bed becomes boudinaged on the south-dipping limb of fold 2, and forms a smooth rounded arc in the core of fold 4 (Figure 14).

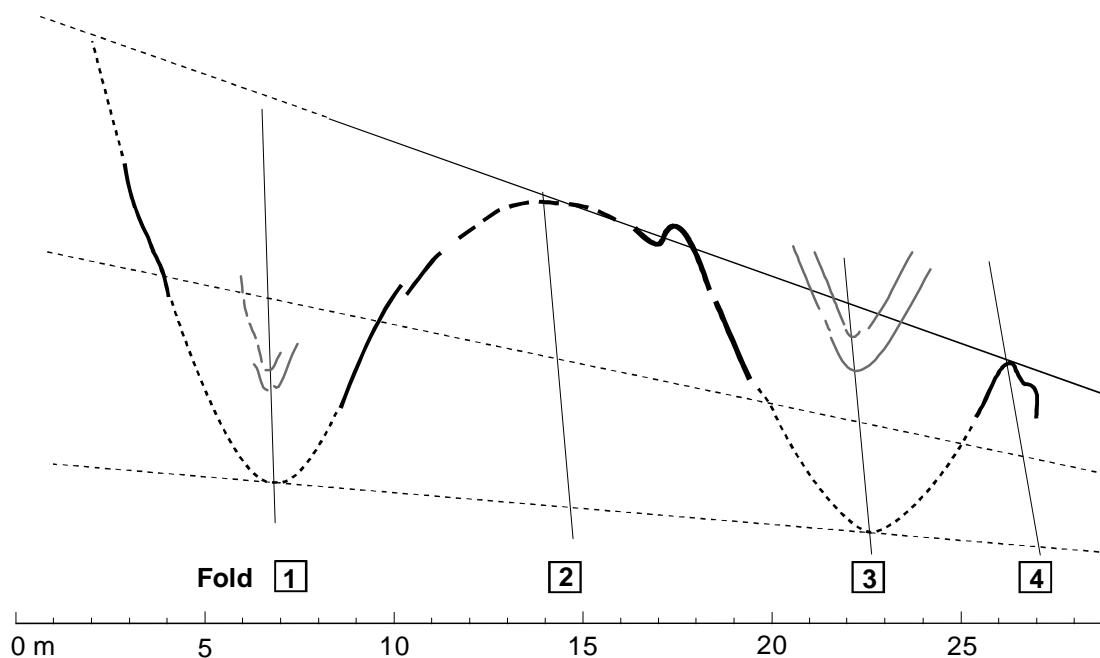


Figure 15. Envelopes of a bed traced through the folds of Section I. Axial planes tilt up to 10° N; the medial axis dips 12° S. Medial axis shortening is about 38 percent, a stretch of 0.62.

Fractures

Most faults of Section I are consistent with layer-parallel shortening. Low-angle thrusts cut beds on the south limb of fold 1 and both limbs of the concentric-like fold (Figure 13). The thrusts form classic wedges as described by Cloos (1961) at 11.5 m and 13.5 m. Thrusts across a set of thinner beds form an immature duplex type structure folded into fold 3 with apparent offset of 1.2 to 1.6 m on the upper thrust, 0.3 m on the lower (Figure 16). The 2.6 m spacing of the thrusts between beds *E* and *F* (Figure 16) is large for ramp spacing compared to the mature duplex structure as modeled by Cruikshank (1989). A thrust lower in the hinge of fold 2 crosses several beds and merges into a sub-horizontal fault cutting the south limb.

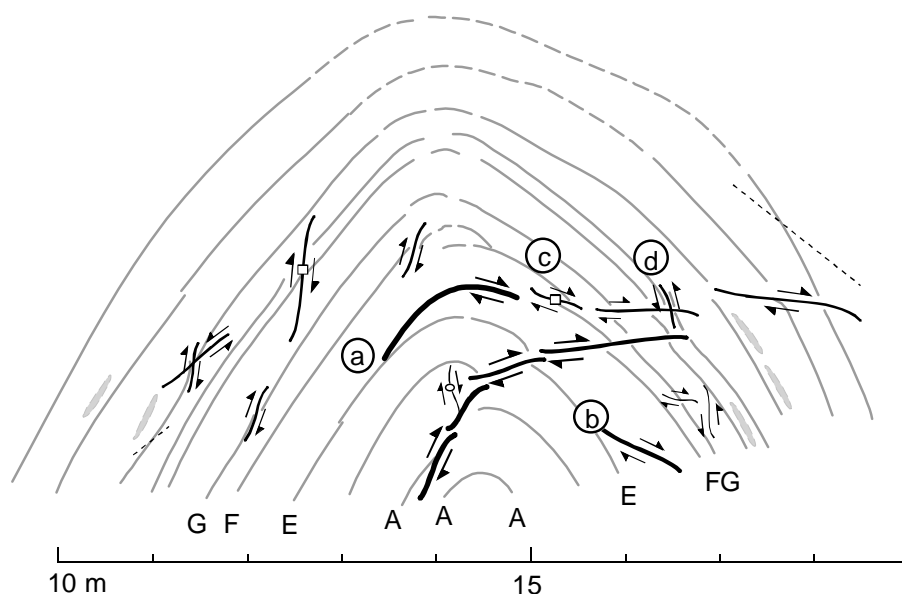
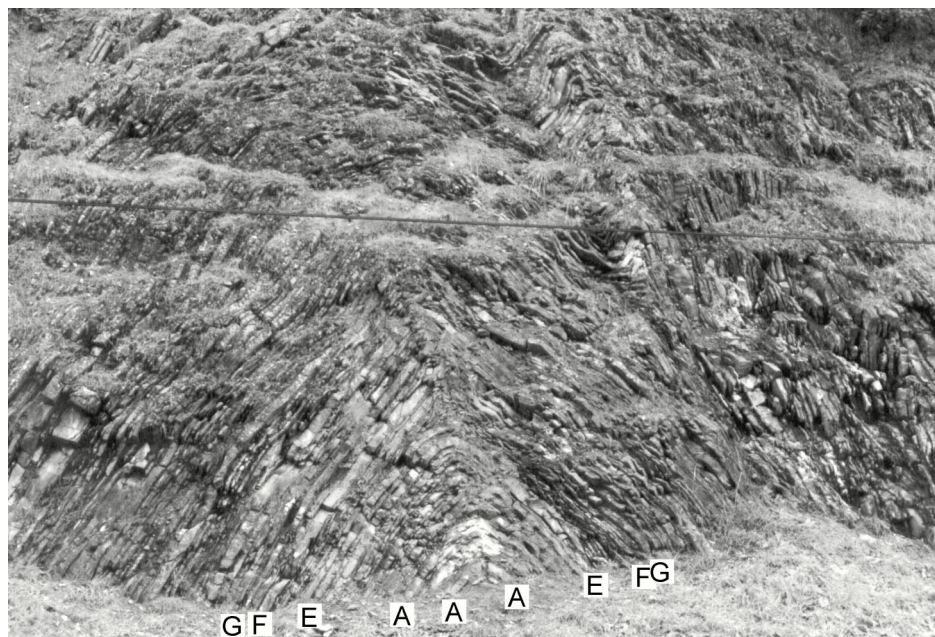


Figure 16. Bedding thrusts and sub-horizontal faults in the concentric-like fold of Section I. Thrusts at *a* and *b* cut across a set of eight thin beds between beds *E* and *F*. Spacing of the thrusts is 2.6 m. Displacement on the upper detachment from *a* to *c* is 1.6 m. The lower slip surface has 1.2 m offset. Bed *E* below the duplication, is 50 percent thicker from the hinge to point *b*. Bed *G* is thickened in the hinge and the area above *c*, above the thrust bed repetitions on *F*. At *c* the upper detachment joins a thrust on layer *F* and then cuts across the limb to the south. The upper cross-cutting fault, with offset of 4 to 6 cm, offsets a bedding thrust at *d*. Extending from a bedding thrust in the interior of the fold, the lower cross-cutting fault has offset up to 16 cm diminishing to the right. The bedding thrust in the core of the fold offsets bed *A* about one meter.

On the south-dipping limb of fold 4, a bedding parallel fault repeats several beds over the length of the limb with top-to-the-south offset (Figure 14). The same set of beds appears thrust again at the base of the hinge, in a top-to-the-north sense, though exposure is poor.

Faulting in the hinges of Section I is mainly confined to sets of thin beds duplicated with a top-to-the-south sense of offset. Thicker beds in fold 2, the concentric-like fold, show minor thickening in the hinge and are jointed just off the crest of the fold. Thicker beds in the core of folds 3 and 4 folded with little evidence of brittle fractures in the hinge, exhibiting a ductile response. Hinges in fold 1 appear compressed, too broken to determine evidence of hinge accommodation.

Removing bedding thrust faults from Figure 13 leaves the series of sub-horizontal faults as shown in Figure 17. The offsets indicated on the south limb of fold 1 may be due to rotation of joint-bounded blocks as limbs rotated in. The interlimb angle of fold 1 is 45° to 50° , which along with broken hinges, suggests continued lateral compression after folding.

The top-to-the-north faults cutting the south-dipping limbs of folds 3 and 4 are in a zone where the interlimb angle is also small, 50° to 55° (Figure 14). The top-to-the-north sub-horizontal faults on the south-dipping limbs of fold 4 cut sets of thinner beds that are offset into thicker adjacent beds. Offset on the faults is less than 10 cm. In the core of fold 4, the arch of a calcareous layer appears to control lateral motion at

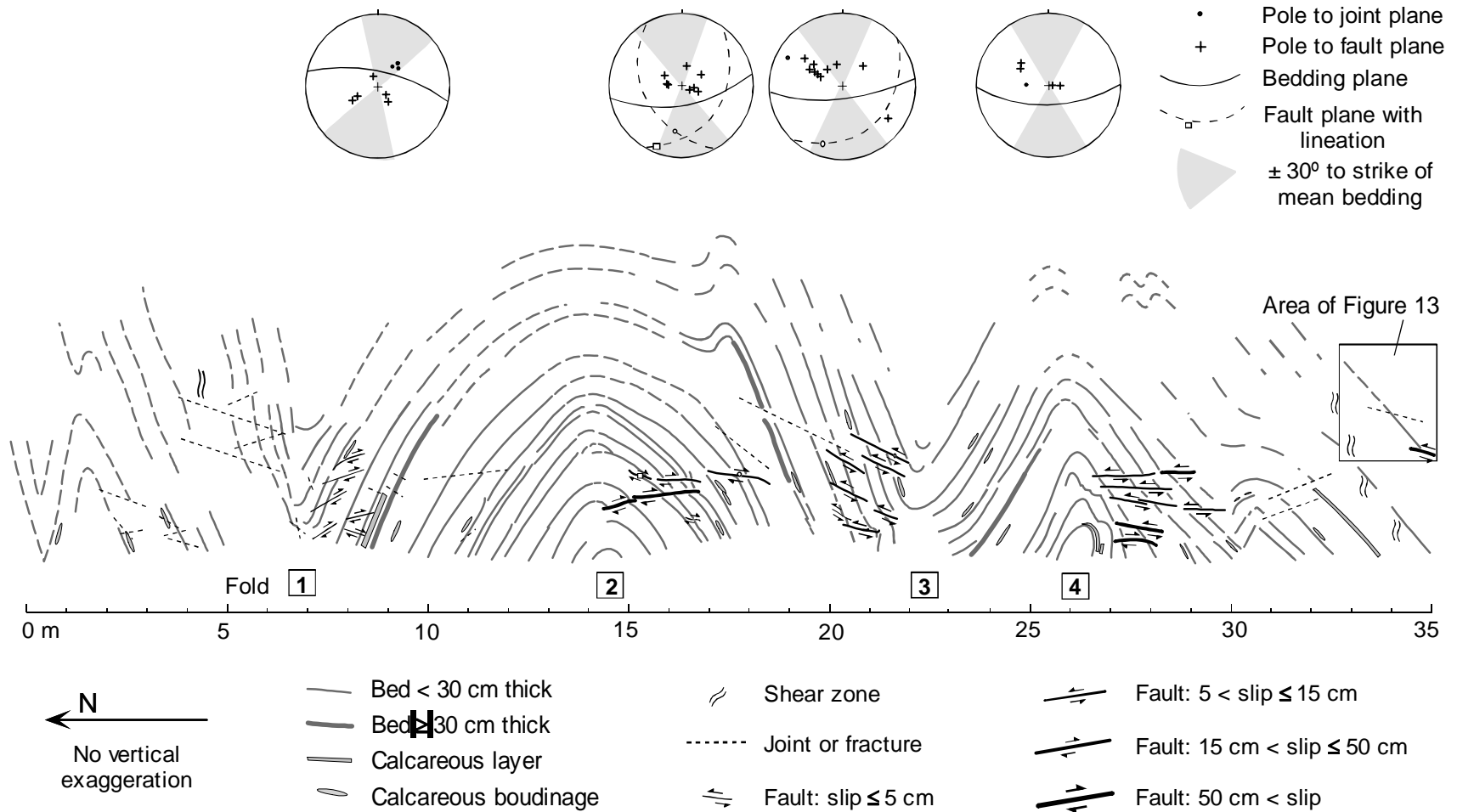


Figure 17. Section I folds and faults not at low angle to bedding. Removing bedding thrusts from Figure 11 leaves only sub-horizontal faults cutting across the south-dipping limbs of folds 2, 3, and 4, and the north-dipping limb of fold 1. These faults appear consistent with continued axial shortening and rotation of limbs, creating interlimb angles of less than 60° .

the base of the exposure (Figure 14). Immediately above, a bed bulges to the south, and thin beds are squeezed into space above and below the bulging thicker bed.

Differing from the pattern of sub-horizontal faults on the limbs of folds 1, 3, and 4 that are in vertical sequences, the faults on the south limb of fold 2 form a band of deformation (Figure 16). The band is bounded by upper and lower top-to-the-south faults extending from upper and lower bedding thrusts. These faults are compatible with continued N-S compression, either rotating existing joints, or faulting where the lateral motion is accommodated by space, weakness, or both.

Age relationships are suggested where the upper sub-horizontal fault cuts the bedding thrust at *d* (Figure 16), implying post-folding N-S compression, and where boudins are imbricated, implying layer-parallel compression after boudinage.

Section II

The fold form and symmetry in Section II is less certain due to poor exposure and variable wavelength (Figure 18). Larger folds have a wavelength 9 to 12 m. Fold form is chevron-like, short limb facing south, except possibly for some shorter wavelength folds which are partly covered. Asymmetry increases to the south. Fold 5 seems to have a small positive asymmetry; fold 10 has high positive asymmetry of 0.8 to 1. Similar to Section I, the folds appear to have a medial plane dipping toward the south. A shear zone at 82 m leads into the next section where steeply dipping beds bound a kink-like fold.

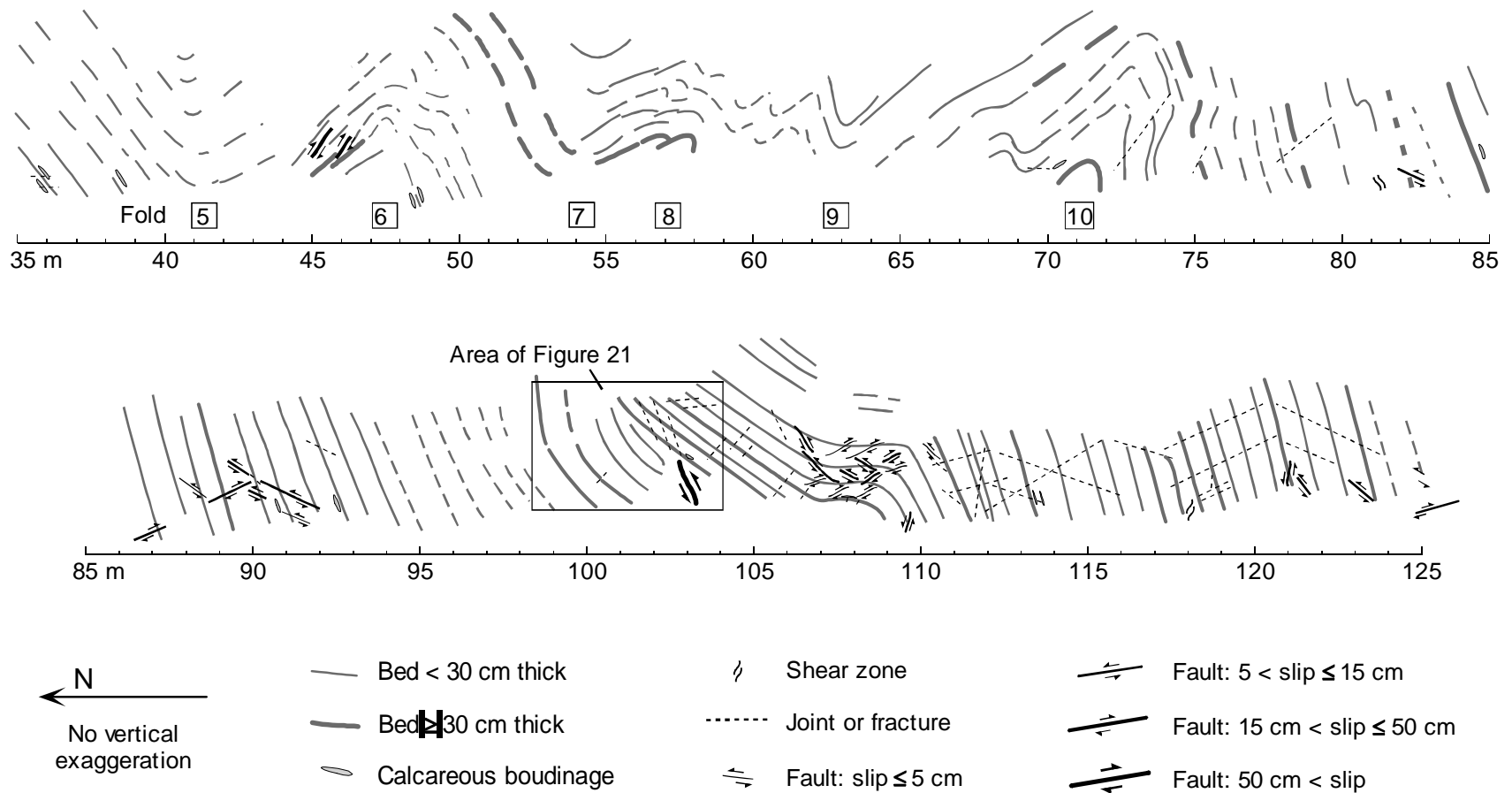


Figure 18. Section II and Section III folds. The asymmetric folds of Section II have bedding thrusts on long limbs and near vertical to overturned short limbs. Bedding is dominated by several 50 to 60 cm strong layers. Shorter wavelength folds are visible above the strong layers. Cover and deformation make it impossible to trace bedding through the section. Section III contains steeply dipping beds bordering a kink-like fold where faults are consistent with layer-parallel shortening. A conjugate fault pattern consistent with post-folding N-S compression is evident in the steeply dipping beds. Offset on these faults is minor, less than 15 cm.

Section III

Exposed between steeply dipping plane parallel beds, the kink-like fold of Section III (Figure 18) has short limb facing north. At 90, 115, and 121 m, steep south-dipping beds north and south of the kink-like fold are cut by conjugate faults consistent with post-folding sub-horizontal compression. Offset on these faults is minor, less than 15 cm. Brecciated shale layers bound the faulted zones.

Within the kink-like fold, beds thicken in the south hinge. This corresponds with the greater inter-limb angle of the hinge (Figure 19). Bed 4 thickens between the hinges where bed separations are duplicated by thrusting (Figure 20).

Variation in bedding interface in the kink-like fold is found above layers 1 and 3 (Figure 20) where 5 to 7 cm thick, soft, tan siltstone forms the upper contact at 102, 104.5, and 107.5 m. At the south end of the siltstone at *b* and *c* (Figure 20), a calcareous nodule is welded to the underlying sandstone (Figure 21). Layer 1 (Figure 20) below the nodule at *b* varies in thickness from 28 cm thick to the north, to 55 cm at the base of the exposure. Adjacent to the siltstone and nodules, bedding is more deformed than higher in the folds. Layer 4 has a bed separation or mechanical layering through both hinges that continues north to the area above *a* (Figure 20). Also above location *a*, the otherwise planar lower surface of layer 5 is rough immediately north of layer-parallel fracturing extending from a fault near the north hinge.

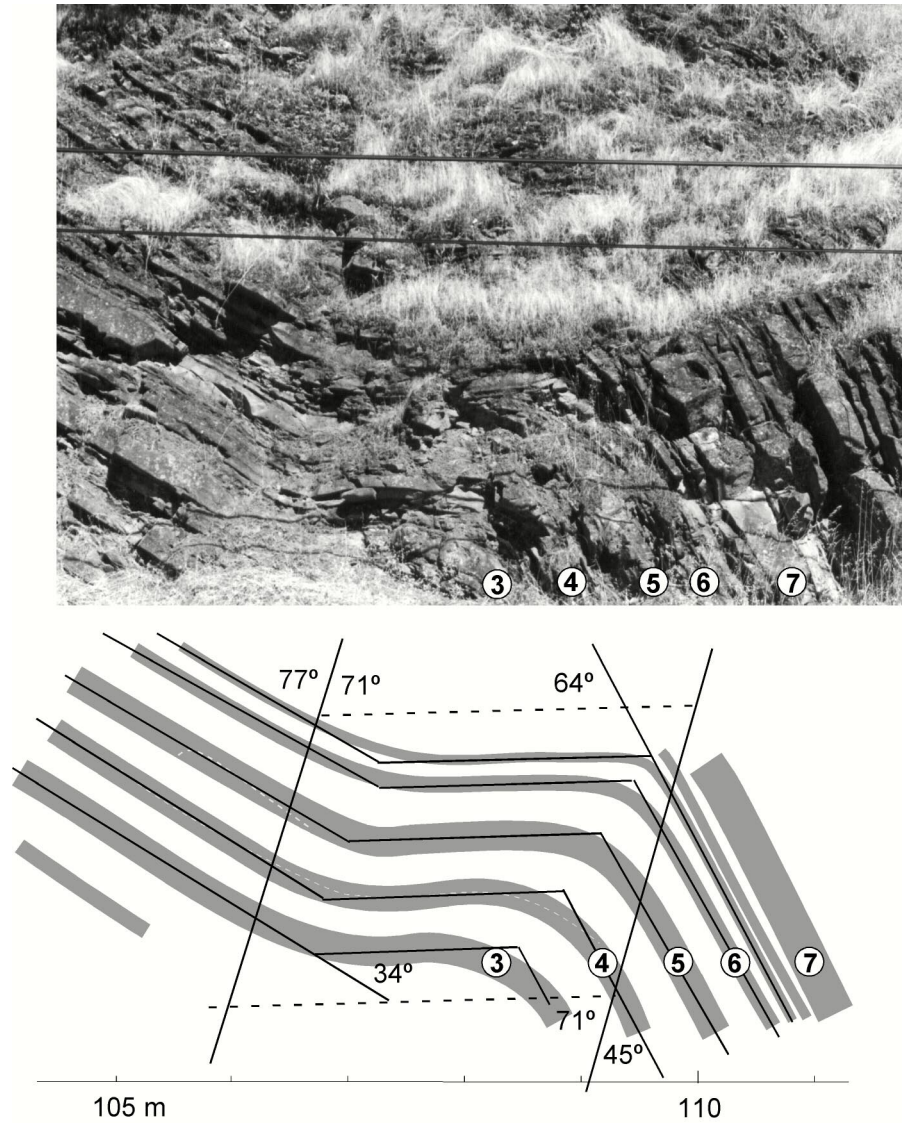


Figure 19. Idealized kink form imposed on schematic drawing of kink-like fold. Traces of the walls form angles of 77° and 44° with the layering outside the fold. The interior and exterior angles of 72° and 44° on the south limb of the fold reflects greater thickening on the south limb than on the north limb where interior and exterior angles are nearly equal.

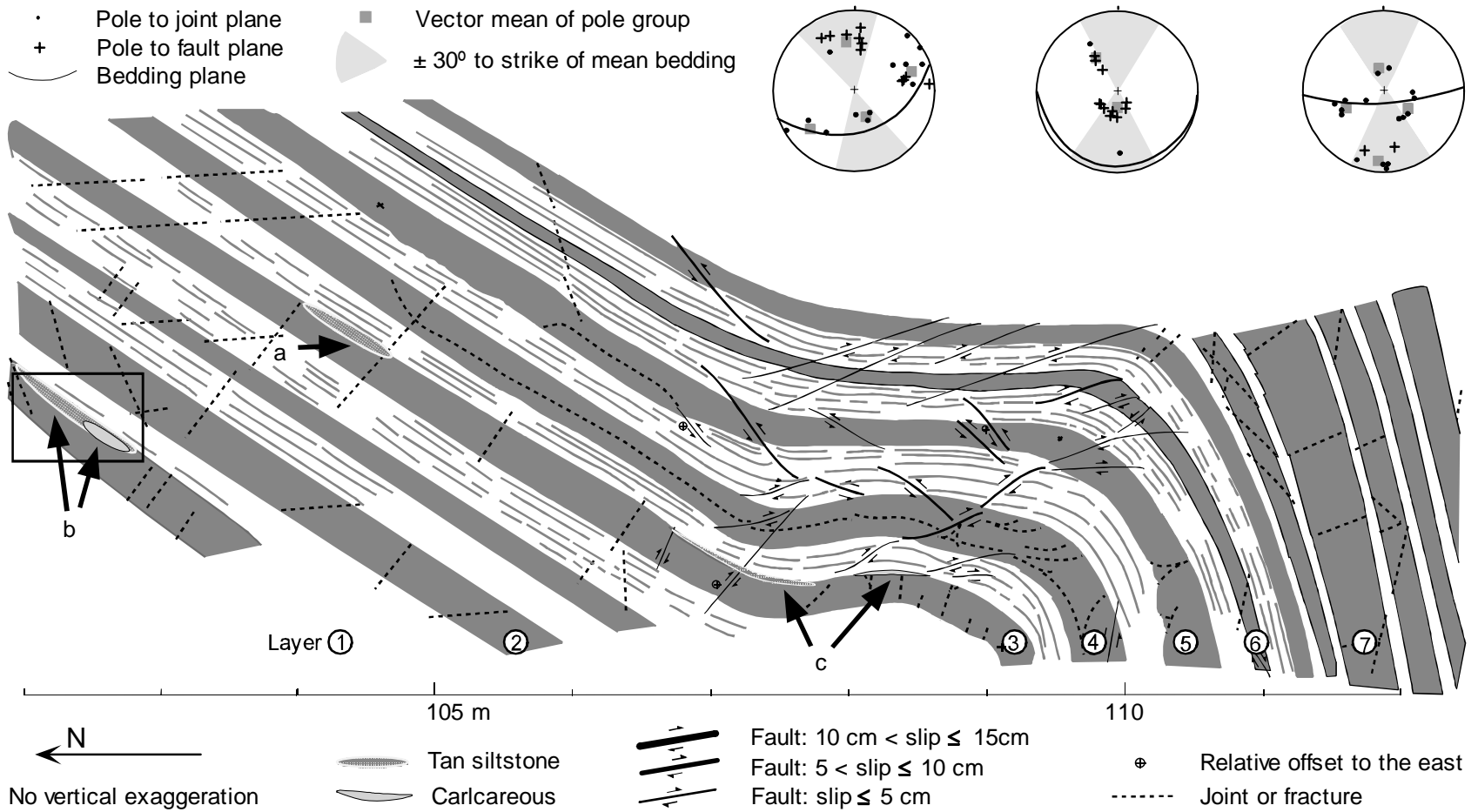


Figure 20. Fractures and contacts in kink-like fold. Thrust faults are consistent with layer-parallel and sub-horizontal shortening and have dip offset except where an E-W component is shown. Stereonets show poles to joint and fault planes are in the same cluster, perhaps an indication of faults with little movement, or faults that formed as joints but later moved. Soft, tan, siltstone 5 to 7 cm thick forms the upper contact of layer 1 at *b*, and of layer 3 at *a* and *c*. A calcareous nodule or layer is associated with the siltstone at *b* and *c*. Rectangle indicates area of Figure 21.



Figure 21. Tan siltstone and associated calcareous nodule at base of kink-like fold of Section III. Welded into sandstone bed, the nodule at *b2* is 8 by 29 cm with 5 cm of siltstone above. Tan siltstone layer, *b1*, extends 80 cm north of nodule. Pen (circled) is 13.5 cm long.

Faults in the kink-like fold are concentrated above layer 3 (Figure 20). Offset is predominantly dip slip and consistent with layer-parallel shortening. The greater offsets of 15 and 11 cm occur on the south-dipping faults through the north hinge. Most other faults have offset of 3 to 6 cm. Normal faults bound a small block on layer 6 just below the south hinge.

Immediately below the main exposure of the kink-like fold, is a fault zone at low-angle to bedding (Figure 22). Poles of a fault plane and fractures above the zone lie in the NW quadrant of the stereonet plot (Figure 20), consistent with layer-parallel

shortening. Several meters below the fault are two thick 35 cm beds. Areas above and to the north of the thick curved beds are covered.

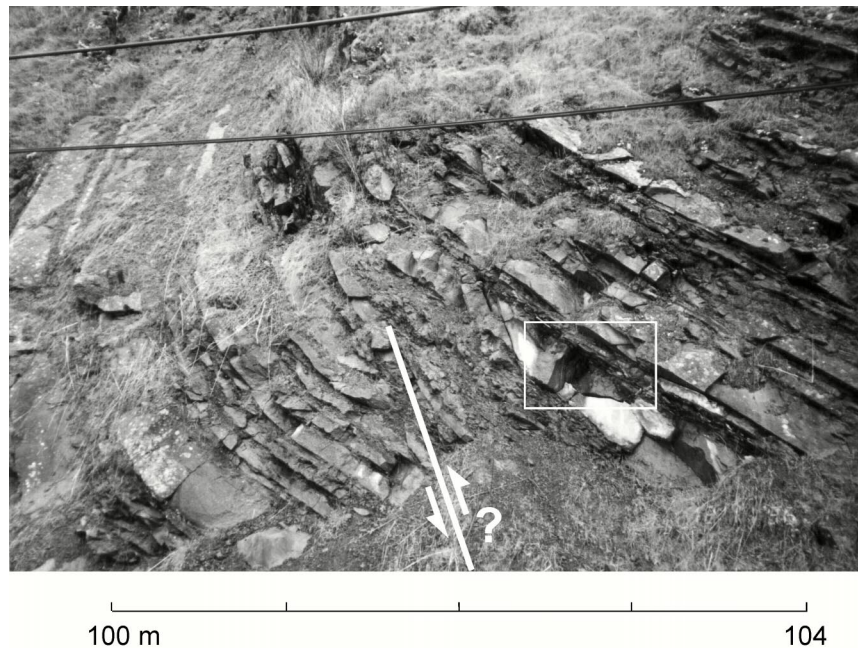


Figure 22. Thrust fault zone immediately north of (stratigraphically below) the kink-like fold. Poles to measured fractures and fault planes lie in NW quadrant of the stereonet plot (Figure 20). Interlimb angle of the thick bed at far left is about 155° . Rectangle indicates area of Figure 21, location of a calcareous nodule and associated tan siltstone.

Sections IV and V

Chevron-like folds in Section IV have high positive asymmetry and wavelengths of 12 to 20 m (Figure 23). Beds on long limbs are repeatedly thrust in a top-to-the-south sense, similar to asymmetric chevron-like folds in other sections. Limbs of the south syncline, fold 18, are exposed over a greater distance than other Section IV beds, with straight beds similar to the south end of Section VI. The

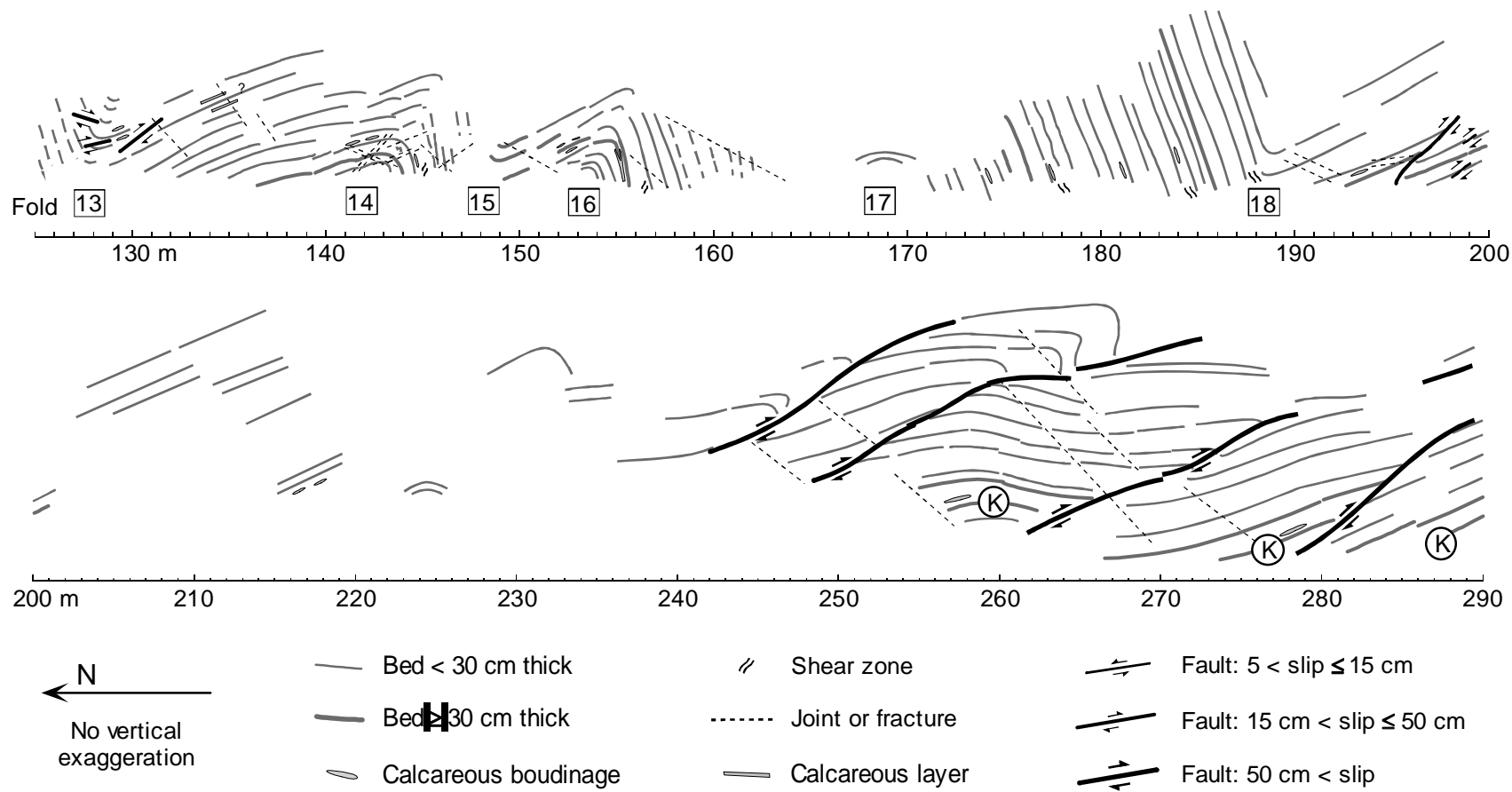


Figure 23. Section IV and Section V folds. In Section IV, asymmetric chevron-like folds having wavelengths of 12 to 20 m are separated by cover from fold 18 at the south end of the section. The chevron-like folds have a top-to-the-south sense of shear with beds on the long limbs repeated by thrust faults. Deeply weathered shale zones occur on steeply dipping limbs at 145, 156, 178, and 185 m. The south end of Section V has a stack of beds repeated by faults at low angle to bedding except at the top of the exposure. A strong fracture pattern in Section V with spacing of 0.5 to 2 times bed thickness at the base of the exposure, is oriented 100/51 S. Bed K is traced through Section VI.

syncline is bordered by covered areas, greater in extent than areas in Sections I to III. South of the cover in Section V, beds repeat by thrusting into a stack at least 20 m high. Beds at the base of the stack are traceable through Section VI.

The steeply dipping limbs of the chevron-like folds have deeply weathered shale horizons at 142, 154, 179, and 185 m, near the exposed cores of folds 14, 16, and 18. Adjacent to the shale zone at 179 m, a bed is deformed into a low amplitude sine wave having wavelength about 2 meters (Figure 10). Pfaff (1986) describes short wave trains of asymmetric chevron-like folds that also exhibit the tendency to have bedding plane faults (indicated by deeply weathered shale layers and slickenlines) more dominantly on the short limbs. The folds described by Pfaff are locally developed on the southeast limb of the Bloomfield anticline, central Pennsylvania.

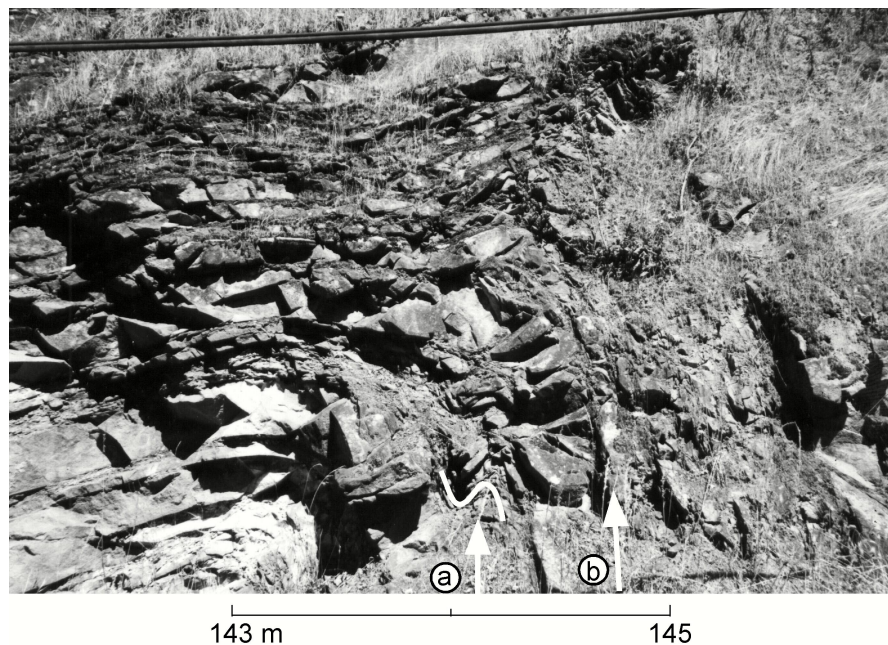


Figure 24. Jointed hinge of fold 14 in Section IV. Thinner beds at *a* are folded into kink-like folds (fold pattern highlighted in white). Calcareous layer at *b* tops a highly jointed sandstone bed.

One of the most closely jointed hinges in the outcrop is fold 14, at 142 m (Figure 24). Small scale kink-like folds are evident in a set of thin beds immediately south of the hinge below a sandstone bed topped by a calcareous layer.

Section VI

Faults in Section VI are typically at low angle to bedding, consistent with layer-parallel shortening (Figure 25). Beds on the long north-dipping limb of fold 21, the north anticline in the section, repeat by thrusting, similar to asymmetric chevron-like folds in other sections. By contrast, the north-dipping limb of fold 23 has a top-to-the-north fault at the base of the exposure that offsets the beds about two meters. The beds are amalgamated without a visible fault plane, but the offset in bed pattern seems to be at low angle to bedding. The top-to-the-north offset is not consistent with flexural slip, but is consistent with layer-parallel shortening before folding as a conjugate to the fault crossing the south-dipping limb of fold 21 (Figure 26).

The top-to-the-south fault crossing the south-dipping limb of fold 21 (Figure 27) is at low angle to the bedding orientation above and below the immediate drag fold, consistent with layer-parallel shortening prior to folding. The steeper south-dipping limbs of the section do not have the thick weathered shale horizons seen in Section IV, though thinner brecciated shale horizons are scattered throughout the exposure. Fold 23 has a bed repetition along one of these shale horizons immediately south of the exposed core at 335 m. Four layers are repeated, two the full 5 to 6 m length of the exposed limb (Figure 28).

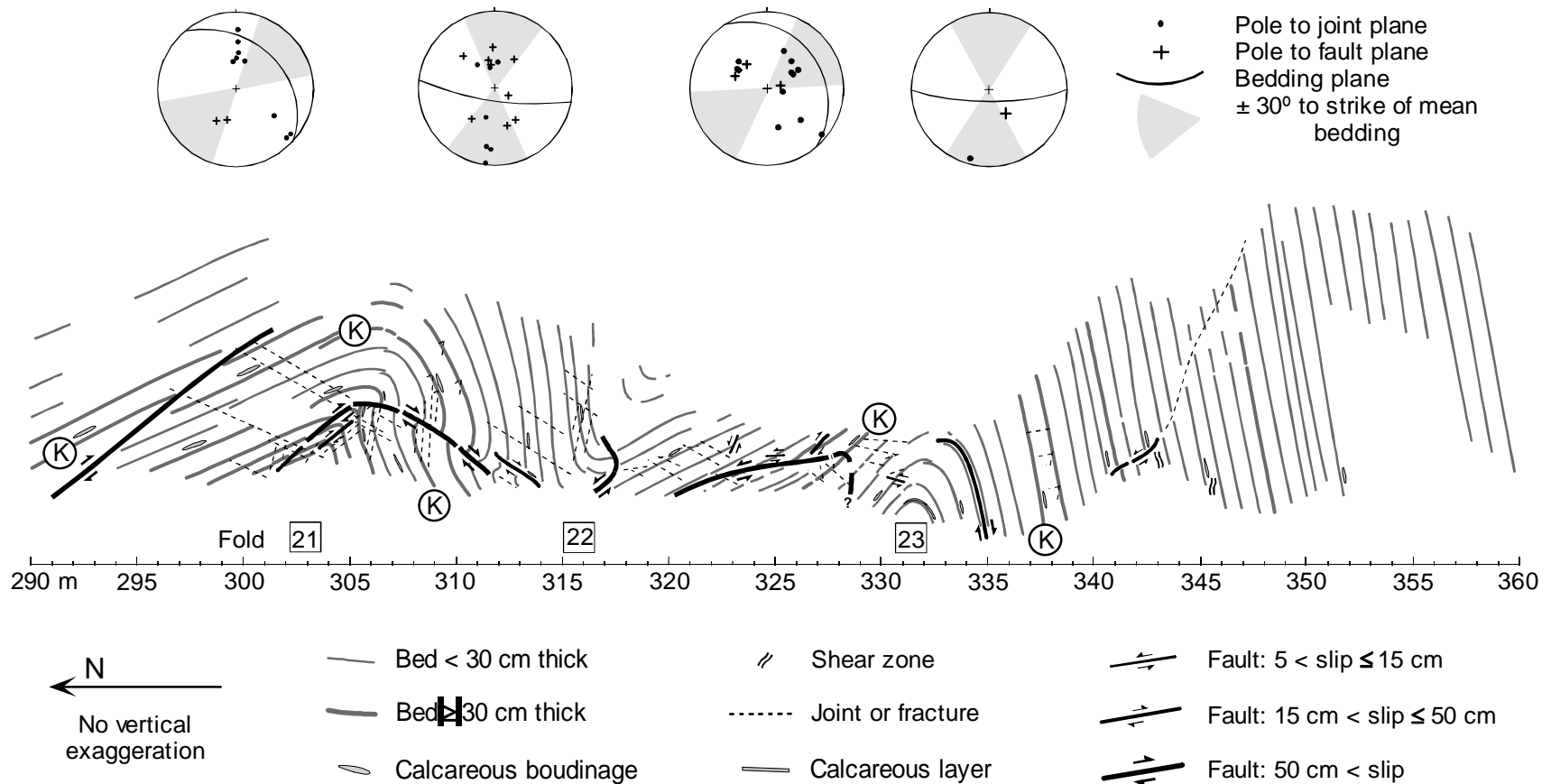


Figure 25. Section VI asymmetric chevron-like folds. A bed followed through the section is indicated with the letter *K*. Several beds repeat through the south-dipping limb of fold 23 at 335 m. Fractures in the section are mainly consistent with layer-parallel shortening as is shown in stereonet above. The fault cutting across the south-dipping limb of fold 21 is at low angle to the bedding beyond the drag fold adjacent to the fault. The top-to-the-north fault at the base of the exposure between folds 22 and 23 also appears to be at low angle to bedding. The top-to-the-north offset is not consistent with flexural slip, but is consistent with layer-parallel shortening before folding. The enveloping surface of the section dips to the south 5°.

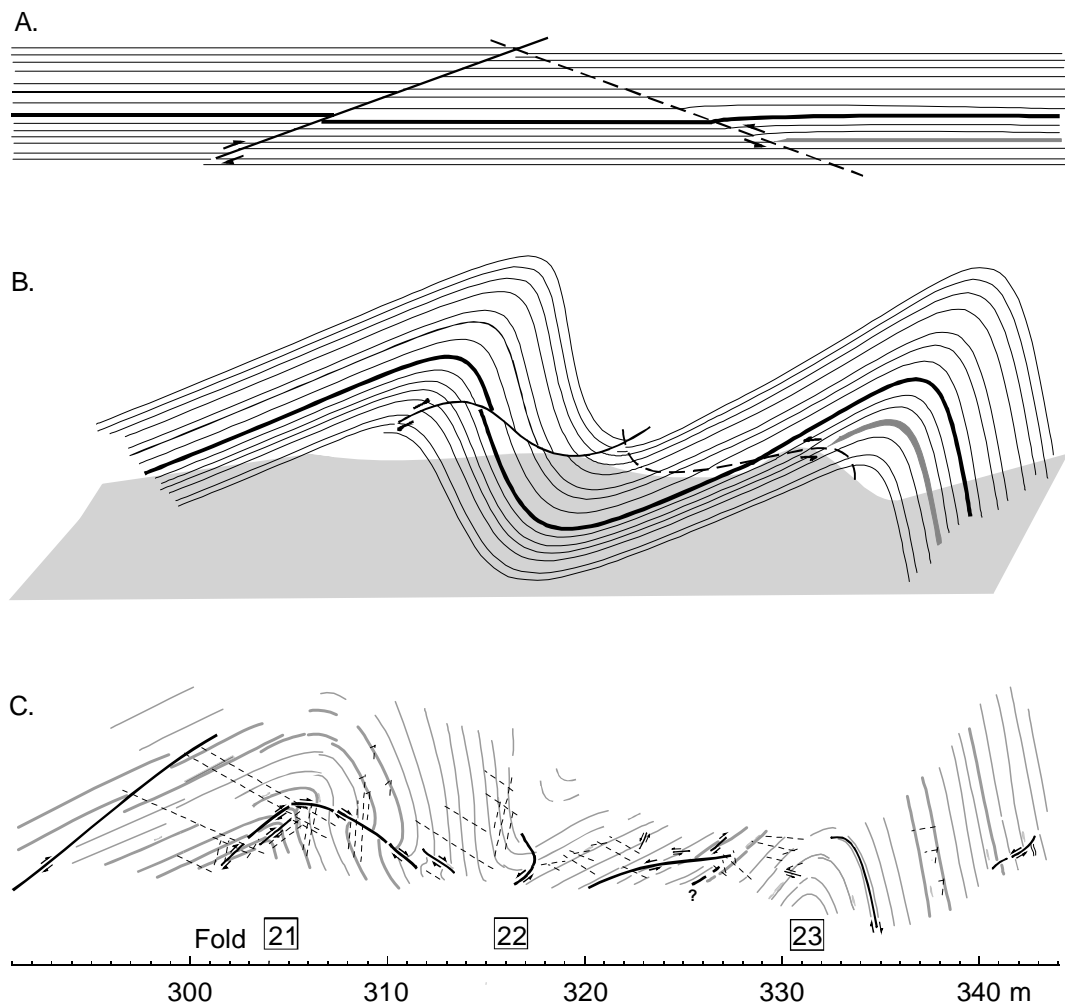


Figure 26. Schematic folding of conjugate fault zones in layers of Section VI. Shading indicates extent of cover at base of exposure. A. Layers before folding are cut or weakened by conjugate faults; shaded bed on right indicates area of visible bed duplication. B. Buckling of layers produces a deformation pattern similar to outcrop. C. Outcrop sketch. The top-to-the-north offset between folds 22 and 23 is not consistent with the top-to-the-south offset in other north-dipping beds of chevron-like folds in the outcrop, or with flexural slip. The offset is consistent with conjugate faults formed before folding and possibly further offset during folding. Offset of beds likely continued during post folding horizontal shortening.

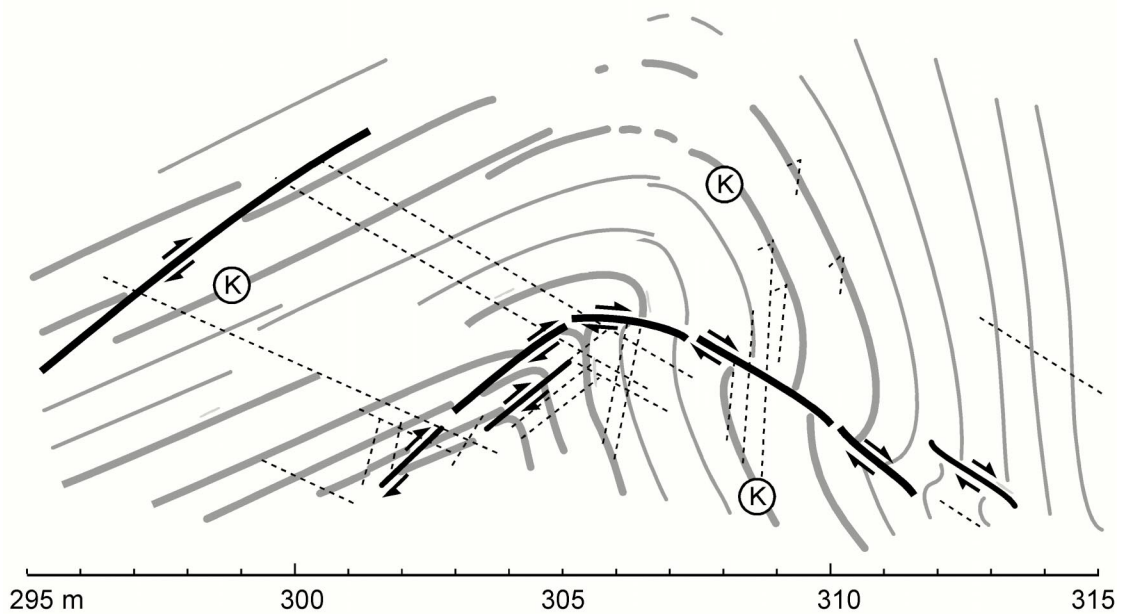
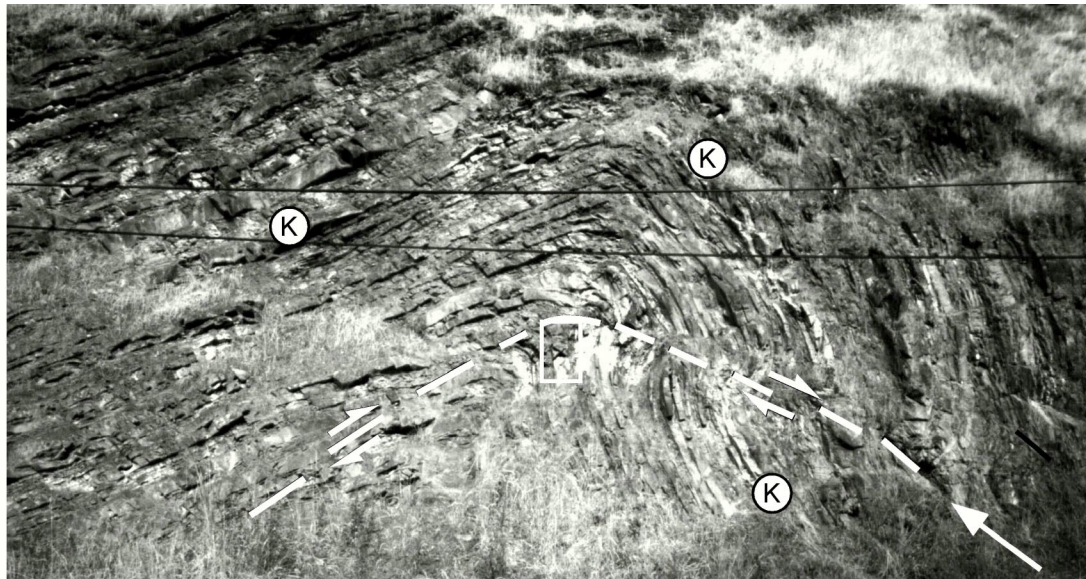


Figure 27. Anticlinal fold 21 in Section VI. Thrust fault on the long dipping north limb extends through hinge and down across the south limb. The letter *K* refers to bed traced through Sections V and VI (Figure 25). Rectangle on photograph shows area of Figure 29.

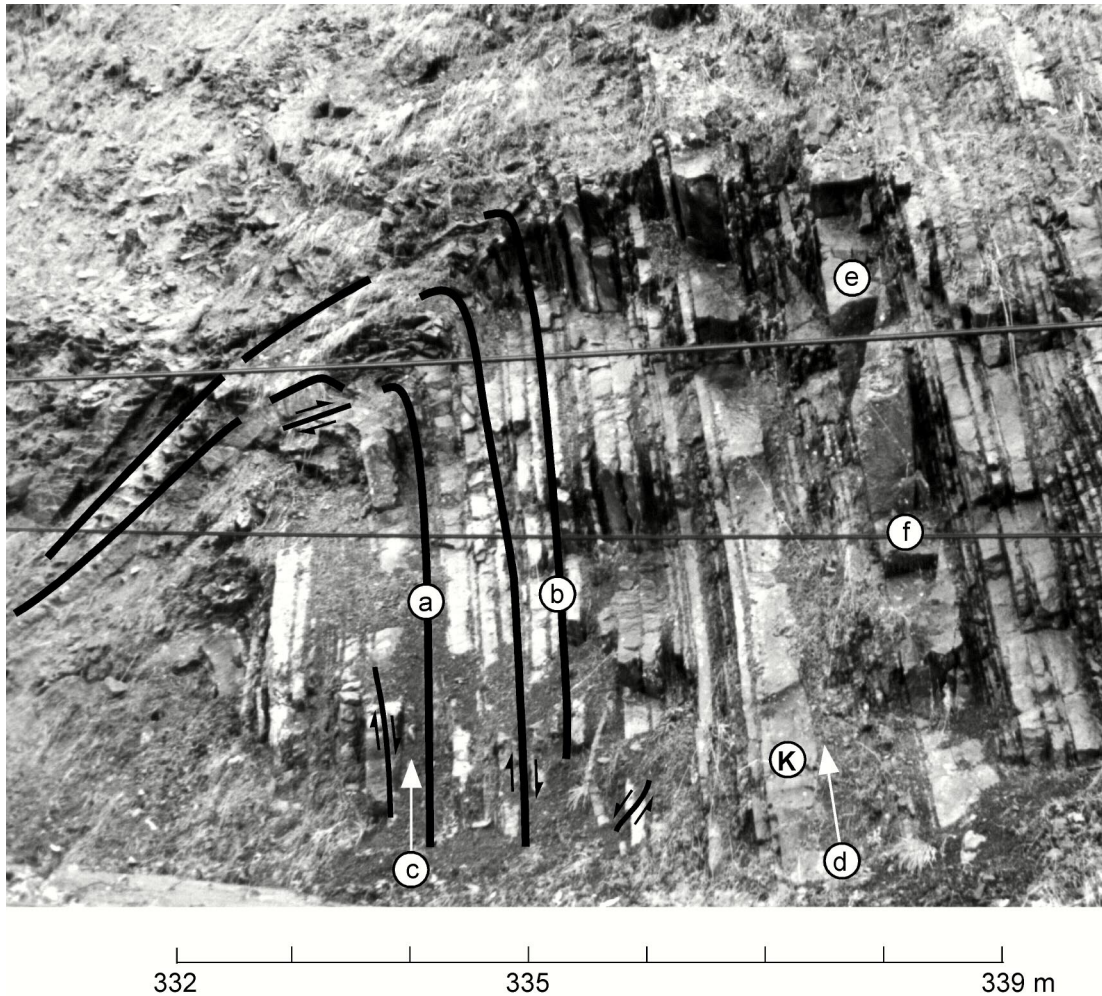


Figure 28. Duplication of layers in south anticline of Section VI. Black lines at *a* and *b* indicate boundaries of bed duplication. The duplication is above a calcareous layer at *c*. The top-to-the-south offset in the bed below the boudins at *c* is not consistent with flexural slip. Jointing normal to bedding at *e* and *f* meets but does not cross fractures at low angle to bedding. Another calcareous boudin layer occurs immediately above bed *K* at *d*.

Layers with a tendency to form boudins, the calcareous layers, are spaced 3 to 4 m apart in Section VI. Layers adjacent to the boudin layers commonly show increased deformation in the form of thickening, jointing, bed duplication, or shale breccia. The duplication of bedding in fold 23 is in layers immediately above a boudin layer (Figure 28). Conspicuous jointing in a 40 cm thick bed at 337 m,

overlies a set of thinner beds having a boudin layer at the base (Figure 28). The near normal joints in the layer do not cut the fractures at low angle to bedding. Near the core of the north anticline, fold 21, at 306 m, boudins fold to the south adjacent to the fault crossing the south limb (Figure 29).



Figure 29. Boudin layer in curve of drag fold in fold 21, Section VI. Layers are near the core of the north anticline at 306 m (Figure 25). The boudins and the upper part of the sandstone layer are drag folded to the south by a fault cutting the south limb (arrow). The lower part of the layer is folded to the north into the anticlinal fold.

Discussion

Locally exposed in one to two wavelength sections, the interbedded sandstone and shale of this study area are folded into concentric-like, kink-like, and chevron-like folds. Apart from the kink-like fold, wavelength and amplitude increase from north to south. Asymmetry, with a top-to-the-south sense of layer-parallel shear, is strong from the south end of Section II to the south end of the outcrop. Lenticular beds and pinch outs are more common in Section I than in other sections. Faults in the outcrop are dominantly thrusts consistent with layer-parallel shortening. Thrusts in the concentric-like fold occur on both limbs, in the chevron-like folds they are mainly on the long limbs. Ramp faults repeat beds the length of a limb in Sections I and VI, on both north and south-dipping limbs. Each section also has an anticline with a thrust fault on the long north-dipping limb that extends through the hinge and across the south-dipping limb. Deeply weathered brecciated shale layers occur on the short steep limbs of the chevron-like folds. Calcareous layers with localized boudinage, are found throughout the outcrop, with closer spacing in Section I than in Section VI, though beds are also thinner in Section I.

Outcrop Fold Package

The variations in asymmetry and wavelength, and shortness of the exposed fold trains (beds could not be traced through the entire outcrop), lead to modeling of the outcrop as a stack of multilayers. These multilayer folds can be described genetically by a folding mechanism, and geometrically by fold form. Since fold form

is not unique to a specific folding mechanism, mechanisms of folding will be examined before fold form.

Folding Mechanism

In a fold and thrust belt, the types of folding and corresponding mechanisms of folding that might be found include a) buckle folding: layer-parallel shortening, b) ramp folding: duplication of strata by faulting, c) drape folding: flexure of strata caused by slip on a buried fault, and d) drag folding: layer-parallel shear on the limb of a higher order fold (Johnson and Fletcher, 1994). As a mechanism for shortening, layer-parallel shortening produces maximum shortening and buckling (Johnson and Fletcher, 1994). Layer parallel shortening is consistent with the most of the faults in the outcrop and for this study, is considered the dominant folding mechanism.

Fold Form

The geometric form of multilayer folds formed in layer-parallel shortening depends on the material properties of the layers and the confining media. Essential properties are a) relative strength of the layers and confining media, b) relative thickness of the layers and confining media, and c) whether contacts are bonded, free slip, or stick slip (Johnson and Fletcher, 1994). Asymmetry of folds is a function of layer contacts and the sense of layer-parallel shear (Pfaff and Johnson, 1989). Though the properties at the time of folding are not known, some assumptions can be made and models applied based on these assumptions.

The layers in the outcrop can be modeled as a multilayer of units with respective relative strength and thickness (Figure 30). Having a thickness greater than the wavelengths of other units, Section III can act as an infinite half-space to units above and below (Johnson and Pfaff, 1989). It is likely a relatively stiff medium since it has greater sandstone to shale ratio and greater bed thickness than other units (Table 3). The upper and lower relatively soft media represent the muddier sections to the north and south of the outcrop.

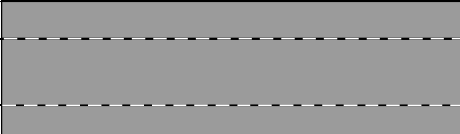
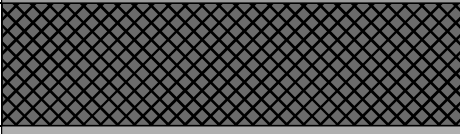
Section	Relatively soft medium	Assumed viscosity contrasts
IV-south		 upper = 1-5 lower = 0.7-1 avg. media = 0.8-1.7
VI		
IV-north		
III		 upper = 0.3-1 lower = 2-10 avg. media = 0.5-1.8
II		
I		
	Relatively soft medium	

Figure 30. Model of folding units in the study outcrop. Multilayer unit thickness is proportional to measured thickness of the section. Since the 35 m thickness of Section III is greater than the 10 to 28 m wavelengths in the upper and lower units, it can act as an infinite half-space to these units. Viscosity contrast is based on bedding properties (Table 3).

Table 3. A summary of bed thickness and sandstone to shale ratios by folding unit. Section IV is split into two units with the layers of fold 18, Section IV-north, stratigraphically above Section VI.

Section	Applicable section thickness (m)	Sandstone thickness maximum (cm)	Sandstone average thickness (cm)	SS : Shale average of ratios
IV-south	16	30	7.4	3.1
VI	20	49	8.1	3.5
IV-north	12	32	8.6	3.7
III	36	60	10.5	3.9
II	7	58	9.8	3.2
I	11	31	4.5	3.9

All the layer, media, and contact properties are pertinent to the fold forms of this study. Relative strength of the confining media determines whether a multilayer will be constrained or concentric in form; ideal concentric folds form in relatively soft media and constrained folds form in relatively stiff media (Figure 31) (Johnson and Pfaff, 1989). Whether contacts have linear or nonlinear slip in layer-parallel shear determines whether kink or drag fold asymmetry develops (Pfaff and Johnson, 1989). Relative strength and spacing of layers determines whether layers will fold independently forming a similar multilayer, and at high amplitude, chevron-like folds.

The sharp hinges in the chevron-like folds of the outcrop have not been reproduced in linear-viscous theoretical multilayers even to high amplitude (Cruikshank and Johnson, 1993), and may require nonlinear material behavior for their

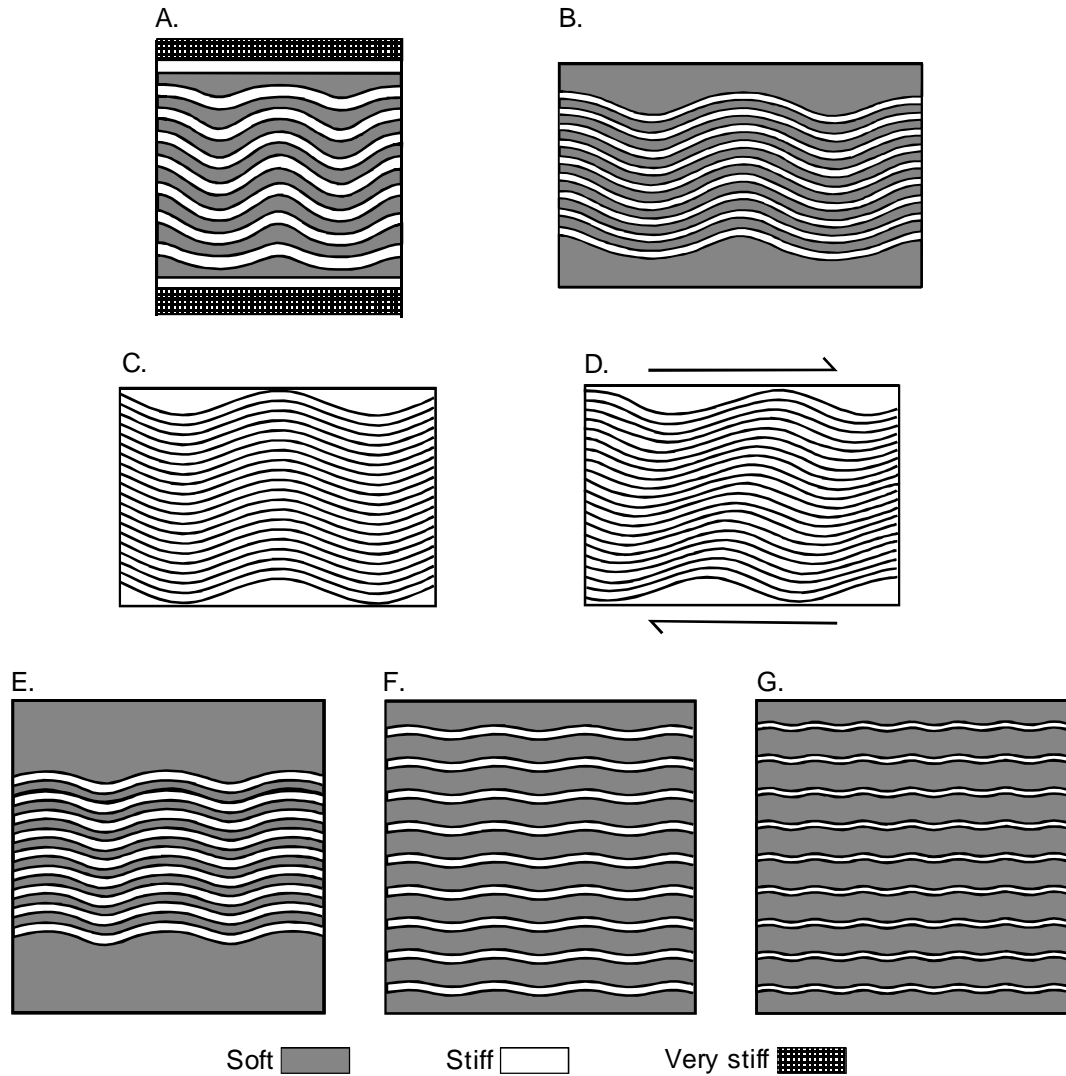


Figure 31. Theoretical multilayer folds. Layers have linear slip or no slip on the layer interfaces. Viscosity contrasts are: $\mu_{\text{stiff}}/\mu_{\text{soft}} = 10$ and $\mu_{\text{very stiff}}/\mu_{\text{soft}} = 10$. A. and B. Constrained folds confined in stiff media and concentric folds formed in soft confining media (after Cruikshank and Johnson, 1993, Figures 7, 8). C. and D. An infinitely thick, similar multilayer of chevron-like folds in layer-parallel shortening, then subjected to layer-parallel shearing deformation (after Pfaff and Johnson, 1989, Figure 6). E., F., and G. Multilayer fold form varies from concentric (E), to similar (G), as stiff layers have greater spacing and a greater degree of independence (after Johnson and Pfaff, 1989, Figure 6).

formation. Nonlinear material behavior of layers in the outcrop is evident by the presence of boudins that do not form in linear-viscous material (Johnson and Fletcher, 1994; Smith, 1977). Distinguishing between linear and nonlinear material behavior, though, is not critical to essential fold form since the behaviors produce comparable fold form and wavelength (Johnson and Pfaff, 1989). Similar folds in the interior of a theoretical multilayer may be used as a precursor of the ideal chevron form. The final fold form is also not affected by whether contacts are bonded or free slip, though folds with free slip grow faster (Johnson and Pfaff, 1989).

Ideal multilayer fold forms are constrained, concentric, and similar (Johnson and Pfaff, 1989) incorporating the basic sinusoidal or chevron fold forms (Figure 31A, B, C). Constrained folds have amplitudes diminishing to zero at upper and lower media contacts. Wide crests and narrow troughs at the upper media interface, and narrow crests and wide troughs at the lower interface characterize concentric-like folds. Similar folds are sinusoidal at low amplitudes and chevron at high amplitudes. Hybrids of ideal multilayers develop if properties are intermediate between end member forms (Johnson and Pfaff, 1989).

Concentric-like Fold

The concentric-like fold of Section I (Figure 32), flattened crest bounded by narrow troughs, is characteristic of the upper layers of theoretical concentric multilayers or layers slightly lower in theoretical constrained multilayers (Figure 31B, A). Crests of layers in the concentric-like fold in Section I are broad above, narrow

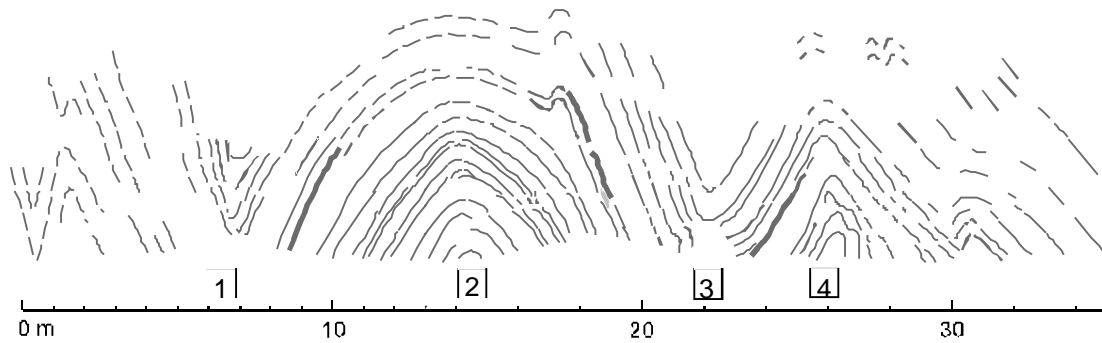


Figure 32. Fold form of Section I.

in the middle, and slightly rounded in the core. Sections II and III provide a relatively stiff medium above Section I (Figure 30). The concentric-like fold in the outcrop is similar to the upper part of the ideal constrained multilayer (Figure 31A).

Chevron-like Folds

Development of a similar multilayer of chevron-like folds is dependent on the relative thickness of stiff and soft interbeds, and the multilayer thickness.

Theoretically, chevron-like folds will develop in a multilayer if the stiff to soft thickness ratio is small, allowing the stiff beds to fold independently (Figure 31G) (Johnson and Fletcher, 1994). Johnson and Fletcher (1994) define the degree of independence, d , as

$$d = \left(\frac{h_2}{L} \right) \left(1 - \frac{\mu_n}{\mu_1} \right)$$

where μ_n is the normal viscosity of the multilayer,

$$\mu_n = \left(\frac{1}{h_1 + h_2} \right) (h_1 \mu_1 + h_2 \mu_2) = \mu_1 \left(\frac{1}{1 + \frac{h_2}{h_1}} \right) \left(1 + \frac{h_2}{h_1} \frac{\mu_2}{\mu_1} \right)$$

L is the wavelength of the folds, h is bed thickness, μ is viscosity, and 1 and 2 refer to stiff and soft respectively (Figure 33). If d is near zero, the beds behave strongly as an ensemble. If d is significantly greater than zero, on the order of 0.5 or greater, the beds fold weakly as an ensemble and the stiff layers will fold independently (Figure 31G) (Johnson and Fletcher, 1994).

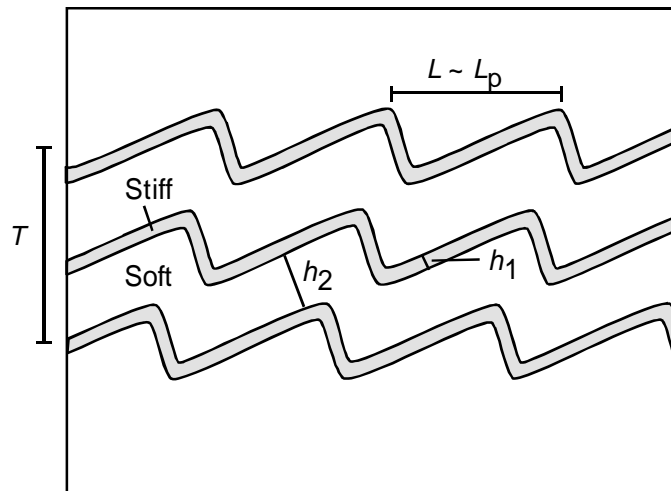


Figure 33. Parameters for multilayer folding models. T is multilayer thickness, L : wavelength, L_p : preferred wavelength, h_1 and h_2 : thickness of stiff and soft layers, respectively.

Assuming viscosity contrast, $\mu_2/\mu_1 = 0.1$, and $h_2/h_1 = 1$, a generous estimate for the outcrop, then $\mu_n/\mu_1 = 0.5$. For the layers to be relatively independent, $d \geq 0.5$, the thickness of soft layers would need to be close to the wavelength of the folds. An increase in the viscosity contrast does not significantly affect the results. With no

indication of sufficiently thick soft layers within the multilayers of the outcrop, the stiff layers must fold dependently. The theoretical similar multilayer of independent stiff layers is not a suitable model for the chevron-like folds.

Chevron-like folds also form in the interior of theoretical concentric or constrained multilayers having a small wavelength to multilayer thickness ratio (Johnson and Pfaff, 1989). Johnson and Pfaff (1989) use a ratio of 0.06 as an example of a confined multilayer in which chevron-like folds will form. Pfaff (1986) refers to the required wavelength to thickness ratio as being much less than one.

For a 28 m wavelength as in Section VI, the multilayer thickness needs to be 466 m to obtain a wavelength to thickness ratio of 0.06. Assuming a multilayer thickness of even 60 to 100 m, with folds of wavelength 12 to 28 m, yields a wavelength to multilayer thickness ratio of 0.2 to 0.28. Even if this is sufficiently less than one, there is still the problem of no visible bounding concentric-like folds above and below the chevron-like folds to match a theoretical multilayer. The chevron-like folds as exposed do not have an equivalent theoretical multilayer in form.

Asymmetry

The properties of the layer interface determine whether drag or kink fold asymmetry develops for a given sense of layer-parallel shear. With nonlinear slip on the interface, the rate of slip during folding is a nonlinear function of contact stress, and the sense of asymmetry of monoclinical kink folds is produced (Pfaff and Johnson, 1989). Linear slip, the rate of slip is a linear function of the contact stress, produces

the sense of asymmetry of drag folds. Concentric and chevron folds are products of linear slip.

Given the sense of layer-parallel shear, orientation of the short limb distinguishes a monoclinial kink fold from a drag fold (Figure 34). The orientation of the short limb, or the vergence, cannot be used as an indicator for the sense of shear. Krabbendam and Leslie discuss folds in the Dalradian of southeast Scotland arguing there is widespread evidence of vergence opposite to the sense of shear (1995). Likewise, Pfaff (1986) describes monoclinial kink folds in the Huasna Syncline, California, and the Wills Mountain Anticline, West Virginia, having vergence opposite to the sense of shear.

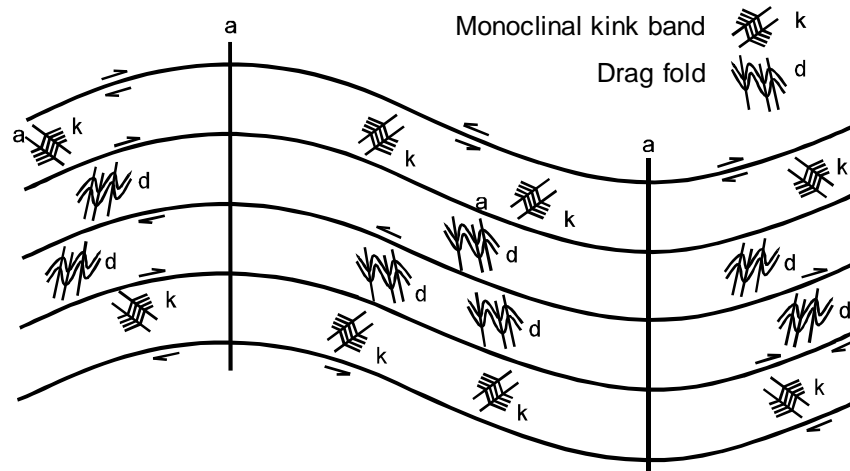


Figure 34. Opposite sense of asymmetry of monoclinial kink and drag folds. The sense of shear responsible for asymmetry of folds is indicated by arrows and implied by position in the larger fold. In right-lateral layer-parallel shear, the short limb faces left in a monoclinial kink fold, and faces right in a drag fold. Traces of axial planes (a) are shown for major and minor folds (after Pfaff and Johnson, 1989, Fig. 1).

In top-to-the-right sense of layer-parallel shear, the short limb of a monoclinial kink fold faces left and layers are offset to the left, the short limb of a drag fold faces right and layers are offset to the right (Figure 34). With the short limbs facing south, the asymmetry of the chevron-like folds in the study outcrop is consistent with drag folds formed in a top-to-the-south sense of layer-parallel shear (Figure 34). This sense of shear is evident in the top-to-the-south thrust faults on long limbs of the chevron-like folds and in the duplex-like structure between Sections I and II. The sense of offset in the kink-like fold is opposite that of the chevron-like folds, but is consistent with top-to-the-south sense of layer-parallel shear (Figure 34).

The top-to-the-south sense of layer-parallel shear of the outcrop indicates that, with the folds on the south-dipping slope of the Oakland anticline, thrust sheet stresses override any simple shear local to the south limb of the anticline (Figure 35). A principal compressive stress oblique to layering and mean top-to-the-south layer-parallel shear is consistent with the geologic setting in a thrust sheet verging NNW.

The alternative to folds forming on a south-dipping slope is for the layers to pass through a trough at the north end of the outcrop. A syncline on the order of the Oakland anticline or even intermediate between it and the study area folds is not evident near the north end of the folds, or on maps of the areas to the east and west. This option also requires a locally developed companion anticline since past geologic mapping shows no area wide evidence of north-dipping beds immediately south of the outcrop. The syncline-anticline option would need more evidence from the field.

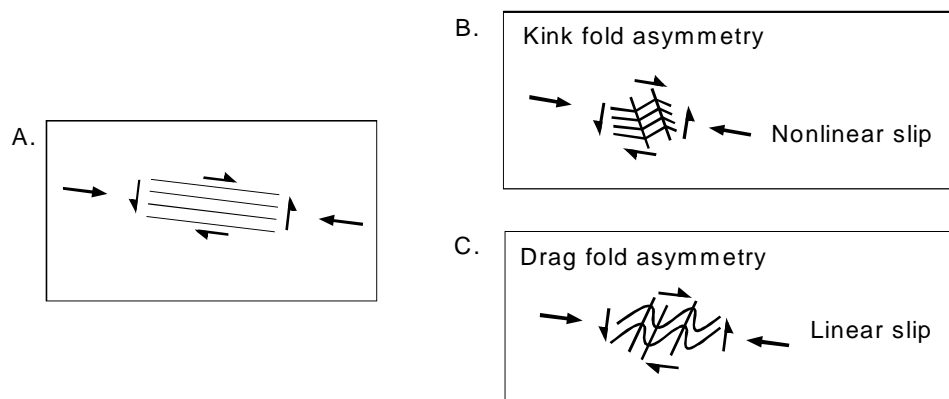


Figure 35. Sense of fold asymmetry for the outcrop setting in a thrust sheet. A. Layer-parallel stress regime. B. Kink fold asymmetry develops in nonlinear slip. C. Drag fold asymmetry develops with bonded contacts or linear slip.

Kink-Like Fold

The asymmetry of the kink-like fold, short limb facing north, is consistent with the top-to-the-south layer-parallel shear evident in the outcrop. The localized tan siltstone and calcareous layers within the kink-like fold (Figure 20) are possible evidence of nonlinear slip, required for the formation of theoretical monoclinical kink folds. Calcareous layers in the outcrop tend to have boudinage, evidence of nonlinear material behavior. The soft tan siltstone may be an indication of diagenesis in response to a local increased resistance to slip. Limited exposure of the layers bordering the siltstone prevents examination of the interface beyond the fold.

Unit Thickness

In mechanical and theoretical models of folded multilayers, thickness of a folded unit is directly proportional to wavelength (Biot, 1961; Currie and others, 1962; Johnson and Fletcher, 1994). The folding unit can consist of more than one layer if

soft interbeds are thin allowing the stiff layers to fold as an ensemble (Johnson and Pfaff, 1989). This applies to the outcrop where stiff layers do not fold independently. The outcrop multilayers can thus be modeled as stiff layers with bonded or free slip.

Bonded layers

For a multilayer of bonded stiff layers or an equivalent single layer, approximate analysis of folding of viscous material shows that the dominant wavelength, L_d , the wavelength that grows most rapidly, is related to the initial thickness of the stiff layer or bonded multilayer, T_0 , by

$$\frac{L_d}{T_0} = 2\pi \sqrt[3]{\mu_{layer} / 6\mu_{media}}$$

where μ is viscosity (Biot, 1965; Johnson and Fletcher, 1994). This approximation is best for greater viscosity contrast. An approximate relation between the dominant wavelength and the preferred wavelength, L_p , (wavelength that attains the greatest amplitude) is

$$L_p \cong L_d S_x$$

where S_x is the stretch (estimated as the ratio of observed wavelength to arclength) (Johnson and Pfaff, 1989). The stretch is about 0.6 and 0.65 in Sections I and VI respectively. In this analysis the preferred wavelength is taken to be equivalent to the observed wavelength.

Because Sections I and VI have relatively stiff and soft media, the media viscosity is an average. The layer to media viscosity ratio may be written as

$$\frac{\mu_{layer}}{\mu_{media}} = \frac{\mu_{layer}}{(\mu_{media})_{average}} = \frac{\mu_{layer}}{\frac{\mu_{upper} + \mu_{lower}}{2}} = \frac{1}{\left(\frac{\mu_{upper} + \mu_{lower}}{\mu_{layer}} \right) \frac{1}{2}}$$

where μ_{upper} is viscosity of the upper medium and μ_{lower} is viscosity of the lower medium (Johnson and Fletcher, 1994). Figure 36 shows the range of layer to average media viscosity ratios for Section I and VI based on the viscosity contrast assumptions of the model outcrop multilayer (Figure 30).

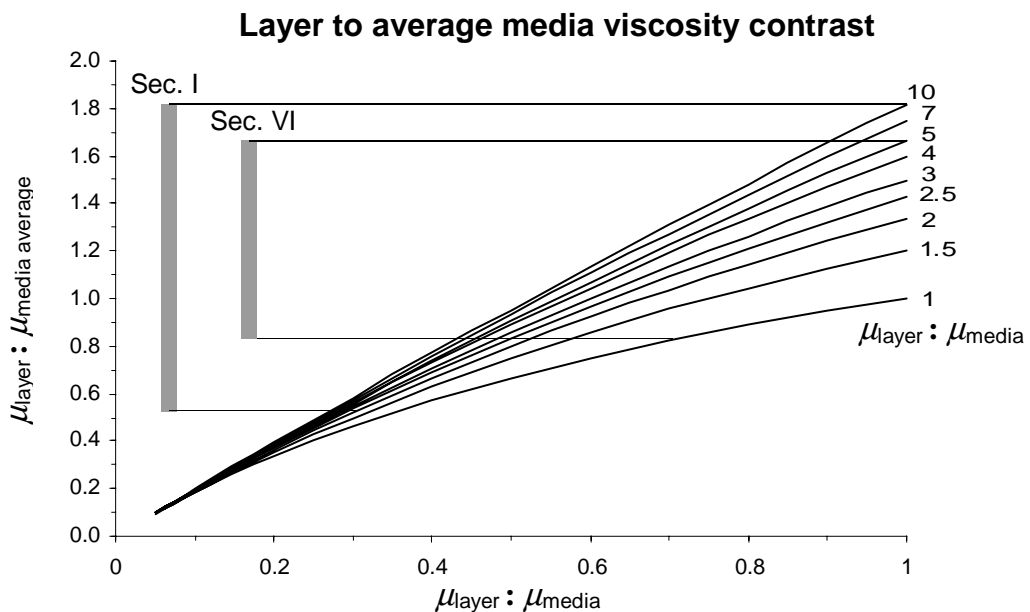


Figure 36. Chart of layer to average media viscosity. In Section I, layer to lower media ratios of 2 to 10, and 0.3 to 1 for the upper media result in a layer to average media viscosity ratio of 0.5 to 1.8. In Section VI, layer to upper media ratios of 1 to 5, and 0.7 to 1 for the lower media, result in a layer to average media viscosity ratio of 0.8 to 1.7.

Applying the above equations to Section I with layer to average media viscosity ratio of 0.5 to 1.8 (Figure 36), yields initial multilayer thickness of 6 to 8 m (Figure 37). An initial thickness of 8 m allows for layer thickening of 25 percent to achieve the final thickness of 10 m (Figure 9). Within the constraints of the initial viscosity assumptions, an 8 m initial thickness corresponds to $\mu_{\text{layer}}/\mu_{\text{avg. media}}$ of 0.5.

In Section VI, assuming $\mu_{\text{layer}}/\mu_{\text{lower media}}$ is 1 to 5 and $\mu_{\text{layer}}/\mu_{\text{upper media}}$ is 0.7 to 1, $\mu_{\text{layer}}/\mu_{\text{avg. media}}$ is 0.8 to 1.7 (Figure 36). A layer to average media viscosity contrast of 0.8 to 1.7 yields initial thickness of 12 to 15 m (Figure 37) compared with a measured thickness of 20 m. An initial thickness of 15 m implies thickening of 33 percent in layer-parallel shortening. Within the constraints of the initial viscosity assumptions, the 15 m initial thickness corresponds to $\mu_{\text{layer}}/\mu_{\text{avg. media}}$ of 0.8.

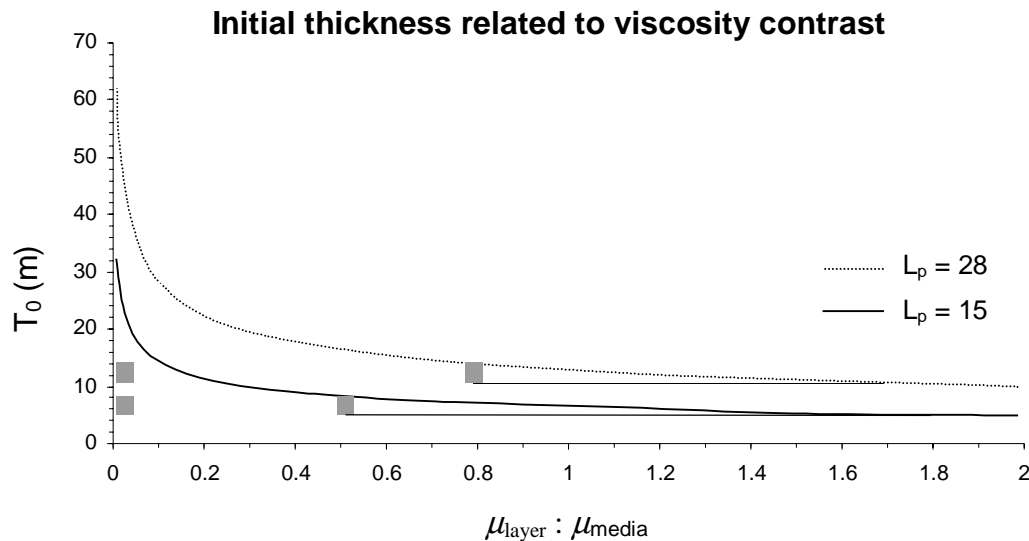


Figure 37. Chart of initial thickness as a function of layer to average media viscosity contrast. Applying the model with a viscosity contrast of 0.5 to 1.8 in Section I, yields initial thickness of 6 to 8 m. In Section VI a viscosity contrast of 0.8 to 1.7 yields initial thickness of 12 to 15 m.

Stiff Layers with Free Slip

Equations for approximating the wavelength to thickness ratio incorporating the number of structural units are presented by Johnson and Pfaff (1989). The equations work best for multilayers of four or more units. For a multilayer in rigid media composed of N structural layers having free slip, the ratio of dominant wavelength, L_d , to multilayer thickness, T , is

$$\left(\frac{L_d}{T}\right)_{Rigid} \cong 1.9 \sqrt[2]{\frac{1}{N}}$$

For multilayers in soft media, Johnson and Pfaff (1989) present a graphical solution for $(L_d/T)_{Soft}$ as related to $(L_d/T)_{Rigid}$ (Figure 38).

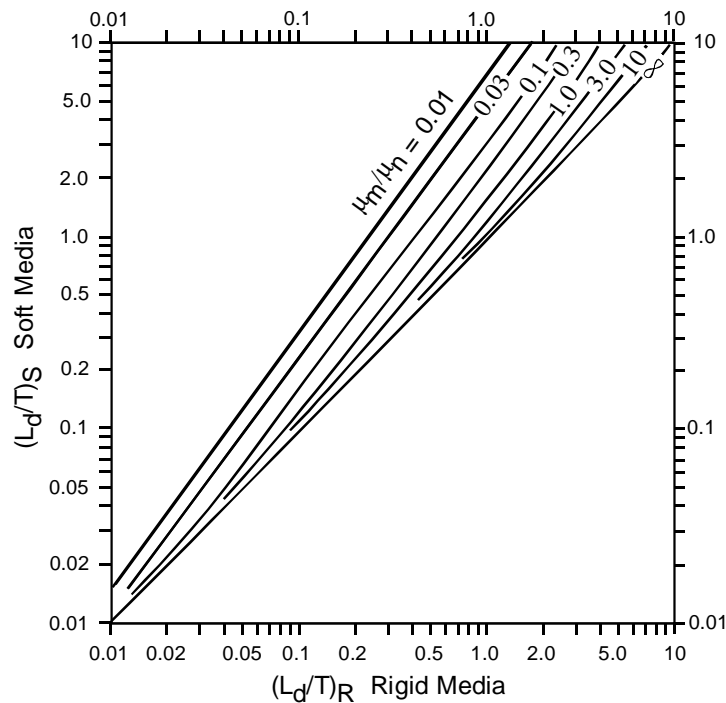


Figure 38. Relation of the wavelength to thickness ratio in rigid and soft media, for various ratios of media to normal viscosity of the multilayer. Normal viscosity is the weighted average viscosity of stiff and soft layers (after Johnson and Pfaff, 1989, Fig. 12).

Table 4. Results of applying the model relating multilayer thickness, number of structural units, and viscosity contrast in a multilayer with free slip. For both Section I and VI, a model of two structural layers produces a viscosity contrast consistent with the range used in the bonded layer model.

Section	I			VI		
S_x	0.6			0.65		
L_p (m)	16			28		
L_d (m)	27			43		
N	8	4	2	4	2	2
T (m)	16	16	16	27	27	26
$(L_d/T)_{\text{Rigid}}$	0.7	1	1.3	1	1.3	1.3
$(L_d/T)_{\text{Soft}}$	2.7	2.4	2	2.3	1.9	2
$(\mu_{\text{media}}/\mu_{\text{layer}})_{\text{average}}$	0.03	0.15	1.5	0.25	2.5	1.7
$\mu_{\text{layer}}/\mu_{\text{media average}}$	33	6.7	0.7	4	0.4	0.6

The relations are applied to yield preferred wavelengths, $L_p = L_d * S_x$, similar to the observed wavelengths in Sections I and VI (Table 4) with a multilayer thickness approximated by total bed thickness plus the amplitude. Section I result for a multilayer thickness of 16 m shows two structural units are required to produce a layer to average media viscosity ratio of 0.7. Evidence in the outcrop may be the relatively thick brecciated shale layer adjoining the lenticular bed in fold 4. Section VI result for a multilayer of 26 m also requires two structural units though there is no comparable field evidence as in Section I. These results may just indicate the folds formed in layers that were more bonded than free slip since the model is best for four or more structural units.

Comparing results of the two models for the concentric-like fold of Section I, show consistency in thickness for an average media to layer viscosity ratio of 1.5. The ratio yields initial thickness of 8 m in the model of bonded layers and final thickness of 16 m in the free slip model, for a vertical stretch of 1.8. Considering the minimum measured shortening is 40 percent, or horizontal stretch of 0.6, the results are reasonable.

Section VI has a similar correspondence between the two models for an average media to layer viscosity ratio of 1.7. The initial thickness of 15 m and final multilayer thickness of 26 m is a vertical stretch of 1.7, slightly less than Section I and similar to the difference in horizontal stretch.

Outcrop Setting

The setting of the folds stratigraphically above the mudstone unit, Tum (Figure 6), provides a contrast in viscosity and possible detachment surface for the initiation of folding or faulting. The abrupt change in bedding orientation observed north of the outcrop at the lower mudstone contact indicates the lower turbidite unit may be in fault contact with the mudstone at this location. This places the outcrop near the base of a splay thrust within the main thrust sheet that extends north 1.7 km to the Cooper Creek Reservoir fault. If the chevron folds in the calcareous concretionary siltstone near the Cooper Creek Reservoir fault are related to the layers in the outcrop, then the possible splay fault at the base of the mudstone unit becomes more significant. The symmetry of the folds in Section I may be due to their position in this splay thrust.

There are three recognized channel fill deposits within the Tenmile Formation, at least one of which, the Rasler Creek tongue, has rounded, white calcareous concretions (Ryu and others, 1992). The turbidites of the study area may be a relatively thin turbidite unit related to another channel fill in the Tenmile Formation or the channel conglomerate of the Bushnell Rock Formation located south of Woodruff Mountain. As a small unit, it would provide greater contrast in material properties with less thickness, enabling shorter wavelength folds to develop.

Previous work in the study area by Perttu and Benson (1980) describe the folds as having formed in beds considerably lithified and at shallow depth due to the continuity of bedding and constant thickness of sandstone beds, even in hinges. It does appear that folding in the study area was not syndepositional. Fluid escape structures and secondary mineralization are absent and faulting and boudinage occurred early in the deformation process. However, the style of folding does not necessitate formation at shallow depths.

The style and extent of deformation in the overburden depends on the distance to major thrust faults and the relative material properties of the overburden. The relative material properties determine how the overburden responds to layer-parallel shortening. Response in the overburden may be of longer wavelength with the appearance of less deformation, such as in the White Tail Ridge Formation. Ryberg's (1984) constraint on folding due to the different style of deformation in the White Tail

Ridge Formation may not be justified. A variation in the amplitude of folds does not exclude the folds from forming at the same time.

Extent of the overburden in the study area at the time of folding depends on the thickness of the turbidite units and the overlying White Tail Ridge Formation, and the relative position of the folds in the turbidites. The overburden does not include the Camas Valley Formation since it appears the principal period of deformation occurred prior to its deposition (Ryu and others, 1996). The White Tail Ridge Formation crops out north of the study area and southwest of Woodruff Mountain (Figure 1).

Intermediate to these locations, including the study area, the White Tail Ridge appears to have been uplifted and subsequently eroded. Uplift was likely associated with movement on the Cooper Creek Reservoir fault and possibly the Bonanza fault.

Assuming the layers of the folds are intermediate within the turbidite unit, an estimate of the overburden at the time of folding is 700 to 800 m and a maximum of 1700 m (Figure 7). A reasonable compromise based on lateral variation in the subbasin is about 1300 m (Figure 4). The White Tail Ridge Formation makes up about 500 m of the total, and undifferentiated Umpqua Group turbidites and mudstone the remainder.

Constraining the beginning of folding is the lithification of sediments some time after deposition in early Eocene. The end of folding is constrained by the end of major N-S shortening. Assuming the shortening subsided coincident with the end of significant offset on the NNW verging Bonanza fault yields an upper time limit of 52 Ma, prior to deposition of the Camas Valley Formation in earliest middle Eocene.

Conclusion

Set in a NNW verging thrust sheet, the outcrop appears to be near the base of a thrust fault, possibly a splay of the Cooper Creek Reservoir fault. The timing of the folding is assumed coincident with the shortening that also produced offset on the Bonanza and Cooper Creek Reservoir faults. This places an upper constraint of 52 Ma, end of the early Eocene, before deposition of the Camas Valley Formation in earliest middle Eocene, a period of transition to the north-south structural alignment of the Tyee basin. A constraint on the onset of folding is lithification of the early Eocene beds.

The exposure of folded turbidite beds displays a complex interplay of folding and faulting. Medial axis shortening attributable to folding is a minimum of 35 to 40 percent, with additional shortening caused by bed repetition in faulting and likely bed thickening. Thrust faults consistent with layer-parallel shortening dominate the system of fractures in the outcrop, occurring before, during, and after buckling of layers to create folds.

In the order of deformation, localized boudins formed before or early in the layer-parallel shortening (Figure 39). Conjugate faulting or weakening, and duplication of beds by ramp faulting, also appear to have initiated early in the shortening, possibly creating a nucleus for folding. The folds of Sections II to VI were subject to a principal compressive stress oblique to layering, creating a mean top-to-the-south layer-parallel shear, with chevron-like folds facing south and a kink-like fold

facing north. Post folding horizontal shortening is evident in the rotation of limbs and in a conjugate faulting and jointing pattern in the outcrop, especially in vertical beds.

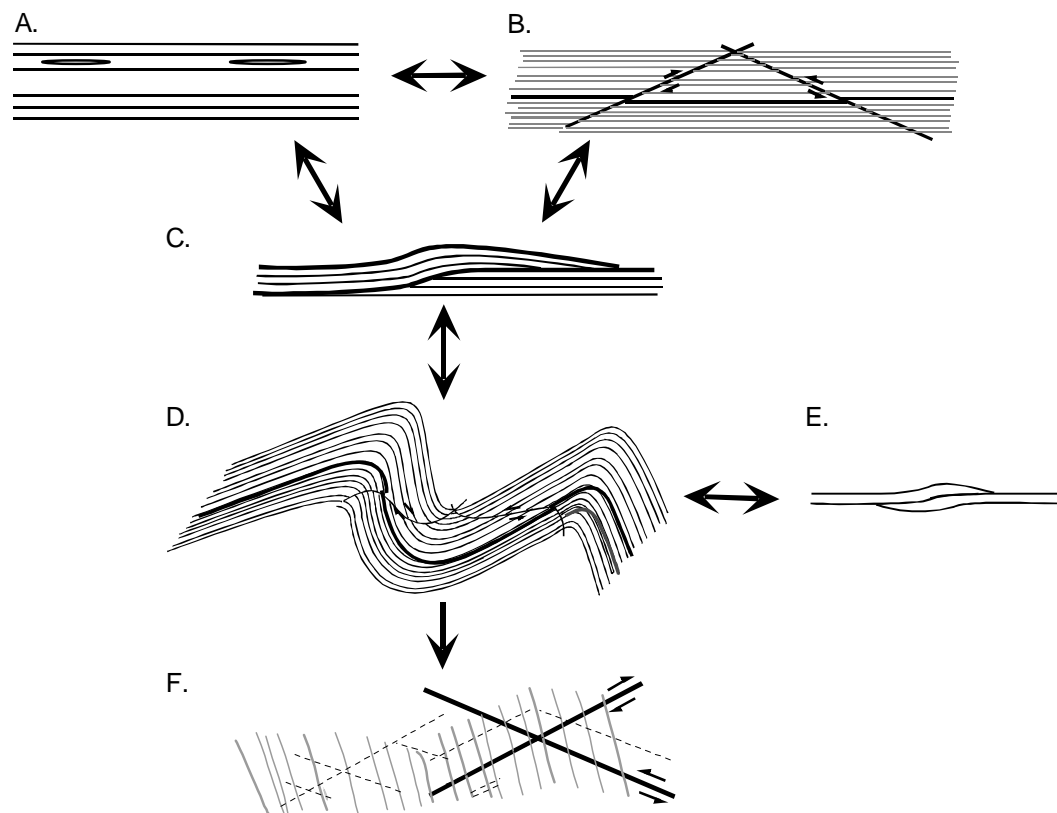


Figure 39. Order of deformation. A. Formation of boudins, and B. initiation of conjugate faults appear early in the deformation. C. Bed duplication with ramp faults also initiates early in the shortening, continuing as folding proceeds. D. Folding on different scales continues subject to a net top-to-the-south layer-parallel shear. E. Wedges form during folding. F. Sub-horizontal shortening continues with conjugate faults in steep beds and rotation of limbs.

Conditions in the multilayer that contributed to the final fold form are

- A relatively thick stiff unit above the thin beds in the upper part of the concentric-like fold contributed to the concentric-like form similar to the upper layers in a constrained multilayer.
- A mean top-to-the-south sense of layer-parallel shear produced an opposite sense of asymmetry in the kink-like fold compared with the chevron-like folds. The short limb of the kink-like fold faces north and the chevron-like folds face south. The top-to-the-south sense of layer-parallel shear is consistent with the setting in a thrust sheet with NNW vergence and overshadows possible top-to-the-north layer-parallel shear caused by flexural slip on the south limb of the Oakland anticline.
- The localized tan siltstone and associated calcareous nodules amalgamated to the sandstone layers within the kink-like fold may be evidence of nonlinear slip on the layer contacts which theoretically is necessary for the formation of ideal monoclinial kink folds.
- The wavelength of the folds in the outcrop varies according to the thickness of the folding units.
- Wavelength to thickness models yield initial thickness of 8 m in Section I and 15 m in Section VI, corresponding to layer to average media viscosity contrasts of 0.5 and 0.8 respectively.

- Modeling the number of structural units in Section I and VI multilayers resulted in two units each, perhaps an indication the layer contacts were more bonded than free slip.
- Boudins in the calcareous layers throughout the outcrop are evidence of non-linear material behavior. Coincident with the calcareous layers and boudins is thickening of adjacent layers or more conspicuous jointing.

The exposure of folds is a cross-section of folding units on the southeast limb of the Oakland anticline going down-section from south to north. This cross-section reveals only short wave-trains going from one folding unit to the next. The apparent folding units going down-section, with wavelengths and total bed thickness:

- Sec. VI asymmetric chevron-like folds, wavelength: 28 m, thickness: 20 m.
- Sec. IV asymmetric chevron-like folds, wavelength: 11-20 m, thickness: 12 m.
- Sec. III steeply dipping beds bordering a kink-like fold, thickness 35 m.
- Sec. II asymmetric chevron-like folds, wavelength: 9-14 m, thickness: 8 m.
- Sec. I concentric-like fold, wavelength: 16 m, thickness: 10 m.

The total measured thickness of the outcrop is about 100 m, with estimated overburden at the time of folding of about 1300 m. The relative thinness of the turbidite unit compared with the Tenmile Formation as a whole, and its strength contrast with the muddier units above and below, allowed the folds to form in layer-parallel shortening at the outcrop wavelengths.

Bibliography

- Baldwin, E. M., 1974, Eocene stratigraphy of southwestern Oregon: Oregon Department of Geology and Mineral Industries Bulletin 83, p. 1-40.
- Baldwin, E. M., and Perttu, R. K., 1980, Paleogene stratigraphy and structure along the Klamath borderland, Oregon, *in* Oles, K. F., Johnson, J. G., Niem, A. R., and Niem, W. A., eds., Geologic field trips in western Oregon and southwestern Washington, Oregon Department of Geology and Mineral Industries Bulletin 101, p. 9-37.
- Biot, M. A., 1961, Theory of folding of stratified viscoelastic media and its implications in tectonics and orogenesis: Geological Society of America Bulletin, v. 72, p. 1595-1620.
- Biot, M. A., 1965, Mechanics of Incremental Deformations: New York, John Wiley & Sons, Inc., New York, 504 p.
- Bouma, A. H., 1962, Sedimentology of some flysch deposits - A graphic approach to facies interpretation: New York, Elsevier, 168 p.
- Cloos, E., 1961, Bedding slips, wedges, and folding in layered sequences: Geologinen Tutkimuslaitos: Bulletin de la Commission Geologique de Finlande, v. 196, p. 105-122.
- Cosgrove, J. W., 1993, The interplay between fluids, folds and thrusts during the deformation of a sedimentary succession: Journal of Structural Geology, v. 15, no. 3-5, p. 491-500.
- Cruikshank, K. M., and Johnson, A. M., 1993, High-amplitude folding of linear-viscous multilayers: Journal of Structural Geology, v. 15, no. 1, p. 79-94.
- Cruikshank, K. M., Neavel, K. E., and Zuo, G. Z., 1989, Computer simulation of growth of duplex structures: Tectonophysics, v. 164, p. 1-12.
- Currie, J. B., Patnode, H. W., and Trump, R. P., 1962, Development of folds in sedimentary strata: Geological Society of America Bulletin, v. 73, p. 655-674.
- Diller, J. S., 1898, Description of the Roseburg quadrangle, U.S. Geological Survey Geological Atlas of the United States, Folio No. 49.
- Duncan, R. A., 1982, A captured island chain in the coast range of Oregon and Washington: Journal of Geophysical Research, v. 87, no. B13, p. 10,827-10,837.

- Heller, P. L., Peterman, Z. E., O'Neil, J. R., and Shafiqullah, M., 1985, Isotopic provenance of sandstones from the Eocene Tyee Formation, Oregon Coast Range: *Geological Society of America Bulletin*, v. 96, p. 770-780.
- Heller, P. L., and Ryberg, P. T., 1983, Sedimentary record of subduction to forearc transition in the rotated Eocene basin of western Oregon: *Geology*, v. 11, no. 7, p. 380-383.
- Heller, P. L., Tabor, R. W., and Suczek, C. A., 1987, Paleogeographic evolution of the United States Pacific Northwest during Paleogene time: *Canadian Journal of Earth Science*, v. 24, p. 1652-1657.
- Irwin, W. P., and Mankinen, E. A., 1998, Rotational and accretionary evolution of the Klamath Mountains, California and Oregon, from Devonian to present time.: U.S. Geological Survey, 98-114.
- Johnson, A. M., and Fletcher, R. C., 1994, *Folding of viscous layers: Mechanical analysis and interpretation of structures in deformed rock*: New York, Columbia University Press, 461 p.
- Johnson, A. M., and Pfaff, V. J., 1989, Parallel, similar and constrained folds: *Engineering Geology*, v. 27, p. 115-180.
- Krabbendam, M., and Leslie, A. G., 1995, Folds with vergence opposite the sense of shear: *Journal of Structural Geology*, v. 18, no. 6, p. 777-781.
- Magill, J., and Cox, A., 1980, *Tectonic rotation of the Oregon Western Cascades*: Portland, State of Oregon Department of Geology and Mineral Industries Special Paper 10, 67 p.
- Molenaar, C. M., 1985, Depositional Relations of Umpqua and Tyee Formations (Eocene), Southwestern Oregon: *The American Association of Petroleum Geologists Bulletin*, v. 69, no. 8, p. 1217-1229.
- Mutti, E., and Ricci Lucchi, F., 1972, *Le torbiditi dell' Appennino settentrionale: introduzione all' analisi di facies*: *Memorie della Societa Geologica Italiana*, p. 161-199. (Translated into English by T. H. Nilsen, 1978, *International Geology Review*, v. 20, no. 2, p. 125-166.
- Perttu, R. K., 1968, *The structural geology of the Woodruff Mountain area, Sutherlin Quadrangle, Oregon* [Honors College thesis]: University of Oregon Honors College, 51 p.

- Perttu, R. K., and Benson, G. T., 1980, Deposition and deformation of the Eocene Umpqua Group, Sutherlin area, southwestern Oregon: *Oregon Geology*, v. 42, no. 8, p. 135-140,146.
- Pfaff, V. J., 1986, On forms of folds: Cincinnati, Ohio, University of Cincinnati, Ph.D. dissertation, 563 p.
- Pfaff, V. J., and Johnson, A. M., 1989, Opposite senses of fold asymmetry: *Engineering Geology*, v. 27, p. 3-38.
- Pyle, D. G., 1988, Geochemical evolution of the Roseburg Formation basaltic rocks, southern Oregon Coast Range: Corvallis, Oregon, Oregon State University, M.S. thesis, 142 p.
- Ryberg, P. T., 1984, Sedimentation, structure and tectonics of the Umpqua Group (Paleocene to early Eocene), southwestern Oregon: Tucson, Arizona, University of Arizona, Ph.D. dissertation, 280 p.
- Ryu, In-Chang, Niem, A. R., and Niem, W. A., 1992, Schematic fence diagram of the southern Tye Basin, Oregon Coast Range, showing stratigraphic relationships of exploration wells to surface measured sections: Department of Geology and Mineral Industries Oil and Gas Investigation 18, 28 p.
- Ryu, In-Chang, Niem, A. R., and Niem, W. A., 1996, Oil and gas potential of the southern Tye Basin, Southern Oregon Coast Range: Department of Geology and Mineral Industries Oil and Gas Investigation 19, 141 p..
- Smith, R. B., 1977, Formation of folds, boudinage, and mullions in non-Newtonian materials: *Geological Society of America Bulletin*, v. 88, p. 312-320.
- Snively, J., P. D., MacLeod, N. S., and Wagner, H. C., 1968, Tholeitic and alkalic basalts of the Eocene Siletz River Volcanics, Oregon Coast Range: *American Journal of Science*, v. 266, p. 454-481.
- Tanner, P. W., 1989, The flexural-slip mechanism: *Journal of Structural Geology*, v. 11, no. 6, p. 635-655.
- Tanner, P. W., 1992, The duplex model: Implications from a study of flexural-slip duplexes, *in* McClay, K. R., ed., *Thrust tectonics*: London, Chapman & Hall, p. 201-208.
- Thoms, R. E., 1975, Biostratigraphy of the Umpqua Group, southwestern Oregon, *in* Weaver, D. W., Hornaday, G. R., and Tipton, A., eds., *Paleogene Symposium and Selected Technical Papers*: Long Beach, California, American Association

of Petroleum Geologists-Society of Economic Paleontologists and Mineralogists-Society of Exploration Geophysicists Annual Meeting, Pacific Sections, p. 513-562.

Wells, F. G., and Waters, A. C., 1934, Quicksilver deposits of southwestern Oregon: U. S. Geological Survey Bulletin, v. 850, p. 58.

Wells, R. E., and Heller, P. L., 1988, The relative contribution of accretion, shear, and extension to Cenozoic tectonic rotation in the Pacific Northwest: Geological Society of America Bulletin, v. 100, p. 325-338.

Wells, R. E., 1998, Geologic map of the Garden Valley 7.5' Quadrangle, Oregon, U.S. Geological Survey, 98-XXX, in press.

Appendix A

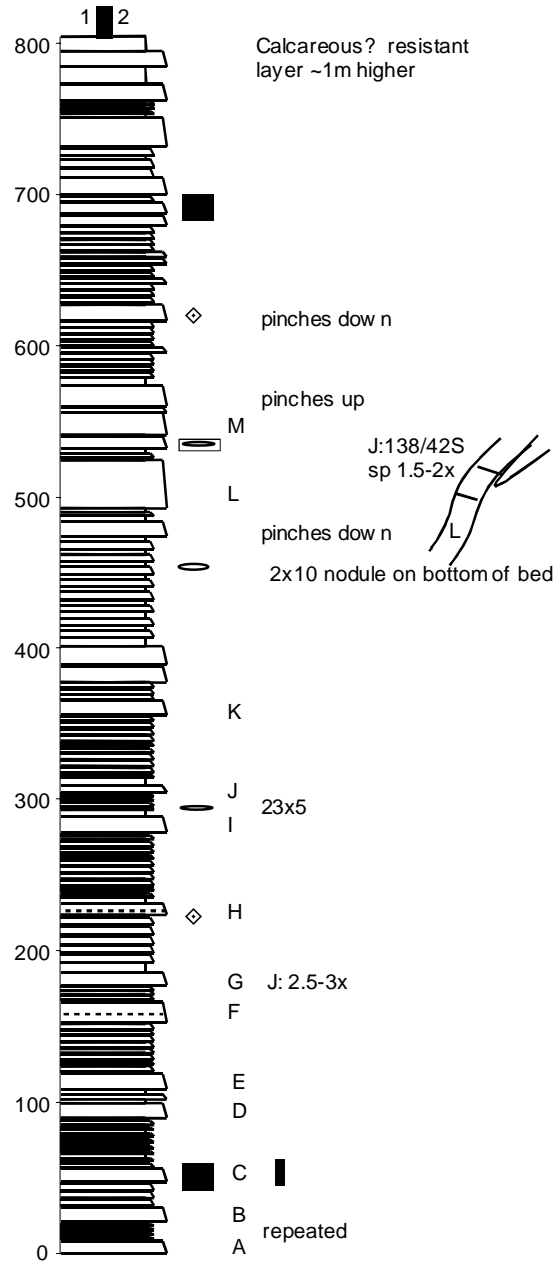
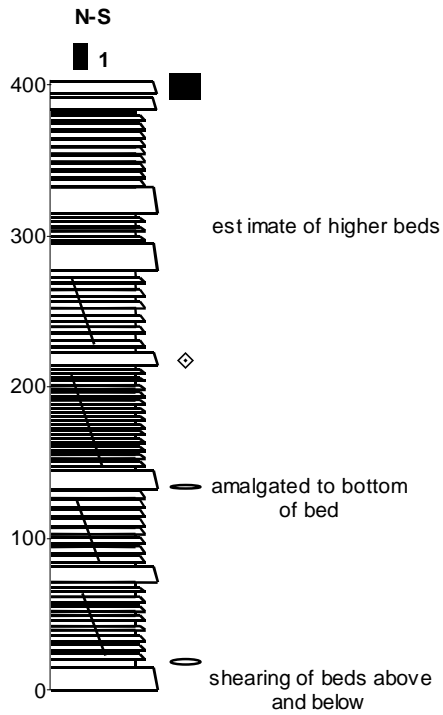
Compilation of data for Figure 7. Estimated thickness of Umpqua Group strata immediately north and south of the study area and east of the Umpqua River as shown in Figure 1. Map distances and bedding dips are based on the Garden Valley 7.5' Geologic Quadrangle (Wells, 1998).

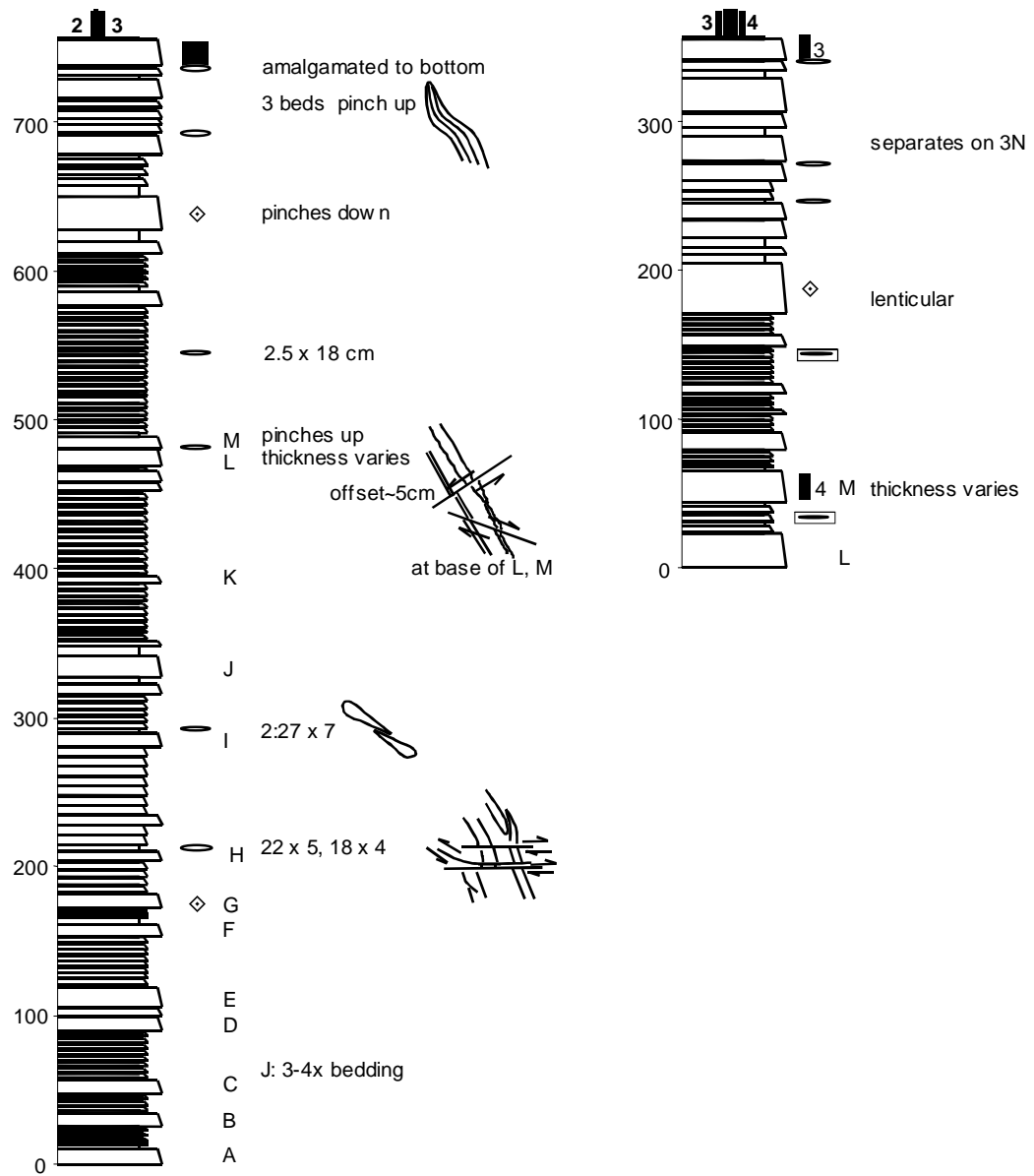
Umpqua Group units	Average map distance (m)	Dip of strata	Average dip	Thickness estimate (m)
White Tail Ridge Formation (½ the syncline)	720	35-41° S	38°	450
Tums: mudstone dominated thin turbidites	1100	8-60° S	40° S	700
Tuss: sandstone dominated turbidites, thick to massive	800	20-34° S	27° S	350
Tum: mudstone	120	25° S	25° S	50
Tuss: sandstone dominated turbidites, thick to massive bedded	1220	10-33° S	25° S	500
Estimated thickness total				2050

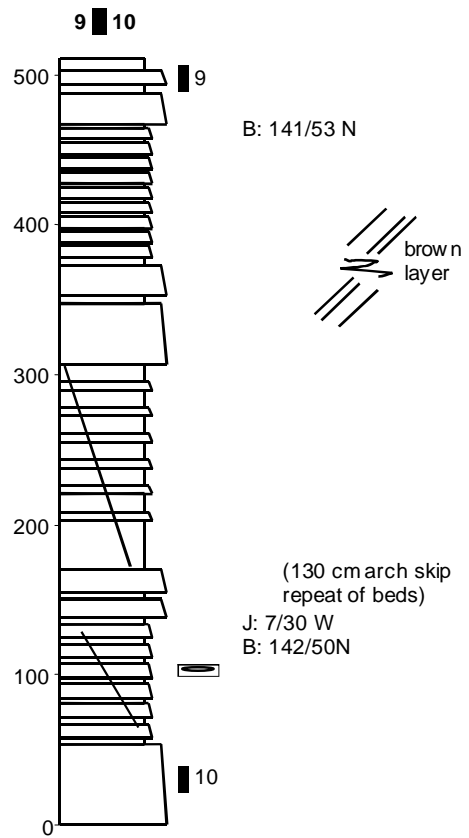
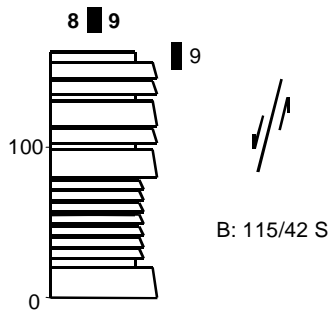
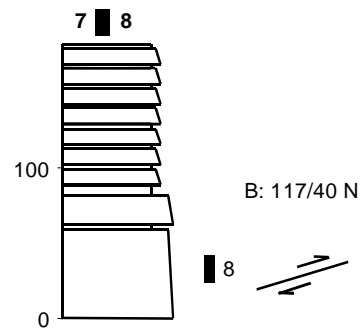
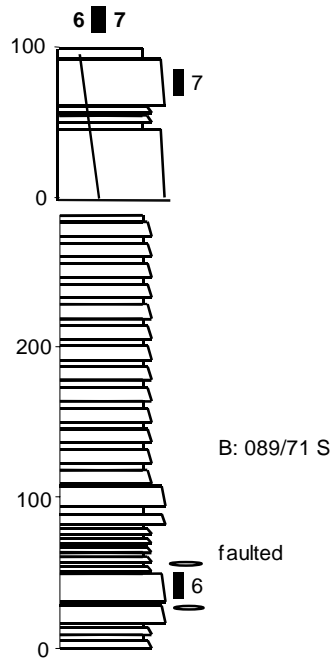
Appendix B

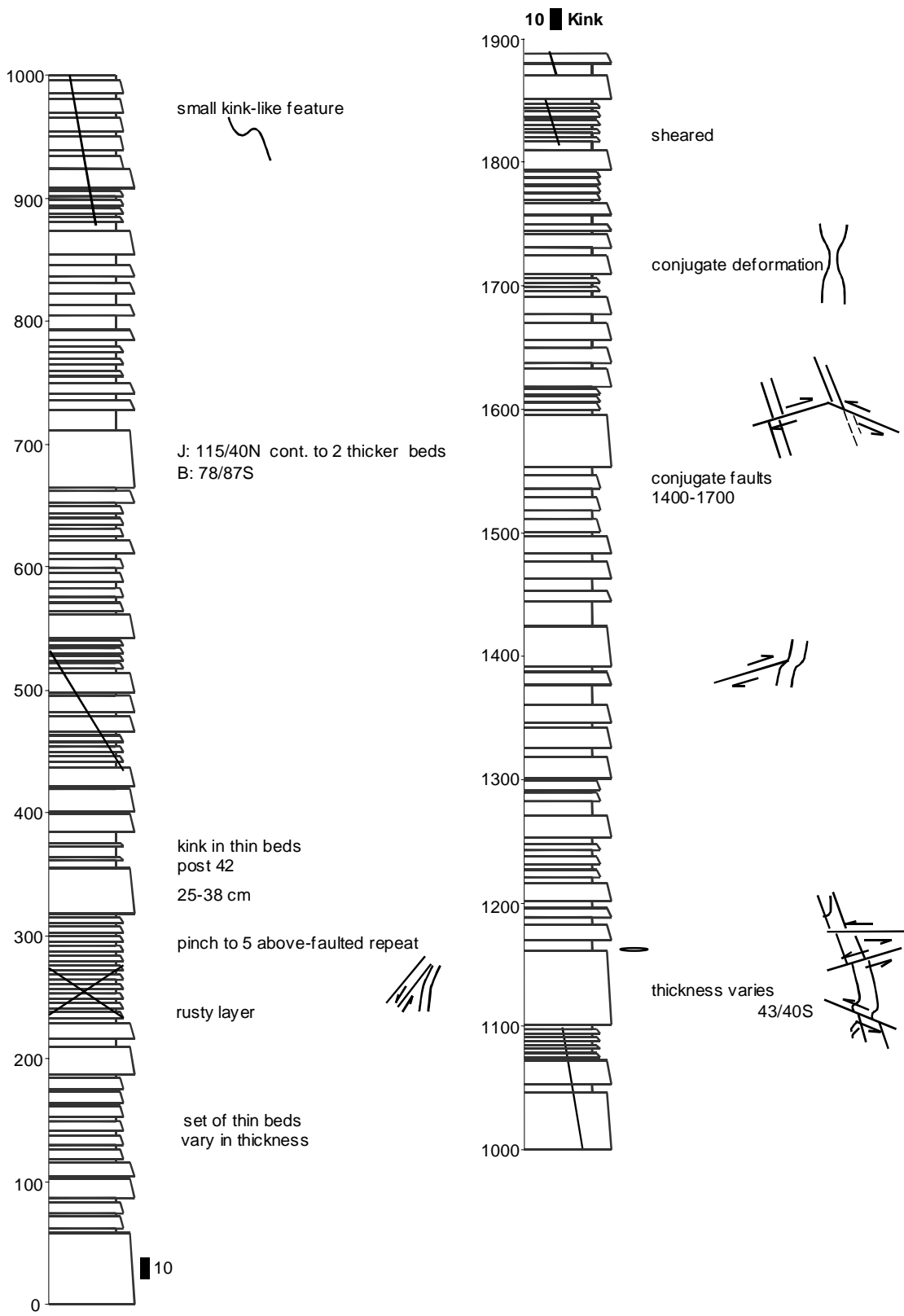
The stratigraphic columns on the following pages illustrate measured sections from north to south, hinge to hinge. An Excel macro was used to draw the columns based on field measurements of thickness and sandstone to shale ratio. Beds less than 10 cm were grouped and averaged. Beds crossed by a diagonal line have poor exposure. Some beds in Sections I and VI are lettered for matching within each section. Symbols used in the column are:

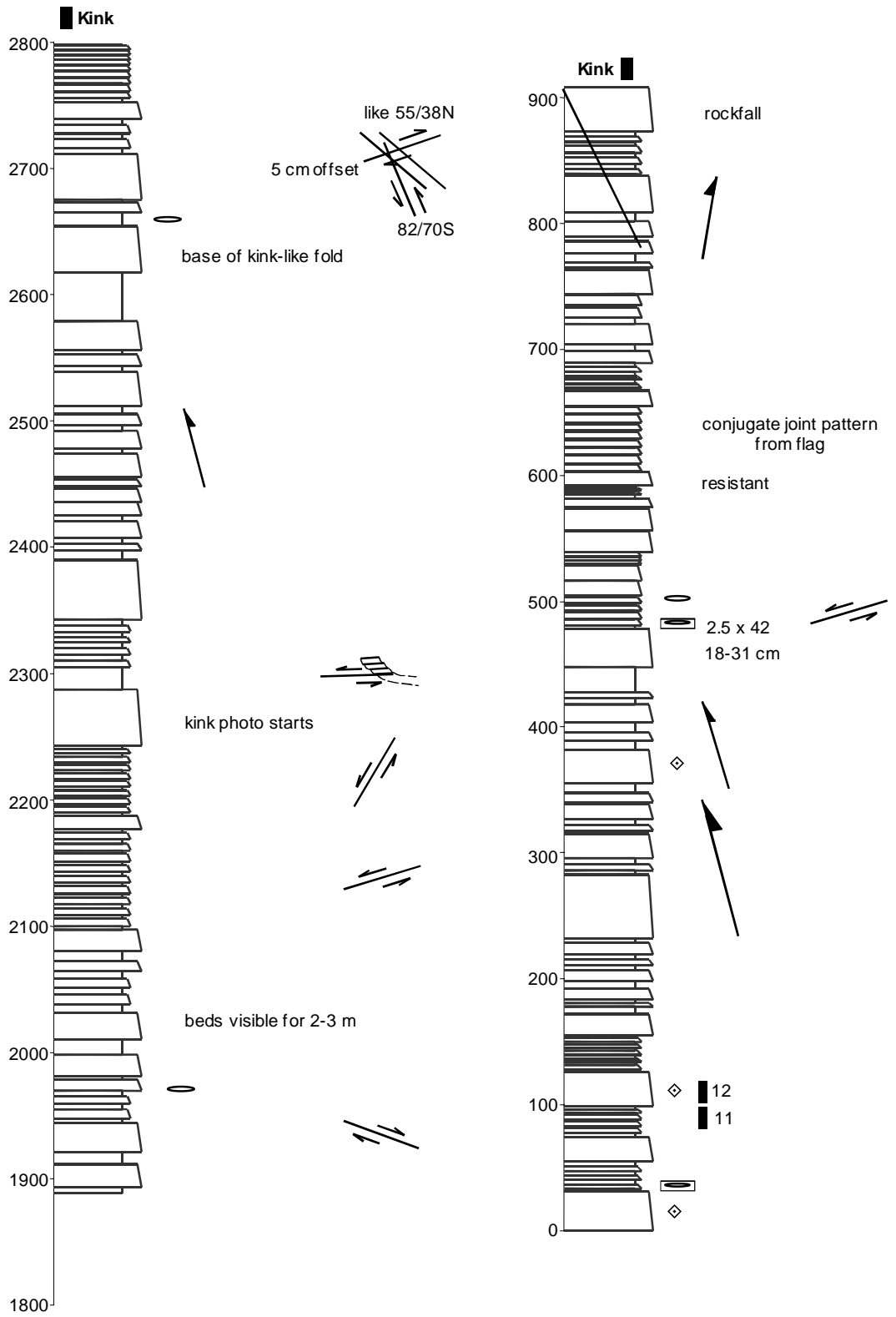
	Hinge survey point		Thinning up sequence
	Flag-survey point		Thickening up sequence
	Calcareous boudin		
	Calcareous layer		

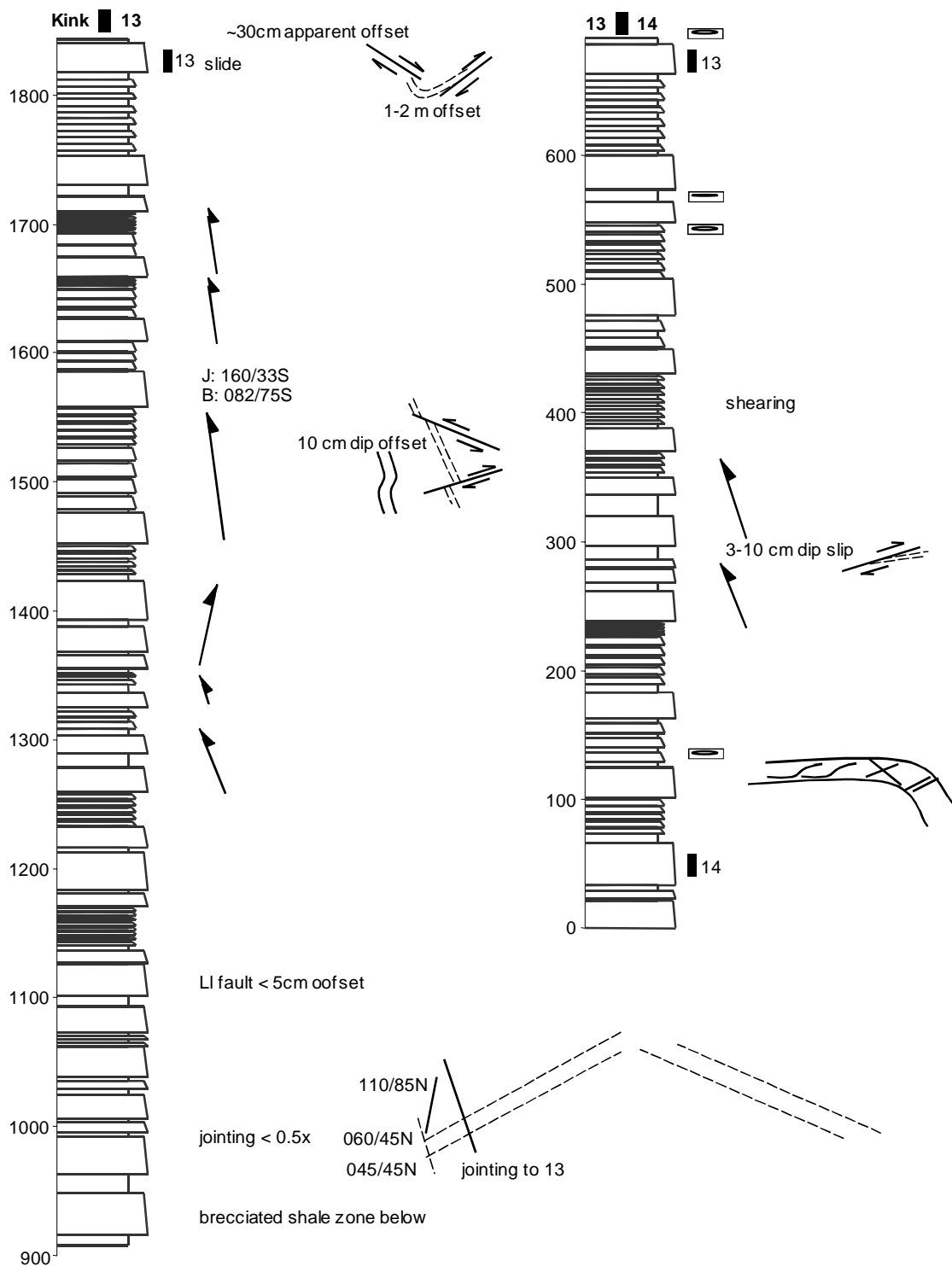


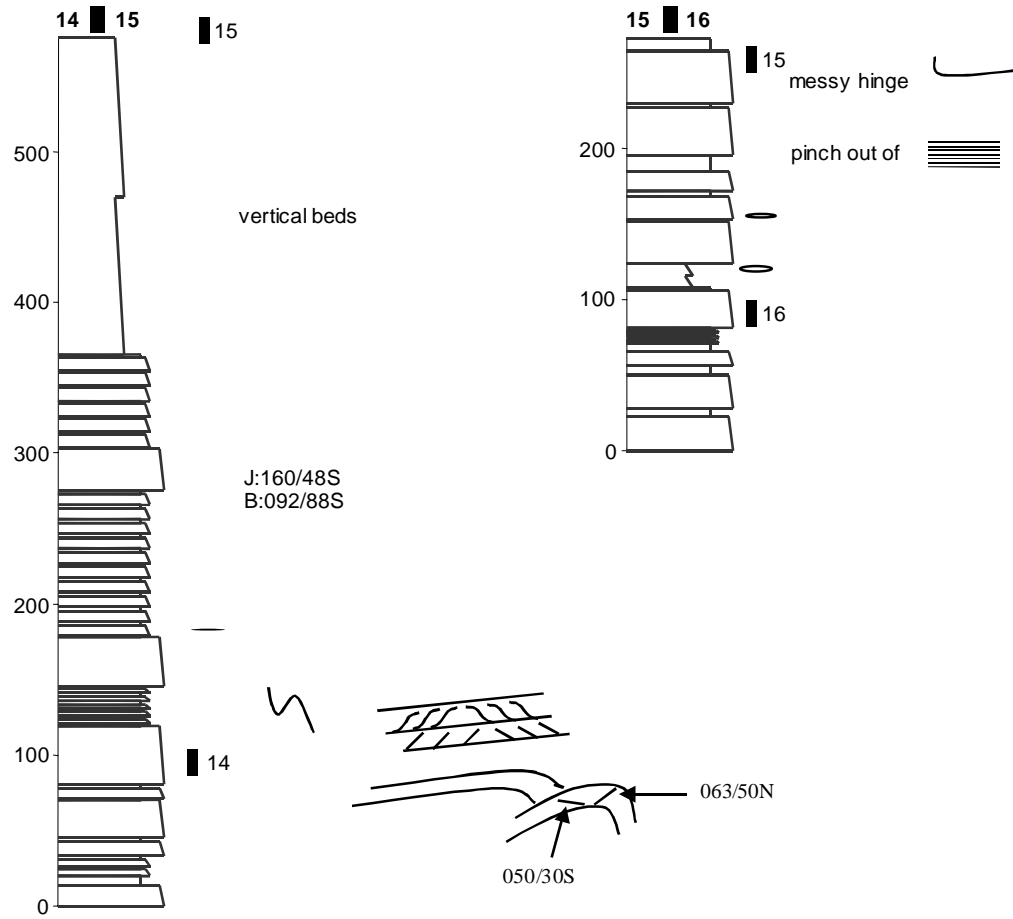


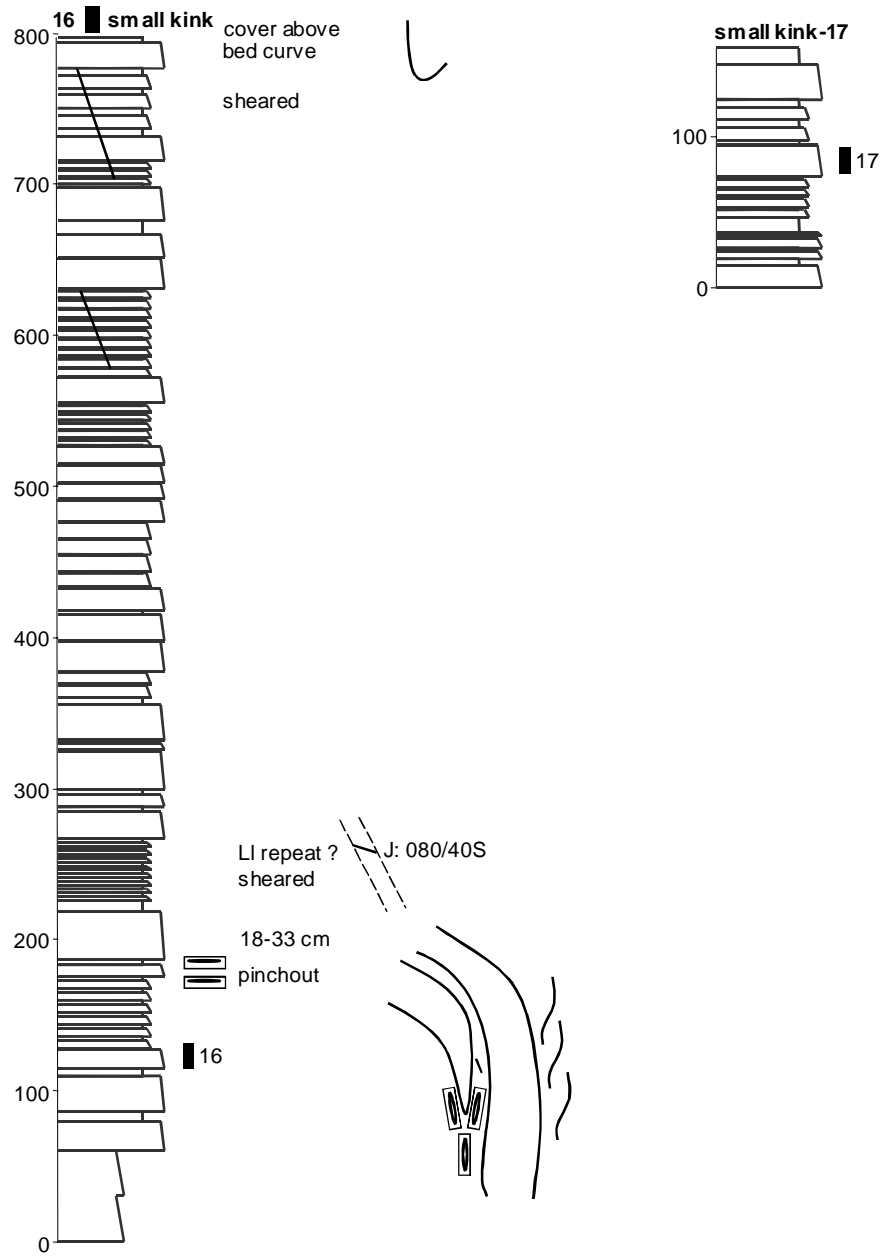


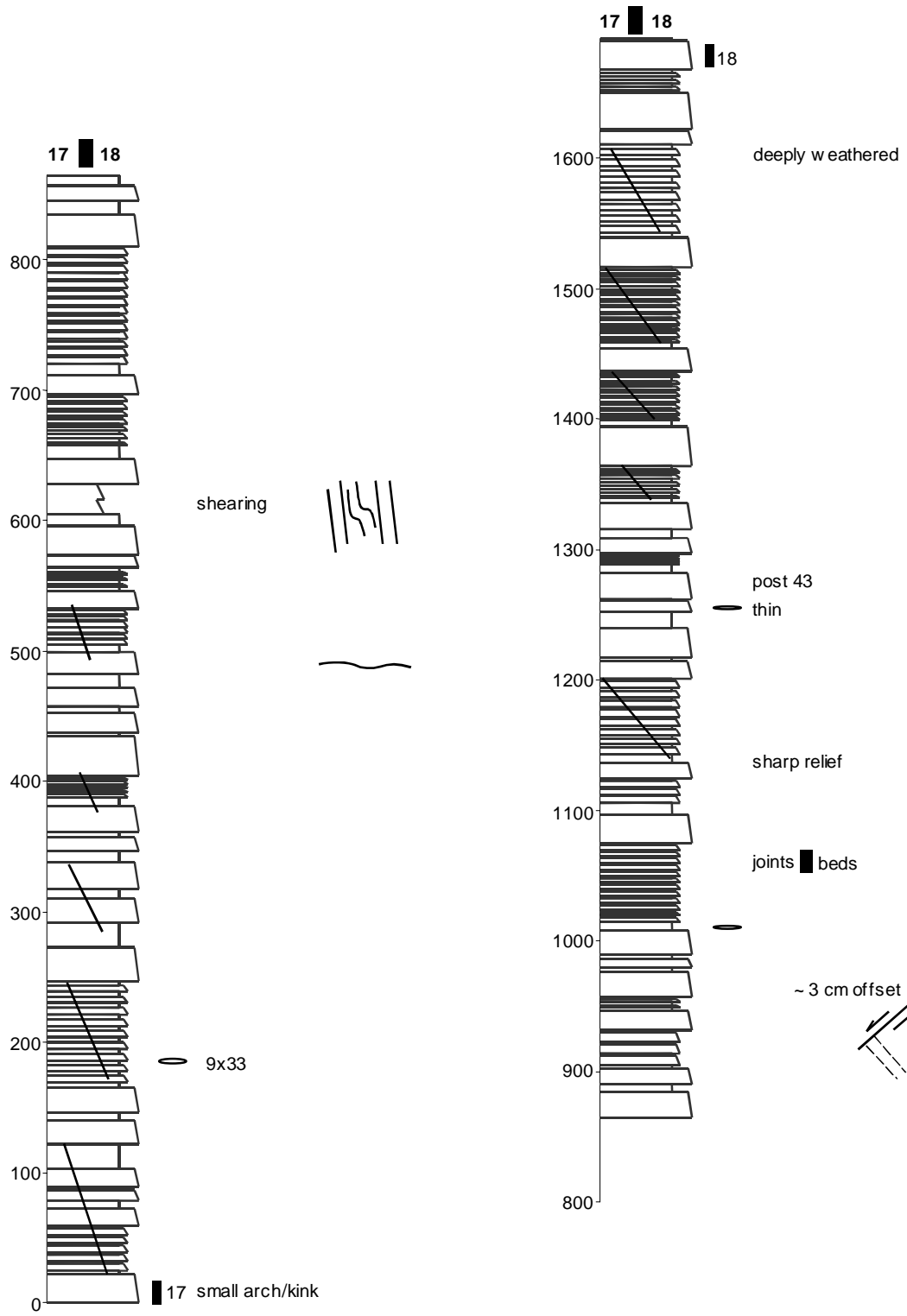


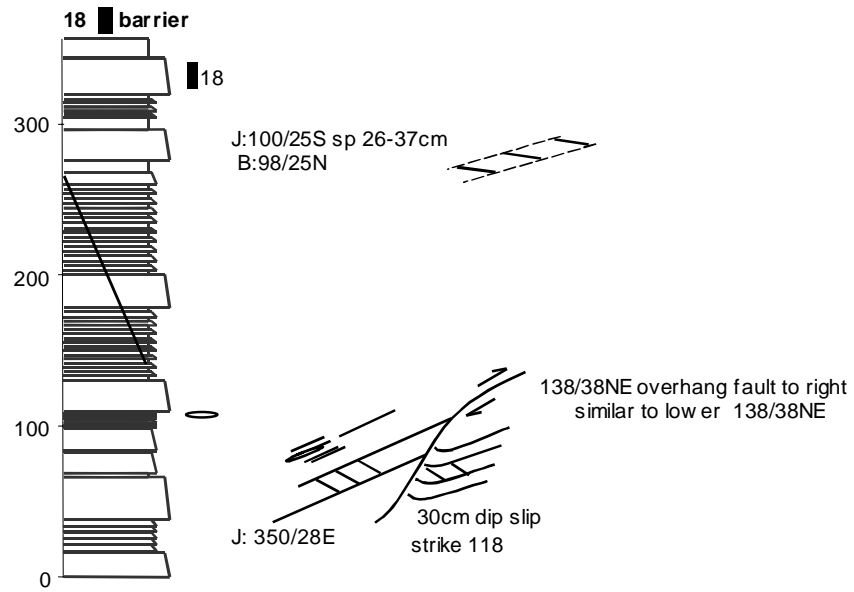


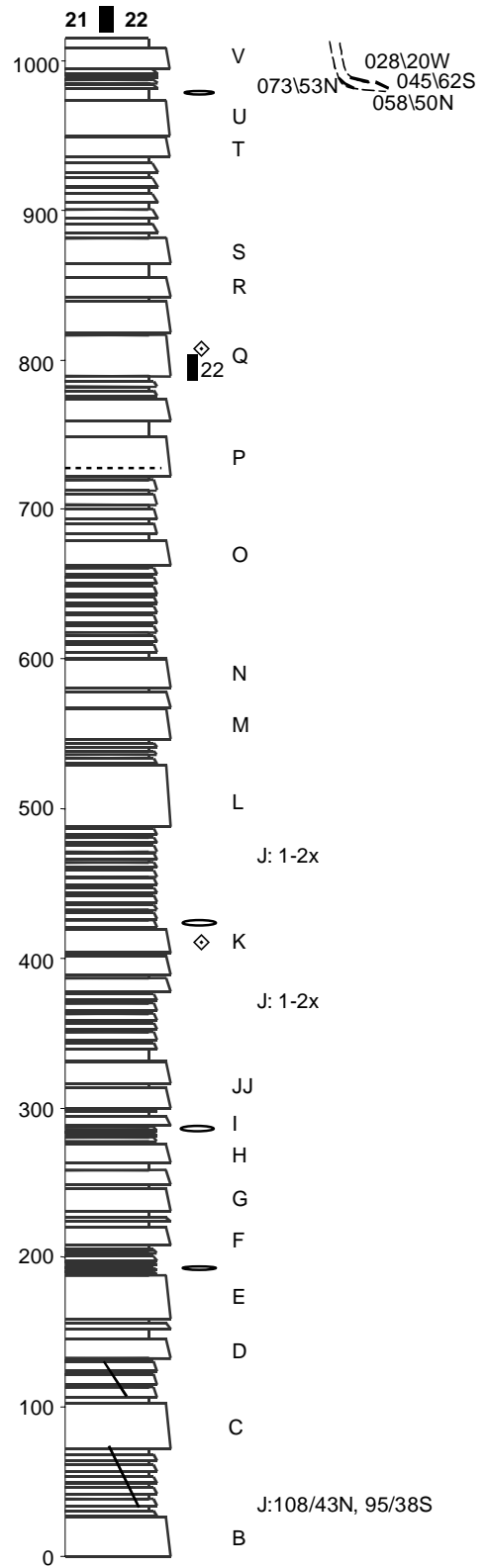
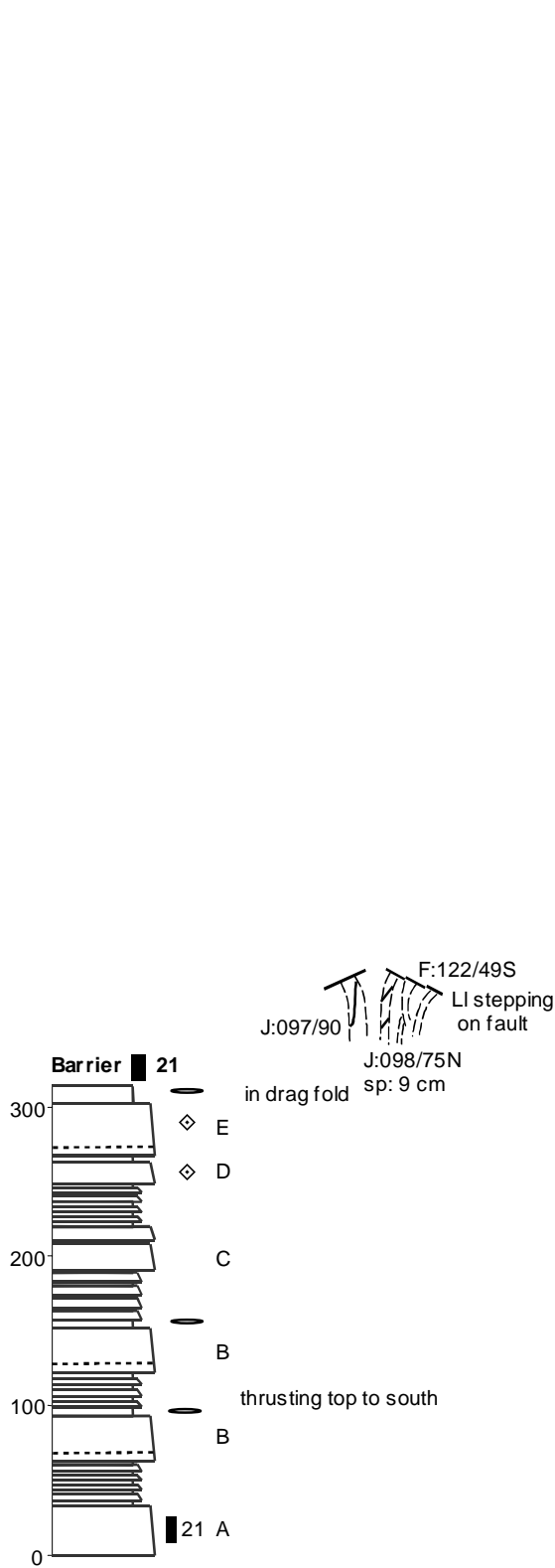


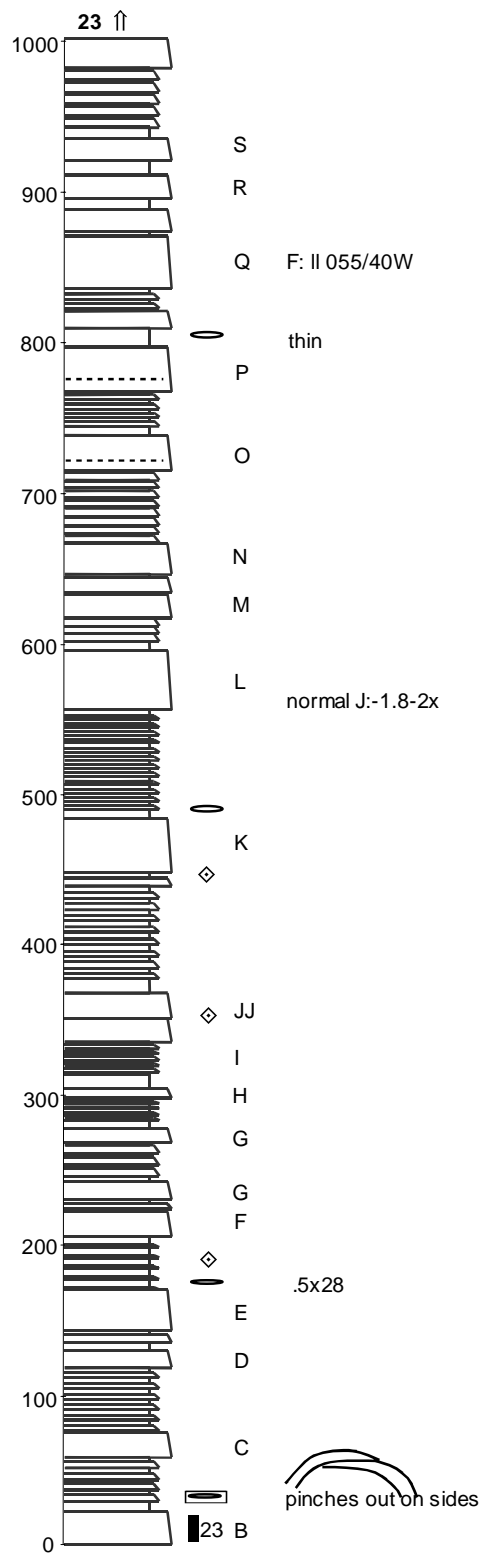
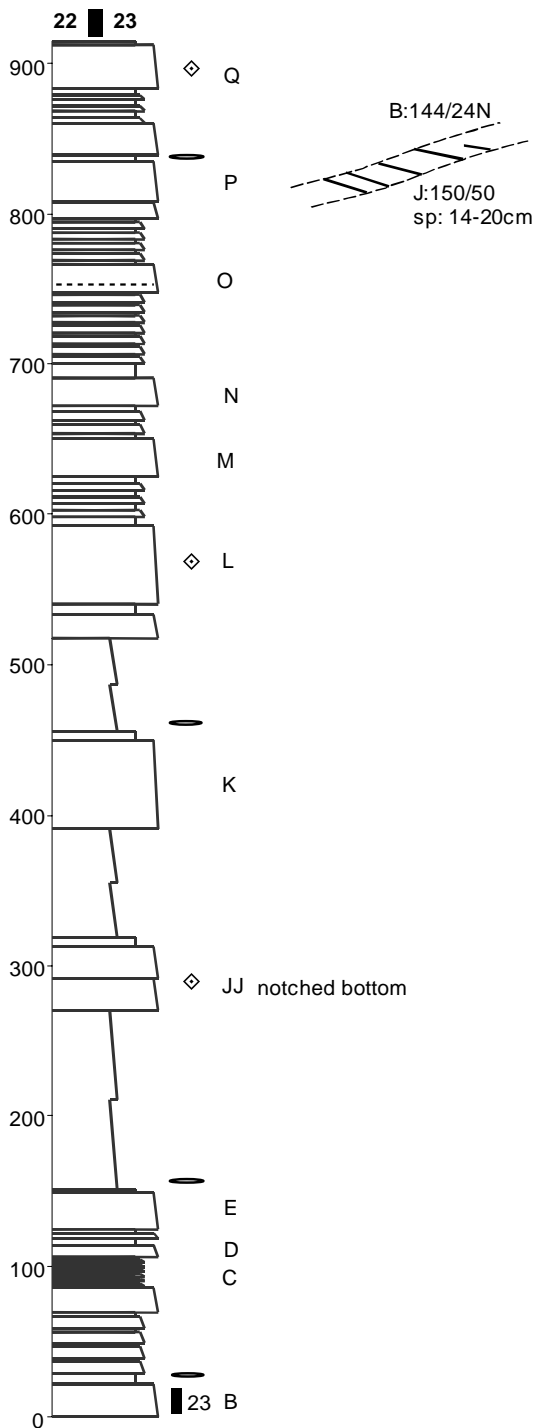


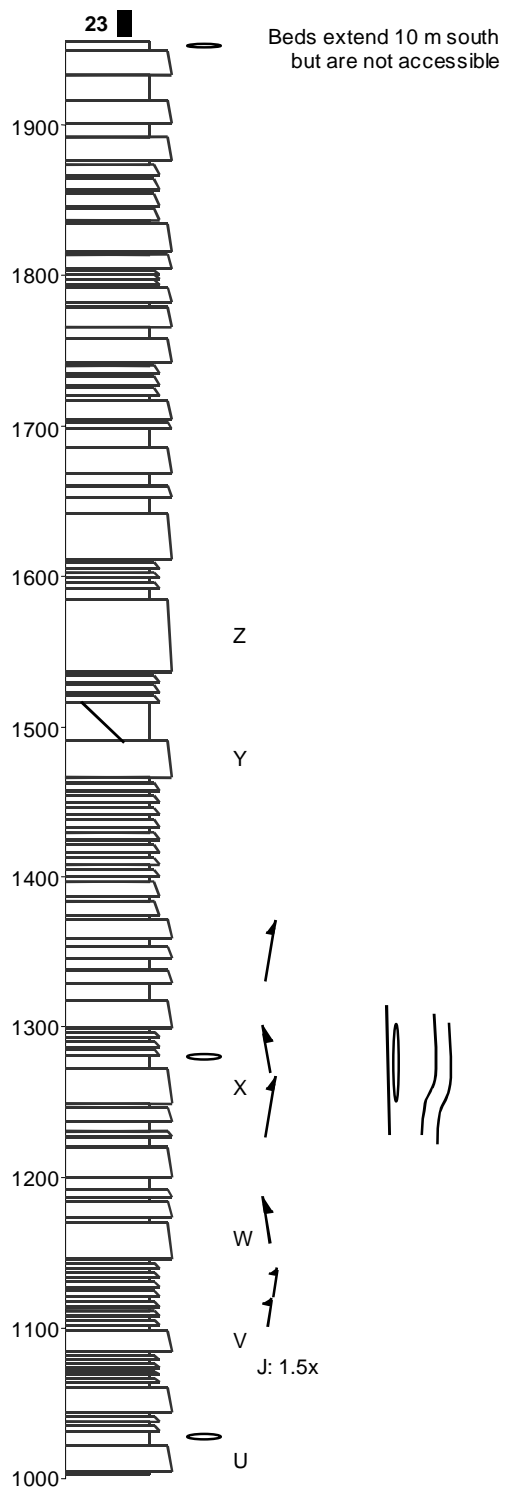












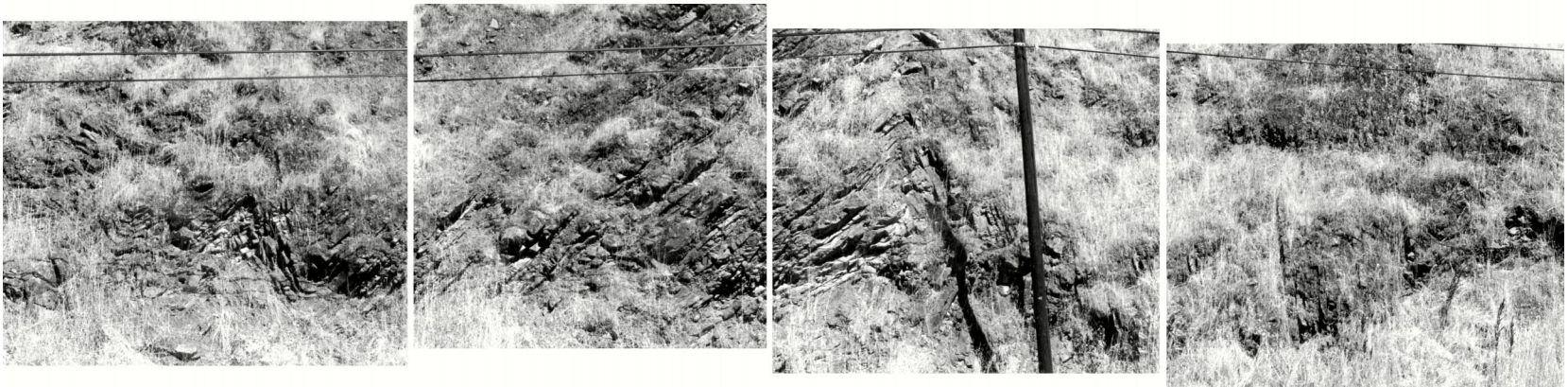
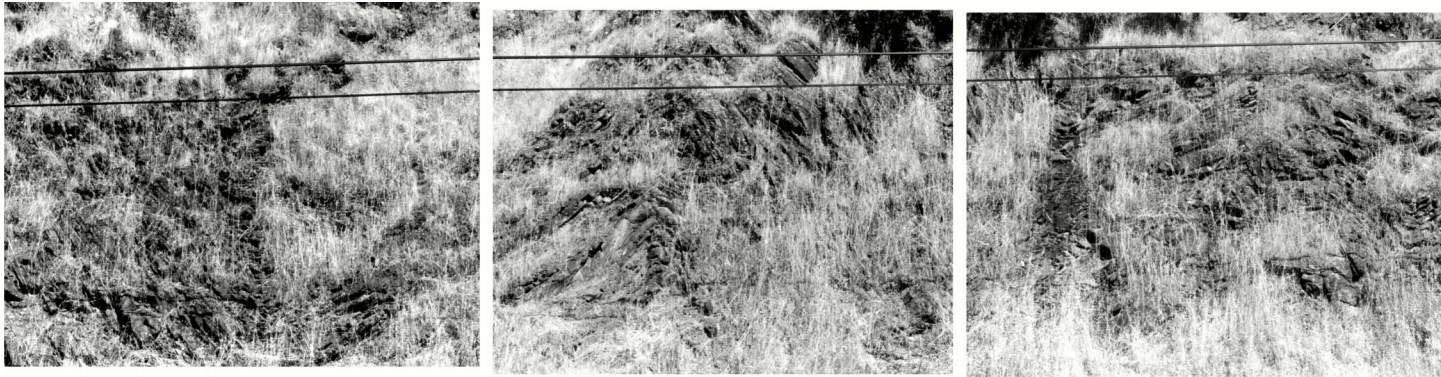
Appendix C

The following pages contain a continuous set of photographs of the outcrop from north to south. The arrangement on each page is from left to right, top to bottom. Photographs were taken normal to the outcrop except for Section VI south where several photographs are along strike of the beds.

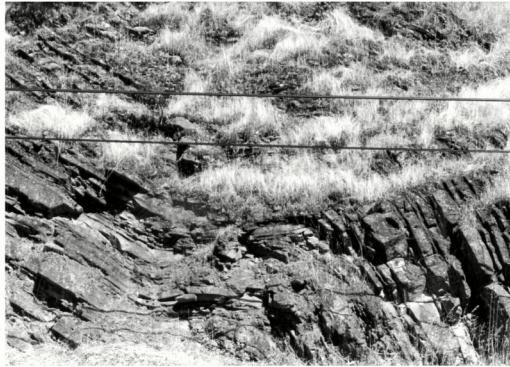
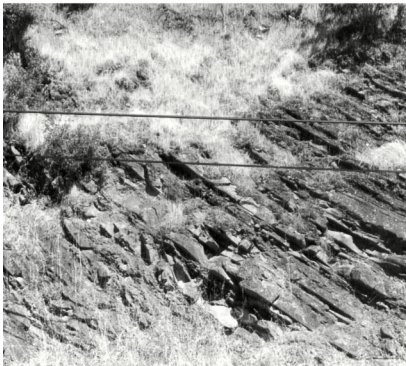
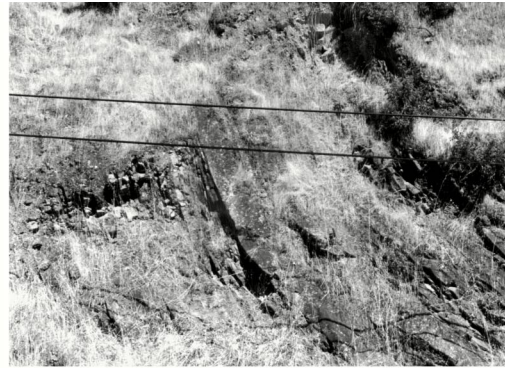
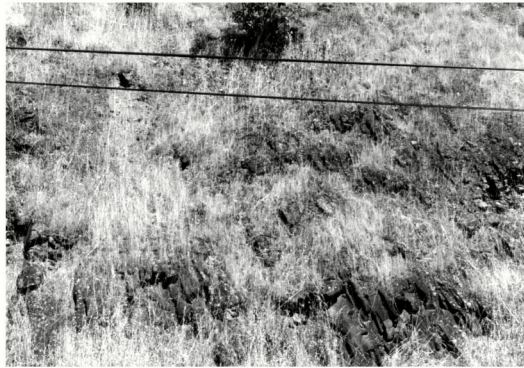
Pocket



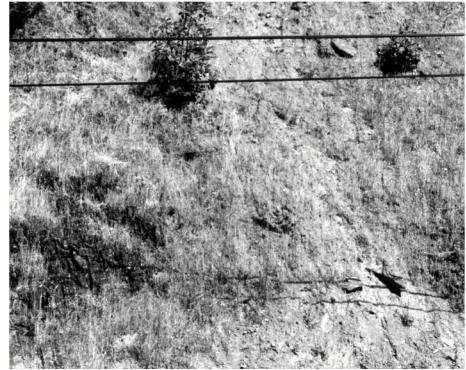
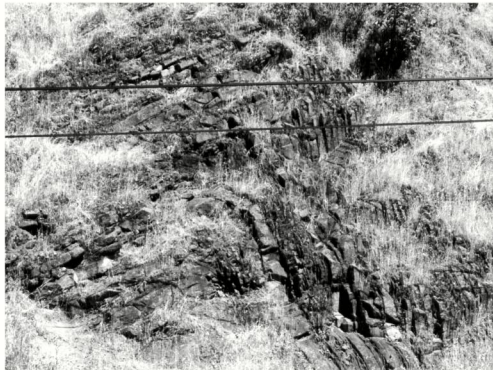
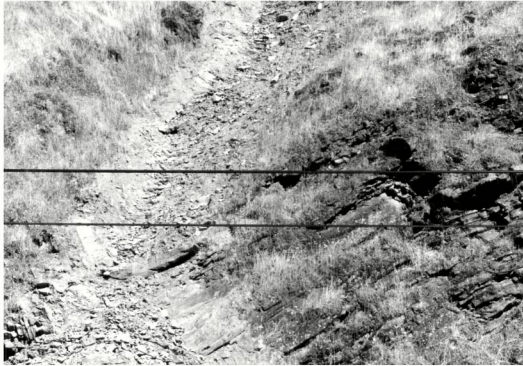
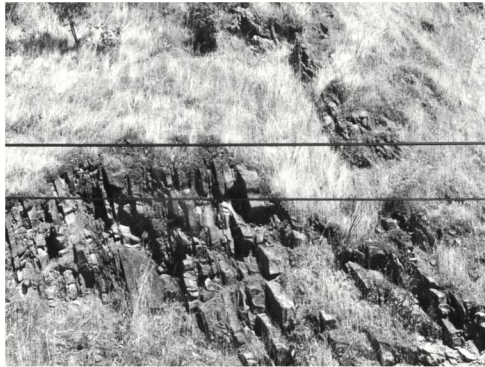
Section I



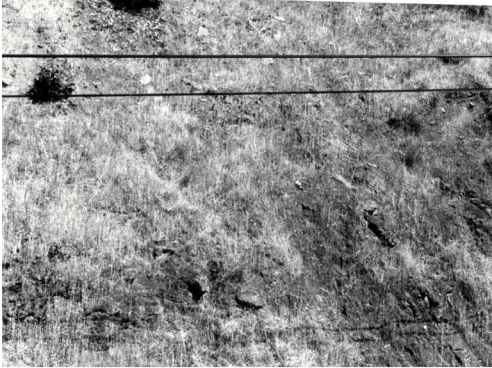
Section II



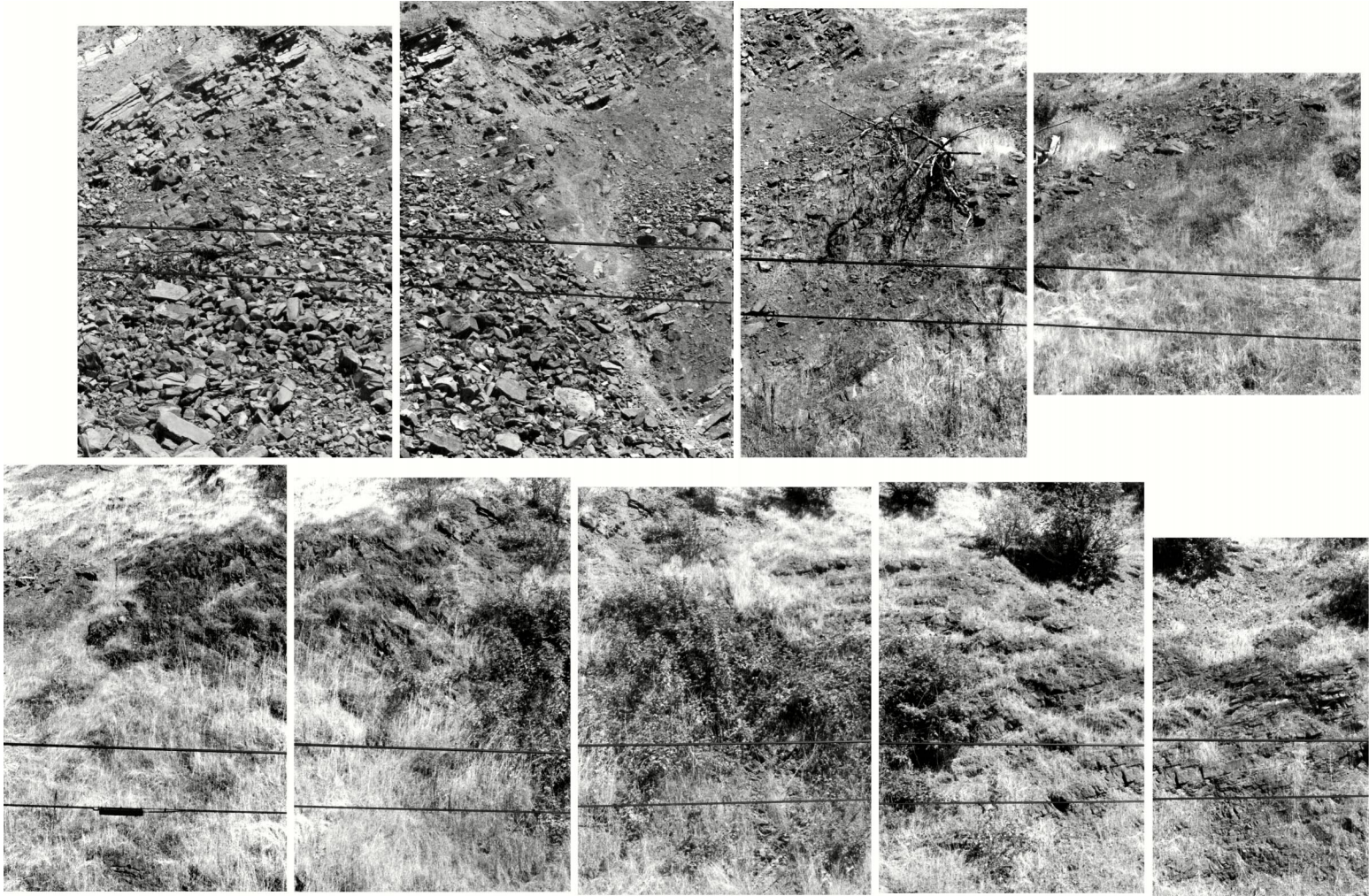
Section III



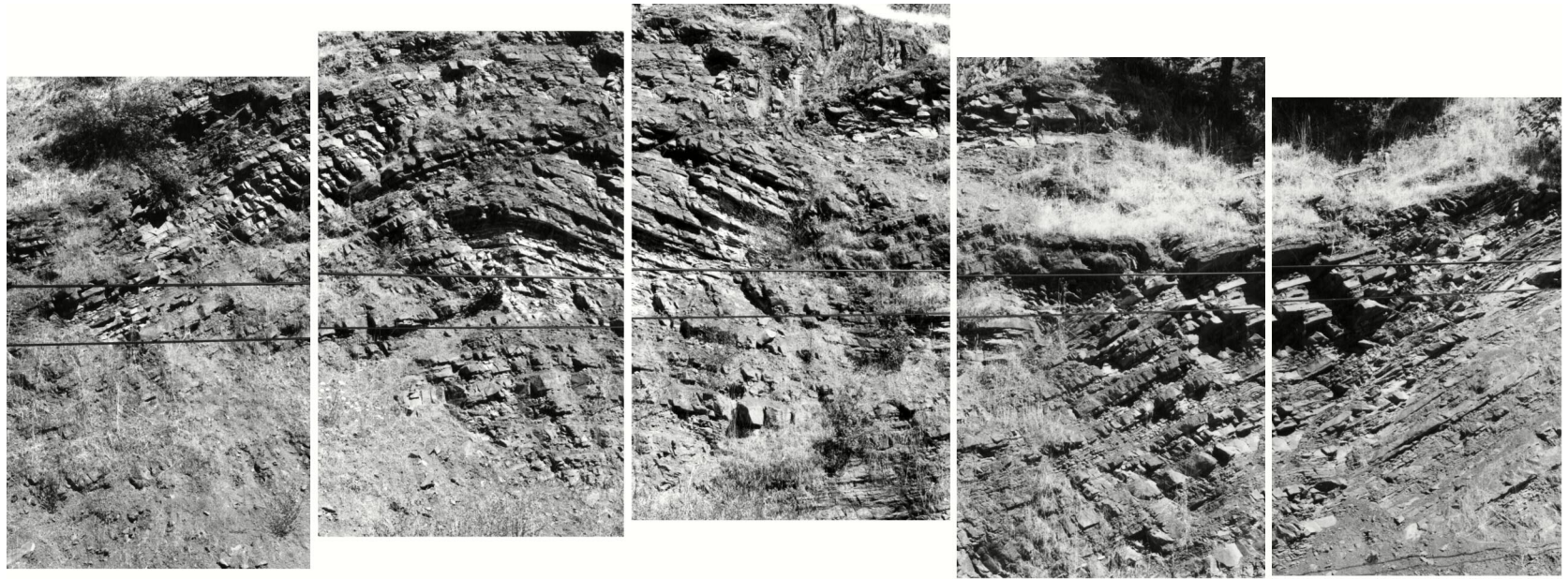
Section IV- north



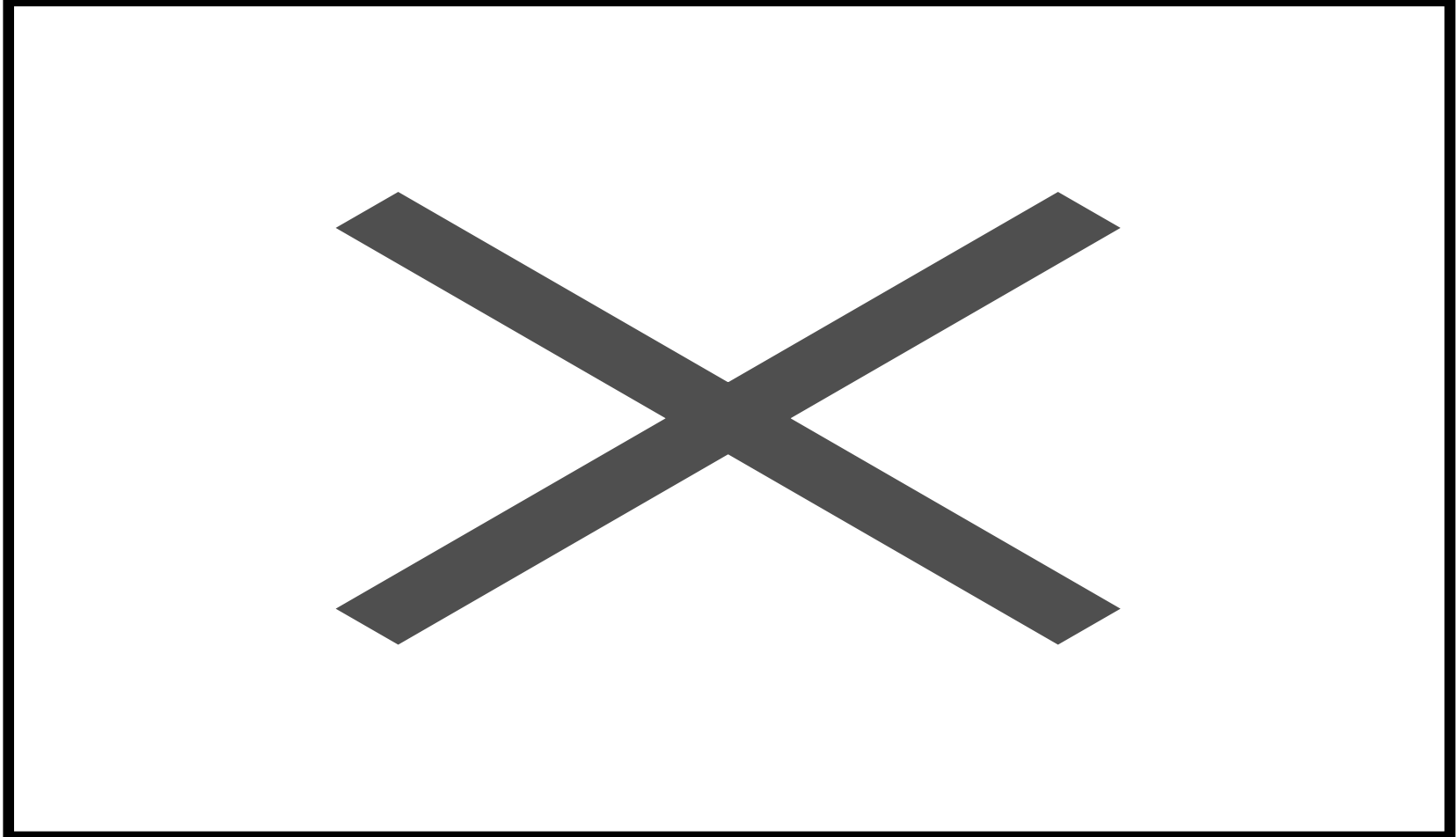
Section IV- south



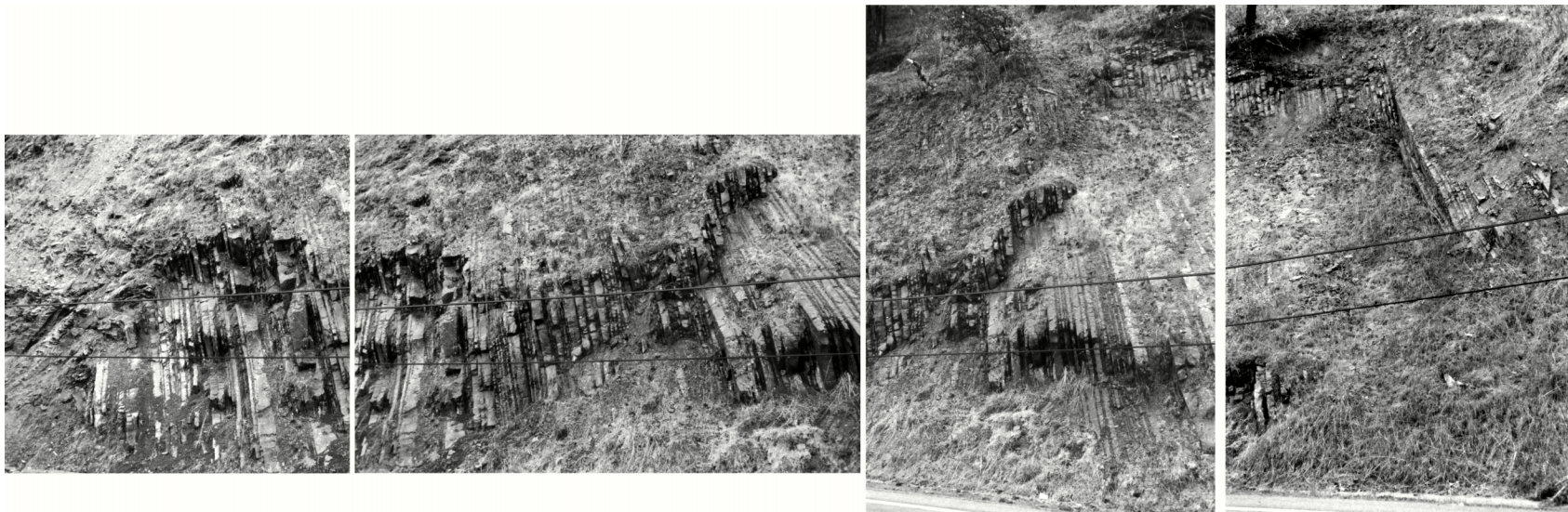
Section V- north



Section V- south



Section VI- north



Section VI- south